UNIVERSITÀ DEGLI STUDI DI NAPOLI

"FEDERICO II"

DIPARTIMENTO DI INGEGNERIA CHIMICA, DEI MATERIALI E DELLE PRODUZIONI INDUSTRIALI

XXVIII° CICLO

TESI DI DOTTORATO IN
INGEGNERIA DEI MATERIALI E DELLE STRUTTURE

Synthesis, physicochemical and biological characterization of layer by layer oil in water nanocapsules

Teresa Fotticchia

TUTORE
Prof. Paolo Antonio Netti

COORDINATORE
Prof. Giuseppe Mensitieri

CO-TUTORE
Dott. Ing. Raffaele Vecchione

Contents

Abstract

Oil in water nanoemulsions (O/W NEs) represent an ideal vehicle for drug delivery thanks to their ability to dissolve large quantities of hydrophobic drugs and protect their cargo from hydrolysis and enzymatic degradation. The stabilization of O/W NEs by means of a polymer coating, obtained through the layer by layer methodology (LbL), and the polyethylene glycol (PEG) conjugation are extremely important respectively to prolong the shelf life of the product and the period of blood stream circulation. In this perspective the first part of my thesis project concerns the complete physicochemical characterization of oil in water nanoemulsions coated with a polyelectrolyte (namely secondary NE) in order to identify polymer concentration domains that are thermodynamically stable and to define the degree of stability through thermodynamic functions depending upon relevant parameters affecting the stability itself, such as type of polymer coating, droplet distance, etc. This study was very important for the build-up of optimal oil in water secondary nanoemulsions (SNE).

The second part of the Ph.D. work was focused on the improvement of O/W SNEs functioning as drug delivery systems in the human body based on the development of a decoration strategy by means of two macromolecules: the PEG as a molecule that increases availability of the nanocarrier in the blood stream, and a peptide as a molecule able to target the nanocarrier to a specific district. Herein, a cell penetrating peptide (CPP) that crosses cellular membranes was chosen as a model, anyway simply removing the peptide or substituting it with a ligand of a specific cell-receptor it is

possible to obtain a nanocarrier that in view of its small size (below 200 nm) can promote passive targeting to tumors through the extravasation mechanism or a nanocarrier prone to active targeting, respectively. The last part of the Ph.D. study was focused on the development of a method able to identify receptors overexpression on specific cell lines. The methodology, based on Isothermal Titration Calorimetry (ITC) coupled with confluent cell layers cultured around biocompatible templating microparticles can be very helpful to identify targets, to address drug design and selectively deliver therapeutics that can cross biological barriers.

CHAPTER I Introduction

1.1. Nanotechnologies and Nanomedicine

Nanotechnology is increasingly considered to be the technology of the future (1), it consists in the confinement of functional systems at the molecular scale. ‘‘There’s plenty of room at the bottom’’ is the title of the lecture that Richard Feynman gave in 1959 at the annual meeting of the American Physical Society introducing the concept of nanotechnology as an important field for future scientific researches (2). During his lecture he asked his audience:

“I don’t know how to do this on a small scale in a practical way, but I do know that computing machines are very large; they fill rooms. Why can’t we make them very small, make them of little wires, little elements, and by little, I mean little?”

This lecture is still seen as a seminal event in the short history of the nano-field. Technological advances had been made in the nano-world since Feynman’s talk. In these years, nanotechnology research has been widely developed in the field of communications, engineering, chemistry, physics, robotics, biology, and medicine. In particular nanotechnology represents a powerful tool in the field of medicine, where it has been utilized for the development of novel drug delivery systems (DDS) through the entrapment of the pharmaceutical agent in nanoparticulate systems aimed to the treatments of a variety of diseases and disorders (3). Nanomedicine offers an avenue where nanoscale systems could easily enter cells and tissues to

interact with DNA and proteins. In other words, the nanoscale systems work as nanocarriers for the delivery of drugs. Since 1970 controlled DDSs have attracted huge interest and great progresses have been reached (4). In fact despite being only several decades old, research in nanomedicine has already led to the development of a wide range of products including diagnostics, and medical devices. Nowadays, there are more than 200 nanomedicine products that have been either approved or are under clinical investigation (5,6). The use of a drug delivery system is useful to enhance the efficacy and safety of therapeutic agents, and overcome any drawbacks of the agents, such as toxicity, low water solubility and poor bioavailability. Moreover, one of the most important advantages of nano-DDS is drug targeting, which may utilize physiology of a normal tissue or pathophysiological properties unique of an ill tissue to address the nano-DDS to a specific target (7,8).

1.2. Common Features of Targeting Drug Delivery Systems

In the design of a DDS it is useful to do a distinction among different types of targeting.

It is known that under certain circumstances (inflammation/hypoxia, first of all, which is typical for tumors, infarcts, and some other pathological sites in the body) the endothelial lining of the blood vessel wall becomes more permeable than in the normal state. As a result, in such areas, particles ranging from 10 to 500 nm in size, can leave the vascular bed and

accumulate inside the interstitial space. If these particles are loaded with a pharmaceutical agent, they can bring it into the area with the increased vascular permeability, and eventually release there the active drug. Such spontaneous accumulation or “passive” targeting, is currently known as enhanced permeability and retention (EPR) effect (9). In other words, high permeability of a damaged vasculature allows macromolecules and nanoparticles to enter the tumor interstitial space, while the compromised lymphatic filtration allows them to stay there. To follow this pathway, the ideal size of the nanocarrier is below 200 nm (10).

Differently from EPR, the nanocarrier delivery to particular locations within the body by targeting specific cell types is called “active” targeting. In other words, it consists in the attachment of ligands to the outer surface of nanoparticles that become able to specifically bind to target receptors present in certain sites such as cell surface or extracellular matrix. For instance, nanocarriers loaded with anticancer drugs can be modified with antibodies that target tumor-specific antigens or with ligands that bind to upregulated receptors present on tumor cells. This interaction induces an uptake by a receptor mediated endocytosis pathway in which plasma-membrane region containing the receptor-ligand complex undergoes endocytosis, becoming a transport vesicle (Fig. 1.1).

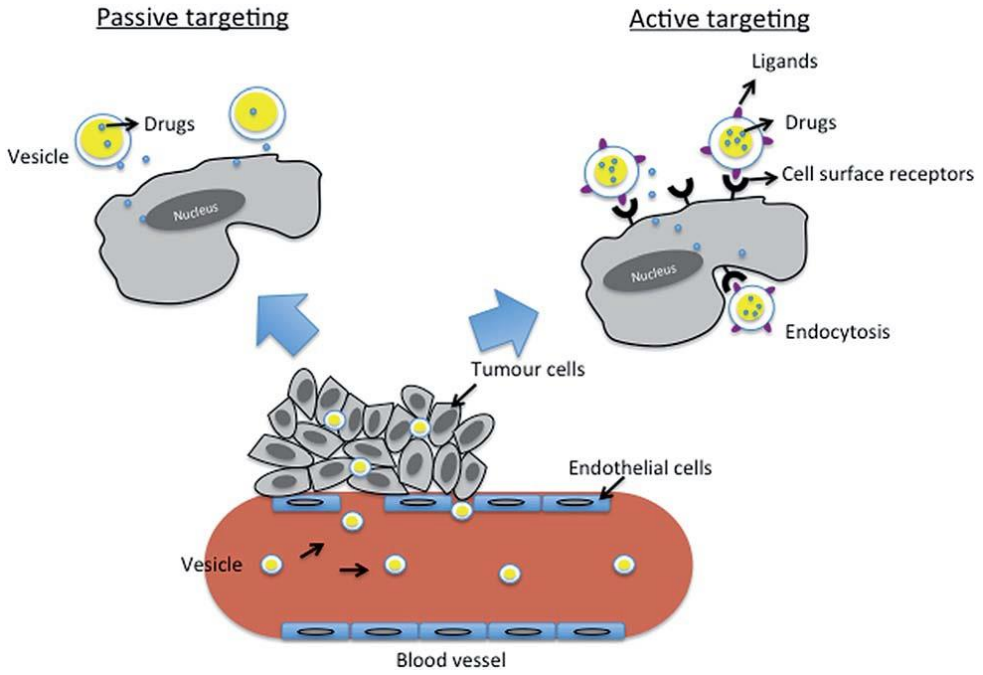

Figure 1.1 *Schematic representations of passive (left) and active (right) drug–tumor targeting. In passive delivery, vesicular nanoparticles extravasate through leaky vasculature, accumulate, and release the encapsulated drugs; whereas in active targeting delivery, ligands attached vesicles extravasated through leaky vasculature specifically bind to cancer surface cell receptors followed by receptor-mediated endocytosis. Drugs could be released either extracellularly, or intracellularly through endocytosis (adapted to ref. 10 and 11).*

The other approach for the delivery of nanoparticles is the use of small naturally derived peptides called cell penetrating peptides (CPPs) or protein transduction domains (PTDs) that cross cellular membranes efficiently. Very generally, CPPs are up to 30 amino acid amphiphilic peptides, which can be internalized by cells by mechanisms that require no energy and are receptor mediated or not. Historically, the first observation was made in

1988, by Frankel and Pabo, who showed that the transcription transactivating (Tat) protein of HIV-1 could enter cells and translocate into the nucleus (13). Subsequently, the group of Lebleu identified the minimal peptide sequence of Tat required for cellular uptake (47YGRKKRRQRRR57) (14). Ever since many other CPPs have been designed; among these the nineteen residues peptide, named gH625, identified as a membrane-perturbing domain in the glycoprotein gH of Herpes simplex virus type I, has attracted much interest (15). gH625, contributing to the merging of the viral envelope and the cellular membrane is able to traverse the membrane bilayer and transport a cargo into the cytoplasm. Although the mechanism of CPPs uptake into the cell is still under debate, this class of peptide is able to trigger the movement of various cargos into cells, including small molecules, peptides, proteins, DNA/RNA, nanocarriers, and other supramolecular aggregates. CPPs thus constitute a new class of potential drug delivery vectors.

Clearly, any type of targeting requires the drug delivery systems to be long-circulating in order to provide a sufficient level of accumulation in the target. Decoration of DDSs with poly(ethylene glycol) (PEG) chains is a well-known strategy to inhibit their clearance and allows them to stay in the blood for extended periods of time. PEG is a coiled polymer of repeating ethylene ether units with dynamic conformation. The movement of PEG chains conjugated on nanoparticles reduces the interaction with opsonin proteins and the subsequent association with macrophages (16). In this way PEGylated nanoparticles generally have an increased circulation time in blood stream with respect to the non-PEGylated nanoparticles (Fig. 1.2).

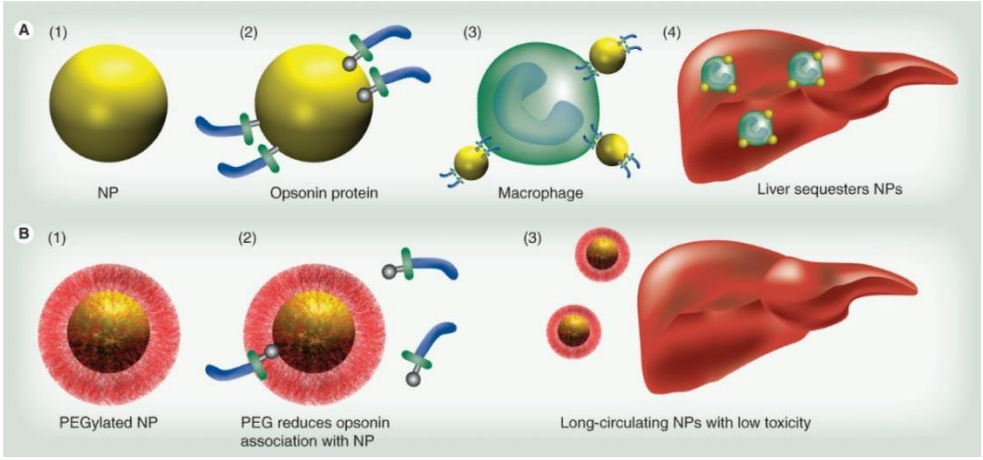

Figure 1.2 *Polyethylene glycol prevents uptake by the reticuloendothelial system (A). Nanoparticles (A1) are coated with opsonin proteins (A2) and associate with macrophages (A3) for transit to the liver (A4). Macrophages stationary in the liver, known as Kupffer cells, also participate in nanoparticle scavenging. (B) Nanoparticles coated with PEG (B1) prevents this opsonization (B2), resulting in decreased liver accumulation (B3) and increased availability of the NP in the blood steam (adapted to ref. 16).*

In this dissertation, we focused on the set up of PEGylated DDSs decorated with a CPPs as a model peptide, anyway simply removing the peptide or substituting it with a ligand of a specific cell-receptor it is possible to fit the nanocarrier respectively for passive or active targeting.

Regarding the composition, nanocarriers can be made of biocompatible and biodegradable materials such as synthetic proteins, peptides, lipids, polysaccharides, biodegradable polymers and fibers (18). Herein, we meanly focused on lipid-based nanoparticles, in particular on nanoemulsions, since the most of newly developed drugs are hydrophobic in nature (19).

1.3. Nanoemulsions

An emulsion is a biphasic system in which one phase is intimately dispersed in the other phase in the form of minute droplets generally ranging in diameter from 0.1 to 100 μm. The dispersed phase is also known as internal phase or discontinuous phase while the outer phase is called dispersion medium, external phase or continuous phase. The term ‘nanoemulsion’ refers to a mini-emulsion which is fine oil/water or water/oil dispersion stabilized by an interfacial film of surfactant molecule having droplet size in the range 20–500 nm. There are three types of nanoemulsions which can be formed: (a) oil in water nanoemulsion (O/W NE) in which oil is dispersed in the continuous aqueous phase, (b) water in oil nanoemulsion (W/O NE) in which water droplets are dispersed in the continuous oil phase, and (c) bi-continuous nanoemulsions. O/W NE can be suitable as the basis of many kinds of foods (e.g., milk, cream, beverages, dressings, etc.) (20), as well as cosmetics (lotions, transparent milks, and crystal-clear gels) (21). Further, their ability to dissolve large quantities of hydrophobics and protect their cargo from hydrolysis and enzymatic degradation makes O/W NEs ideal vehicles for the purpose of drug delivery. Digestible oils such as soybean oil, sesame seed oil, cottonseed oil and safflower oil are often used to prepare O/W NEs where to dissolve the lipophilic drugs. An O/W NE is generally produced by homogenizing oil and water together in the presence of an emulsifier that rapidly adsorbs to the surface of oil droplets during homogenization improving the NE stability (22). A vigorous blending of only oil and water may yield a crude temporary emulsion, which upon standing, will separate in two distinct phases due to the coalescence of the

dispersed globules, whereas the presence of an emulsifier makes the nanoemulsion a stable system. An emulsion formed by small anionic droplets coated with a layer of emulsifier is called primary emulsion (Fig. 1.3).

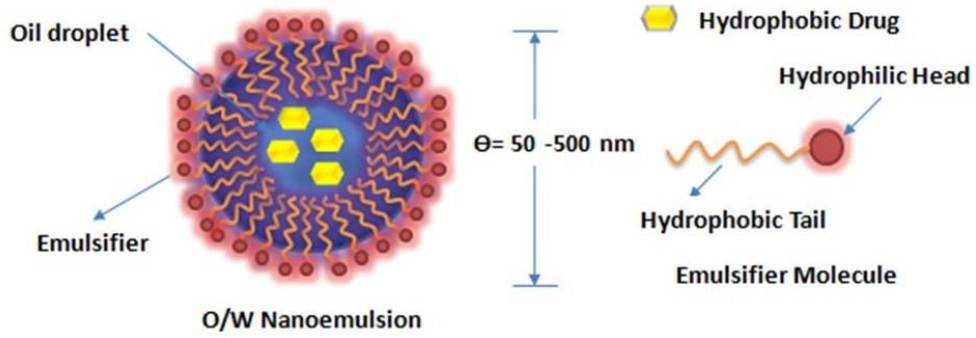

Figure 1.3 *Illustration of an oil in water nanoemulsion stabilized by an emulsifier molecule (primary nanoemulsion) (adapted to ref 23).*

However, even though stabilized by the use of emulsifiers, emulsions do not typically have a sufficiently long shelf life and they present destabilization mechanisms such as creaming, sedimentation, coalescence and Ostwald ripening (24). The combination of lipids and polyelectrolytes is often used as a facile method to optimize the physicochemical properties of nanoemulsions; an example is represented by SNEs. A secondary emulsion is formed by a primary emulsion coated with a layer of a polyelectrolyte that is produced by adding the polymer to the primary emulsion. The electrical charge on the droplets increases from negative to positive when the polyelectrolyte is added to the emulsion indicating that the polymer is

adsorbed to the droplet surface. It has been shown that the stability, to avoid the aggregation of lecithin-coated emulsion droplets induced by thermal processing, freeze-thaw cycling and high calcium ion contents, can be improved by coating the droplets with a polyelectrolyte (25-26). Layer by layer methodology is one of the most common strategies used to obtain thin polymeric films around O/W NEs.

1.4. Layer by Layer Methodology Applied to Multilayered Polymer Nanoemulsions

Layer by layer technique is based on the sequential adsorption of oppositely charged polyelectrolytes on a charged substrate. This technique was firstly proposed by Iler in 1966 for the alternate assembly of oppositely charged layers of colloidal particles (27). The same concept was adapted 25 years later by Decher and co-workers that reported the fabrication of multicomposite films of charged materials through LbL adsorption from aqueous solutions (28). Since then, extensive work has been carried out on the application of this technique to the fabrication of ultrathin films on surfaces of any size and shape, ranging from flat surfaces to round template particles (29). A significant step for the preparation of polyelectrolyte nanocapsules was done by Sukhorukov et al. in 1998 that fabricated hollow capsules by layer-by-layer assembly of polyelectrolyte film–coated colloidal particles and subsequent removal of the colloidal core (30). Further, in recent years LbL adsorption of polyelectrolytes has resulted also a convenient method of formation of a shell at emulsion cores which is

designed to incorporate lipophilic drugs (31). The polymeric coating can be used to regulate the release rate of encapsulated active components in the nanoemulsion (32). Moreover, the shell can be easily functionalized to reduce the interactions between the capsules and the immune system (PEGylation for ‘‘stealth effect’’) and to immobilize target specific ligands for intelligent delivery systems. This chemistry uses a series of layer-by-layer deposition steps of oppositely charged polyelectrolytes (33). The first step starts with colloidal particles carrying surface charges (e.g., a negative surface charge). Polyelectrolyte molecules having the opposite charge (i.e., polycations) are readily adsorbed to such a surface due to electrostatic interactions. Not all of the ionic groups of the adsorbed polyelectrolyte are consumed by the electrostatic interactions with the surface. As a result, the surface charge of the coated particle changes its sign and is now available for the adsorption of a polyelectrolyte of again opposite charge (i.e., a polyanion) (Fig. 1.4).

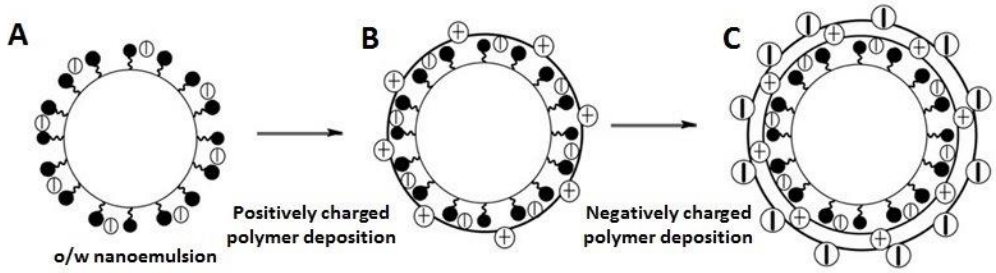

Figure 1.4 *Schematic representation of LbL methodology applied on O/W NE. O/W NE results negatively charged due to the surfactant adsorbed on its surface (A). A positively charged polymer is added to the nanoemulsion solution determining the formation of a polymer coating around the oil droplets and a switch of charge of the colloidal system (B). A negatively charged polymer is added in order to create a second polymeric layer and provide a negative charge to the LbL O/W NE (adapted from ref. 33).*

The use of LbL assembly has a number of advantages. For example, LbL assembly can be performed in entirely aqueous solutions, requiring no exposure to organic solvents. This is important for biomolecules such as nucleic acids and proteins, which have limited solubility in non-aqueous solutions and are susceptible to denaturation. The size and shape of the capsules can be engineered by simply altering the template used for polymer adsorption. A large range of polymers can be used to prepare the capsule wall, resulting in the ability to finely tune the composition, permeability, stability, and surface functionality of the capsules. The assembly process is relatively cheap, requiring only simple laboratory equipment, and can be performed with inexpensive materials. For these reasons, LbL assembly is considered a promising method for the creation of efficient therapeutic delivery devices (35).

Herein we showed how Isothermal Titration Calorimetry is able to provide important information related to the LbL assembly on O/W NEs, and the subsequent attachment of the nanocapsules to macromolecules.

1.5. Isothermal Titration Calorimetry in Nanotechnology

Isothermal titration calorimetry (ITC) is a valuable method aimed at characterizing the energetics of molecular interactions evaluating the heat absorbed or released upon molecular interactions, at constant temperature and pressure (36). ITC is able to provide the complete thermodynamic profile (i.e., binding constant (K_b), enthalpy change (ΔH), entropy change (ΔS), Gibbs energy change (ΔG)) and the stoichiometry of interaction in a single experiment. In Fig. 1.5, it is represented a schematic illustration of a typical ITC instrument. Since this methodology has the ability to determine the different energetic contributions to the binding affinity without introduction of labels on the ligands, it can be considered the technique of choice for the study of complex systems where the use of a label may introduce artifacts. So far, ITC has been widely used to study molecular interactions in biological systems (e.i. protein-protein, DNA-DNA, protein-DNA), anyway in recent years it has shown great potential in nanotechnology field (37) where it has been proved to be a useful tool to study the energetic of assembly of polymeric nanoparticles giving information on the thermodynamic signature of the nanodevice formation. Further, calorimetric analysis of nanoparticles is a growing field due to

ready availability of the instrumentation in core facilities and reduced sample requirements of modern calorimeters. In particular, ITC resulted extremely important to find the optimal conditions of polymer coating around a nanotemplate. In particular, Mertins and Dimova thermodynamically characterized the interaction of chitosan with small liposomes and the organization of the polysaccharide on the membrane of the vesicles. ITC was particularly important in this study for assaying the enthalpy changes arising from binding of the positively ionized chitosan to neutral and negatively charged liposomes. The equilibrium constant, the interaction stoichiometry, and the molar enthalpy of binding chitosan monomers to phospholipids from the external leaflet of the vesicle membrane were obtained from the isotherm curves (38). Further, ITC has resulted a valuable methodology to quantify the energetics of interactions of nanoparticles with proteins or nucleic acids. For instance, Mosquera et al. performed ITC experiments to understand association efficiency and loading capacity of insulin into the polymeric nanoparticles under different pH conditions and achieve the best NP system capable to simultaneously modulate and control the insulin delivery in order to favor the best sustained protein release (39).

In this dissertation it will be illustrated how ITC can be extremely important in the build-up of a nanocarrier both to find the optimal conditions of polymer coating around the nanoemulsion and to gain information about the interaction between the oil in water secondary nanoemulsion and a protein. In the first case, we performed a complete physicochemical characterization to identify polymer concentration domains that are thermodynamically stable and to define the degree of stability through thermodynamic functions

depending upon relevant parameters affecting the stability itself, such as type of polymer coating, droplet distance, etc. This is very important to prolong the shelf life of products and make them suitable for a variety of applications ranging from nutraceutics to cosmetics and pharmaceutics. In the second case, we studied the interaction between the streptavidin and a polylysine secondary nanoemulsion functionalized with biotin. In this way with a simple calorimetric titration we gained information about the amount of functionalizable groups exposed on the nanoparticle surface.

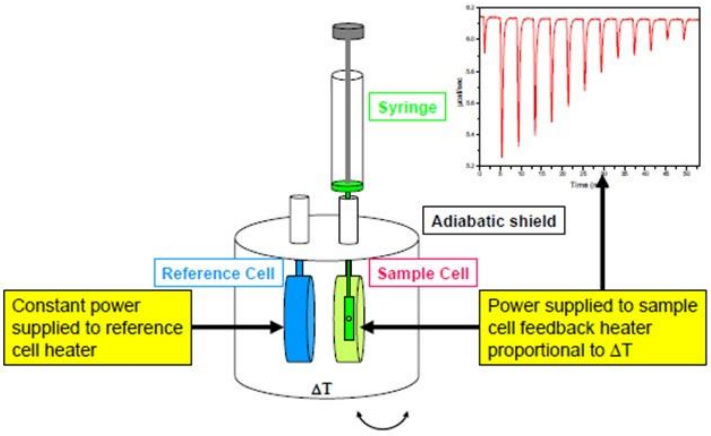

Figure 1.5 *Illustration of an ITC instrument. A typical ITC instrument consists of two equivalent cells positioned in an adiabatic jacket. The temperature of each cell is monitored and maintained at a constant temperature through an electronic feedback loop that controls thermoelectric heaters located near each cell. During the experiment the titrant, which is in the injection syringe, is added to the sample cell. If the reaction is exothermic, heat evolves and the temperature of the sample cell increases. The feedback loop responds by reducing the power to the resistive heater around the sample cell to restore the differential*

temperature between the cells to zero. This mechanism gives rise to a power versus time curve with more positive peaks at the beginning and gradual decrease of them. At saturation when no reaction is taking place, the baseline reproduces a constant power consumption proportional to the power needed to maintain the difference in temperature between the cell and the adiabatic jacket. Small peaks are still observed due to effects such as buffer dilution. On the contrary, an endothermic reaction shows negative initial peaks that gradually become more positive. The area under each peak represent the heat involved in the reaction, the integration, subtraction of background areas and normalization for injected moles of titrant, gives the enthalpy involved in the process as a function of the ratio between titrant and titrate concentrations. The total differential enthalpy results negative in exothermic reactions and positive for endothermic reactions (40).

1.6. Thesis Purpose

The first purpose of this thesis was to synthetize and characterize, from a thermodynamic point of view, O/W SNEs in order to obtain all the information needed to prolong the shelf life of the product. A new method based on Isothermal Titration Calorimetry was used to define the degree of stability depending upon relevant parameters affecting the stability itself, such as type of polymer coating and droplet distance. The second purpose was to decorate O/W SNEs with PEG chains and with a cell penetrating peptide in order to improve respectively its circulating time in blood stream and capability to cross an endothelial cell layer. Biological tests were conducted on the decorated O/W SNE showing a better transcytosis through an endothelial barrier and most importantly a much higher accumulation in

the endothelial barrier as compared with the non-decorated counterpart. The last aim of this thesis was to set up a new method able to quantify the amount of a specific receptor on the cells surface in order to identify targets, to address drug design and selectively deliver therapeutics. In this regards, ITC measurements coupled with confluent cell layers cultured around biocompatible templating microparticles were conducted to evaluate the number of transferrin receptors (TfRs) onto the cell membrane and study the energetics of their interaction with the transferrin.

References

1) Safari, J.; Zarnegar, Z. *Advanced drug delivery systems: Nanotechnology of health design A review*. Journal of Saudi Chemical Society. 2014, 18, 85–99
2) Feynman, R. *There is planty of room at the bottom*. Engineering and science 1960.
3) des Rieuxa, A.; Fieveza, V.; Garinota, M.; Schneiderb, Y. Véronique Préat. *Nanoparticles as potential oral delivery systems of proteins and vaccines: a mechanistic approach.* J Control Release. 2006;116(1):1–27.
4) Qiu, Y., Park, K. *Environment-sensitive hydrogels for drug delivery*. Adv. Drug Deliv. Rev. 2012, 64, 49-60.
5) Etheridge, M.L.; Campbell, S.A.; Erdman, A.G.; Haynes, C.L.; Wolf, S.M.; McCullough, J. *The Big Picture on Nanomedicine: the state of investigational and approved nanomedicine products*. Nanomedicine. 2013, 9, 1−14.
6) Sonke, S. *Clinical translation of nanomedicines*. Current Opinion in Solid State and Materials Science. 2012, 16, 287-294.
7) Sonke Svenson, Yuanzeng Min, Joseph M. Caster, Michael J. Eblan, and Andrew Z. Wang.
8) Moghimi, S.M.; Hunter, A.C.; Murray, J.C. *Nanomedicine: current status and future prospects*. FASEB J. 2005, 19, 311-330.
9) Markman, J. L.; Rekechenetskiy, A.; Holler, E.; Julia Y. Ljubimova, J. Y. *Nanomedicine therapeutic approaches to overcome cancer drug resistance*. Adv Drug Deliv Rev. 2013, 65: 1866-79.

10) Gaumet, M.; Vargas, A.; Gurny R.; Delie, F. *Nanoparticles for drug delivery: the need for precision in reporting particle size parameters*. Eur. J. Pharm. Biopharm., 2008, 69, 1.

11) Maeda, H.; Wu, J.; Sawa, T.; Matsumura, Y.; Hori, K. *Tumor vascular permeability and the EPR effect in macromolecular therapeutics: a review*, J. Control. Release. 2000, 65, 271–284.

12) Salim, M.; Minamikawa, H.; Sugimurab, A.; Hashim, R. *Amphiphilic designer nano-carriers for controlled release: from drug delivery to diagnostics*. Med. Chem. Commun. 2014,5, 1602-1618.

13) Peer, D.; Karp, J.M.; Hong, S.; Farokhzad, O.C.; Margalit, R.; Langer, R. *Nanocarriers as an emerging platform for cancer therapy*. Nature Nanotechnology. 2007, 751 – 760.

14) Frankel, A.D.; Pabo, C.O. (1988). *Cellular uptake of the tat protein from human immunodeficiency virus*. Cell. 1988, 55(6):1189-93.

15) Vivès, E.; Schmidt, J.; Pèlegrin, A. *Cell-penetrating and cell-targeting peptides in drug delivery*. Biochim, 2008, 1786(2):126-38.

16) Galdiero, S.; Falanga, A.; Vitiello M.; , Browne, H.; Pedone, C.; Galdiero, M. *Fusogenic domains in herpes simplex virus type 1 glycoprotein H.* J. Biol. Chem. 2005 , 280 , 28632-43.

17) Moril, A.; Klibanov, A. L.; Torchilin, V.P.; and Huangl, L. *Influence of the steric barrier activity of amphipathic poly(ethyleneglyco1 and ganglioside GM, on the circulation time of liposomes and on the target binding of immunoliposomes in vivo*. FEBS letters. 1991, 284, 263-266.

18) Zhao, L.; Seth, A.; Wibowo, N.; Zhao, C.; Neena, M.; Chengzhong Yu, C.; Anton, P.J. Middelberg. *Nanoparticle vaccines.* Vaccine. 2014, 32, 327–337.

19) Narvekar, M.; Xue, H. Y.; Eoh, J. Y.; Wong, H. L. *Nanocarrier for Poorly Water-Soluble Anticancer Drugs—Barriers of Translation and solutions.* AAPS PharmSciTech. 2014, 15(4): 822–833.

20) Puri, A.; Loomis, K.; Smith, B.; Lee, J. H.; Yavlovich, A.; Heldman, E.; Blumenthal, R. *Lipid-Based Nanoparticles as Pharmaceutical Drug Carriers: From Concepts to Clinic*. Crit Rev Ther Drug Carrier Syst. 2009, 26(6): 523–580.

21) Brusewitz, C.; Schendler, A.; Funke, A.; Wagner, T.; Lipp, R. *Novel poloxamer-based nanoemulsions to enhance the intestinal absorption of active compound*s. Int. J. Pharm. 2007, 329(1-2):173-81.

22) Jaiswal, M.; Dudhe, R.; Sharma, P. K *Nanoemulsion: an advanced mode of drug delivery system*. Biotech. 2015, 5, 123-127.

23) Patravale, V. B.; Mandawgade, S. D. *Novel cosmetic delivery systems: an application update*. Int. J. Cosmet. Sci. 2008; 30(1), 19-33.

24) Kendall, G. What is Pharmaceutical Nanoemulsion? University of Nottingham. 2013.

25) Chique, K. R.; Puertas, A .M.; Romero-Cano, M. S.; Rojas, C.; Urbina-Villalba, G. *Nanoemulsion stability: experimental evaluation of the flocculation rate from turbidity measurements*. Advances in Colloid and Interface Science. 2012, 178, 1–20.

26) Ogawa, S.; Decker, E. A.; McClements, D. J. *Influence of environmental conditions on the stability of oil in water emulsions containing droplets stabilized by lecithin–chitosan membranes*. J Agric Food Chem. 2003;51:5522–7.

27) Guzey, D.; McClements, D. J. *Influence of environmental stresses on O/W emulsions stabilized by beta-lactoglobulin–pectin and beta-lactoglobulin– pectin–chitosan membranes produced by the electrostatic layer by layer deposition technique*. Food Biophys. 2006;1:30–40.

28) . Iler, R. K. *Multilayers of colloidal particles.* Journal of Colloids and Interface Science. 1966, 21, 569-594.

29) Voigt, A.; Buske, N.; Sukhorukov, G. B.; Antipov, A. A.; Leporatti, S.; Lichtenfeld, H.; Bäumler, H.; Donath, E.; Möhwald, H. *Novel polyelectrolyte multilayer micro- and nanocapsules as magnetic carriers*. Journal of Magnetism and Magnetic Materials. 2001, 1–2, 59–66.
30) A.T. Hubbard (Ed.), Encyclopedia of Surface and Colloid Science, Marcel Dekker, New York, 2002 (Chapter 3).
31) Sukhorukov, G. B.; Donath, E.; Davis, S.; Heinz Lichtenfeld, Caruso, F.; Popov, V. I.; Möhwald, H.. *Stepwise polyelectrolyte assembly on particle surfaces: a novel approach to colloid design*. Polymers for Advanced Technologies. 1998, 9, 10-11, 759-767.
32) Preetz, C.; Rübe, A.; Reiche, I.; Hause, G.; Mäder, K. *Preparation and characterization of biocompatible oil-loaded polyelectrolyte nanocapsules*. Nanomedicine. 2008, 4(2):106-14.
33) Formation of Biocompatible *Nanocapsules with Emulsion Core and Pegylated Shell by Polyelectrolyte Multilayer Adsorption*. Langmuir. 2010, 26 (15), 12592–12597.
34) Donath, E.; Sukhorukov, B.; Caruso, F.; Davis S. A.; Möhwald, H. *Novel Hollow Polymer Shells by Colloid-Templated Assembly of Polyelectrolytes* Angewandte Chemie., 1998, 37, 2201-2205.
35) Johnston, A. P.R.; Cortez, C.; Angelatos, A. S.; Caruso, F. *Layer-by-layer engineered capsules and their applications.* Current Opinion in Colloid & Interface Science. 2006, 11, 203.
36) Ladbury, J. E.; Doyle, M. L. Biocalorimetry 2: Applications of Calorimetry in the Biological Sciences; John Wiley & Sons: Chichester, West Sussex, England, 2004.
37) Robert, J.; Falconera and Brett M. *Collins Survey of the year 2009: applications of isothermal titration calorimetry*. Molecular recognition. 2010, 24:1-16.
38) Mertins O.; Dimova R. *Binding of Chitosan to Phospholipid Vesicles Studied with Isothermal Titration Calorimetry*. Langmuir. 2011;27:5506-15.
39) Robles E.; Villar E.; Alatorre-Meda M.; Burboa M. G.; Valdez M. A.; Taboada P.; Mosquera V. *Effects of the Hydrophobization on Chitosan–Insulin Nanoparticles Obtained by an Alkylation Reaction on Chitosan*. J. Appl. Polym. Sci. 2013;129,822–34.
40) Giancola, C.; Fotticchia, I.; Fotticcchia, T.; Mattia, C. A. *Chitosan-based Nanoparticles Studied by Isothermal Titration Calorimetry*. Journal of Thermal Analysis and Calorimetry, 2015, 1-9.

CHAPTER 2 Thermodynamic Signature of Secondary Nanoemulsion by Isothermal Titration Calorimetry

2.1.Introduction

Oil in water nano-emulsions (O/W NEs) are being increasingly investigated for their ability to dissolve large quantities of hydrophobic compounds and protect their cargo from hydrolysis and enzymatic degradation, therefore improving hydrophobic drug bioavailability. This makes O/W NEs ideal vehicles for the purpose of drug delivery (1−6). Moreover, these colloidal systems can be used as multifunctional platforms, allowing for the cancer-research-related field to benefit from simultaneous imaging and targeted drug delivery (7−9). In addition, O/W NEs can be suitable for gene therapy (10) and as the basis of many kinds of foods (e.g., milk, cream, beverages, dressings, etc.) (11,12), as well as cosmetics (lotions, transparent milks, and crystal-clear gel) (13−17). The main limitation of O/W NEs is their poor stability over time because they are thermodynamically unstable systems (18). One strategy to improve emulsion stability, proposed by McClements and his group, is to produce secondary emulsions obtained with a polyelectrolyte thin layer, adsorbed through the interaction with an ionic emulsifier of opposite charge standing on the surface of the starting primary emulsion (19). When the polymer concentration is varied, it is possible to control the level of polymer coating and obtain O/W NEs with increasing stability before the occurrence of another mechanism of aggregation, the so-

called depletion flocculation. However, at the moment, emulsion stability is only evaluated experimentally or based on theoretical considerations that determine the level of coating. No methods have been proposed up to now to evaluate the stability of secondary nano-emulsions from a thermodynamic point of view, therefore precluding the possibility to correctly assess the stability of such a system. Herein, we use isothermal titration calorimetry (ITC) to study the evolution of the polymer deposition around primary nano-emulsions and obtained novel results regarding thermodynamic stability domains. Thus far, ITC has been widely used to study molecular interactions in biological systems and only in a few cases applied to nanosystems (20−26). Particularly, Mertins and Dimova employed ITC to observe the interaction of chitosan with zwitterionic liposomes organized in vesicles. They described the thermodynamic parameters of the overall adsorption process by a single binding event; the liposome aggregation was mainly detected by dynamic light scattering (DLS) measurements. In our study, for the first time, we investigated in depth the binding between a primary nanoemulsion and a polyelectrolyte using a state-of-the-art nano-ITC technique, gaining information on the thermodynamic signature of two well-defined adsorption events. A third event was also detected by ITC and attributed to an aggregation phenomenon. Polyelectrolytes of two different classes were chosen to explore the validity of our approach: chitosan, a polysaccharide, and poly-L-lysine, a polypeptide. ITC provided useful information on the strength of the adsorption in terms of thermodynamic functions, for both systems. In addition, for what concerns the level of polymer coating around primary emulsions, we showed herein that, after a first saturation, a complete coating of the droplets is only possible at much

higher concentrations; the saturation method, conversely, is based on ζ-potential measurements and provides the saturation condition by identifying the ζ-potential plateau (27). The two distinct events were completely characterized and quantified in terms of thermodynamic parameters. For this purpose, two different sets of ITC measurements were designed ad hoc. The precise evaluation of the level of polymer coating around primary emulsions is very useful when the emulsion has to be used as a template for the preparation, via layer by layer, of polymer nanocapsules, very promising as multifunctional nanocarriers in nanomedicine (27−29). Further, the ITC enabled a clear understanding of when the flocculation starts, allowing for the achievement of the best conditions for an optimal coating.

2.2.Materials and Methods

2.2.1. Sample Preparation

Chitosan low molecular weight [CT-LMW, 127 kDa, degree of deacetylation (DD) = 84%] and poly-L-lysine (PLL, 4−19 kDa) were purchased from Sigma-Aldrich. Chitosan solution was prepared dissolving 10 mg in 1 ml of 0.1 M acetic acid solution (pH 3) by vigorous stirring overnight; the obtained solution was then filtrated. Chitosan solutions at different concentrations were obtained diluting the bulk solution with 0.1 M acetic acid solution at pH 4 to be able to dissolve chitosan; PLL solutions were prepared by dissolving 50 mg in 1 ml of Milli-Q water (final pH 6.0).

First, a 10 wt % oil in water pre-emulsion was prepared by dissolving the surfactant (egg lecithin) in the oil phase (soybean), stirring the sample for 40 min at 60 °C and 180 revolutions per minute (rpm) speed, and then performing sonication runs of 10 s for 1 min at 60% of the sonication amplitude. Then, the oil phase was added to the aqueous phase, 5 mL at a time, and mixed using an immersion sonicator with runs of 10 s for 8 min. The pre-emulsion was finally homogenized for 3 single cycles and 200 steps at a pressure of 1330 bar by a high-pressure homogenizer (110P series microfluidizer) to obtain the final nano-emulsion (180−200 nm, ∼−30 mV, pH 4.3). Soybean oil and fat-free egg lecithin with 80 wt % phosphatidylcholine (Lipoid E80) were purchased from Lipoid. In some preparations, we needed higher oil concentrations; therefore, we also prepared a O/W NE at a concentration of 20 wt % (2000 bar), keeping the same lecithin/oil ratio to obtain about the same size. All of the steps of the process were the same as described for the 10 wt % O/W NE. The first positively charged layer of polymer (chitosan or PLL) was obtained by adding in one shot the polymer solution to the emulsion solution under vigorous stirring (1500 rpm). The second layer was obtained in the same way by adding the negatively charged polymer to the positively charged secondary nano-emulsion.

2.2.2. ζ-Potential Measurements.

ζ-Potential titration experiments were performed by a Malvern Zetasizer. In this technique, a voltage gradient is applied across a pair of electrodes of the cell containing the particle dispersion. Charged particles are attracted to the oppositely charged electrode, and their velocity can be measured and expressed in unit field strength as an electrophoretic mobility. ζ-potential is the electrostatic potential that exists at the interface of the nanoparticle, which is related to both the surface charge and the local environment of the particle. It was automatically calculated from the electrophoretic mobility based on the Smoluchowski equation, $\nu = (\varepsilon E/\eta)\zeta$, where ν is the measured electrophoretic velocity, η is the viscosity, ε is the electrical permittivity of the electrolytic solution, and E is the electrical field. In these titration experiments, different samples were prepared varying the concentration of chitosan or PLL in water, expressed as a weight/weight percent, from 0 to 0.020 wt % and keeping constant the weight/weight percent O/W NE at 1 wt %. Before each experiment, 50 μl aliquots were withdrawn from each sample and diluted 1:40 (v/v) with 20 mM acetic acid solution at pH 4 for chitosan-based secondary nano-emulsions or Milli-Q water at pH 6 for PLL-based secondary nano-emulsions. The diluted samples were poured into disposable cells, and the ζ-potential was determined at least 3 times for each sample. Measurements were recorded at 25 °C. ζ-potential values were plotted as a function of the weight ratio between polymer (chitosan or PLL) and O/W NE. Each titration experiment was performed 3 times; the errors on ζ-potential values were calculated on three measurements.

2.2.3. Nano-emulsion Size Measurements

Nano-emulsion size measurements were also performed by a Malvern Zetasizer. In particular, the particle size distribution was measured by laser DLS (λ= 632.8 nm). This technique correlates the fluctuations of scattered light intensity I(t) during time with the Brownian motion of colloidal particles associated with the diffusion coefficient D, which is related to the hydrodynamic radius Rh of the particles. A detecting angle of 173° was used. All samples were diluted up to a droplet concentration of approximately 0.025 wt % using Milli-Q water in the case of primary emulsions; PLL-based secondary emulsions and an acetic acid Milli-Q water solution (pH 4, 20 mM) were used in the case of chitosan-based secondary emulsions. A default refractive index ratio (1.52) and three measurements of 5 runs (1 run lasting 100 s) were used in the calculations of the particle size distribution.

2.2.4. Isothermal Titration Calorimetry

ITC experiments were performed using a nano-ITC low volume calorimeter (TA Instruments) equipped with a reference and sample cell of 170 μl. All titrations were carried out at 25 °C using a 50 μl syringe at a stirring rate of 250 rpm. The sample cell was always filled with the O/W NE, and the reference cell was always filled with Milli-Q water. All solutions were degassed for 5 min before starting the experiments to eliminate air bubbles. The pH of each solution was monitored before experiments to ensure the

same values in the cell and in the syringe. The pH was adjusted when required. Two sets of ITC experiments were performed. In the first set, the titration experiments were performed by a single injection of 50 μl of chitosan at a concentration from 0.01 to 0.08 wt % or PLL at a concentration from 0.01 to 0.06 wt % into the reaction cell filled with 1.34 wt % O/W NE to have a final emulsion concentration of 1 wt %. The relative amount of polymer and nano-emulsion was expressed in terms of the ratio (R) between the concentration of chitosan or PLL and the concentration of nano-emulsion, both expressed as a weight percentage. The comparisons between the two polymers were made in the R range between 0.003 and 0.018. The heat released for each injection was evaluated over 1200 s. In the second set, higher values of R (between 0.018 and 0.27) were evaluated by stepwise titration experiments with 25 aliquots of 2 μl of chitosan or PLL solution at 1 wt % injected with 200 s intervals into the working cell filled with 1.1 wt % O/W NE, to link the last concentration of the single-injection experiment with the first concentration of the stepwise titration experiment. The time interval between two consecutive injections was chosen to reach the thermodynamic equilibrium before the next injection. In the case of PLL, the same experiments were also conducted at two more different concentrations of nano-emulsion (~5 and ~10 wt %). In particular, single-injection titration experiments were conducted by injecting 50 μl of PLL from 0.044 up to 0.33 wt % into the reaction cell filled with 6.5 wt % O/W NE or injecting 50 μl of PLL from 0.088 up to 0.79 wt % into the reaction cell filled with 13 wt % O/W NE, depending upon the final concentration of nanoemulsion (5 and 10 wt %, respectively). The heat released for each injection was evaluated over 1200 s. Ratios between 0.003

and 0.019. were explored, and then higher values of R were evaluated by injecting stepwise 25 aliquots of 2 μl of 2.5 or 5 wt % PLL solution, with 200 s intervals, into the working cell filled with 5.1 or 10.2 wt % O/W NE, respectively. Heat produced by chitosan or PLL dilution was evaluated by performing a control experiment, titrating each polymer into the buffer alone. The interaction heat for each injection was calculated after correction for the heat coming from polymer dilution. The resulting corrected injection heats were plotted as a function of the weight ratio between polymer and O/W NE concentrations, fitted with a model for one set of binding sites and analyzed with a nonlinear least-squares minimization algorithm, using the program NanoAnalyze software, version 2.4.1 (TA Instruments). ΔbH° (binding enthalpy change in kJ mol−1), Kb (binding constant in M−1), and stoichiometry (N = binding sites, calculated at the inflection point as the ratio between polymer and O/W NE concentrations) were the fitting parameters. The Gibbs energy and entropy change contributions were calculated using the relationships:

$\Delta_b G° = -RT \ln K_b$, (R = 8.314 J mol^{-1} K^{-1}, and T = 298 K)

$T\Delta_b S° = \Delta_b H° - \Delta_b G°$.

The errors on the heat of the single titration experiments were calculated on the average of three measurements. The errors on thermodynamic parameters K_b, $\Delta_b H°$, and stoichiometry were based on the percentage of confidence of the fitting procedure, and the errors on $\Delta_b S°$ and $\Delta_b G°$ were derived by the theory of error propagation.

2.3.Results and Discussion

Polymer coatings around primary emulsions are typically studied by measuring the ζ-potential. In particular, there is a switch in the ζ-potential of the colloidal system when the polymer is added a little at a time. A plateau in the ζ-potential is associated with the saturation of the surface by means of the polymer coating. We performed the ζ-potential as a reference analysis; to gain a deeper insight in the stoichiometry of layer by- layer interactions and to analyze the energetics of nanoparticle assembly, we carried out ITC experiments. The methodology is based on the measurement of the heat absorbed or released following titration through injecting a solution of one of the interacting molecules (the ligand) into a cell containing a solution of the other molecule (a macromolecule).

2.3.1. ζ-Potential Analysis

The ζ-potential of the O/W NE was negative (ζ = −35.4 mV) in the absence of chitosan, which can be attributed to the presence of charged carboxylic acid groups along the lecithin chain. When the chitosan concentration is increased, the ζ-potential initially became increasingly less negative, with a point of zero charge at around 0.00023 wt % chitosan, and reached a plateau for higher concentrations (Fig. 2.1A). The saturation ratio was reached at around 0.01 wt %. In the case of PLL, the same emulsion formulation was used (ζ = −31.2 mV). The point of zero charge was reached at around

0.0011 wt %, with the saturation concentration at around 0.01 wt % (Fig. 2.1B). However, no indications about the affinity between polymers and primary emulsion can be registered through the ζ-potential analysis. Moreover, because the ζ-potential is highly sensitive to the environmental conditions, slight differences in the ion concentration can affect measurements, which are typically scattered, making it difficult to assess the concentration at which the plateau is reached.

2.3.2. Isothermal Titration Calorimetry Analysis

The switching of the charge after polymer addition to the primary emulsion can be attributed to chitosan or PLL adsorbed on negatively charged oil nanodroplets, giving rise to secondary emulsions, whose stability is reached at well-defined values of ζ-potential, where the plateau starts. An understanding of the forces driving the self-assembly at the interface requires a comprehensive account of the thermodynamic parameters (ΔH° and ΔS°). Here, we employed ITC to measure the equilibrium adsorption constant, enthalpy of adsorption, and adsorption stoichiometry. The ITC measurements show that a more complex interaction than just electrostatic interaction occurs for both systems and gives information on the stoichiometry and affinity constant as well as enthalpy changes in the interacting molecules. In particular, the ITC analysis allowed for the identification of two binding events, followed by an aggregation event. The two binding events were not completely resolved in a single titration

experiment, which comprise two significantly different ratios of concentrations. Thus, to better characterize and separate these different binding events, two sets of experiments were designed, as described in the Materials and Methods. Briefly, in the first experiment, a set of single injections was accomplished in the range of R values of 0.003− 0.018; in the second experiment, a typical titration experiment was performed in the range of R values between 0.018 and 0.27. Panels C and D of Fig. 2.1 and Fig. 2.2 are thermograms for the binding of chitosan or PLL to the O/W NE at 25 °C, along with the integrated heats and the corresponding best fit binding models for each system. The thermodynamic data are collected in Table 2.1. The binding constants are always higher for the first event with respect to the second event; in the case of PLL, the affinity is stronger than that of chitosan. Table 2.1 shows that the I event is characterized by an exothermic binding and ΔH° values are smaller for chitosan and greater for PLL. The II event is almost athermic in the case of chitosan and exothermic for PLL, with a low ΔH° value. In both systems, the binding is accomplished by a favorable ΔS°, indicating that both the I and II events are entropically driven.

The thermodynamic signatures are shown in Fig. 2.3. The first event can be mainly attributed to the predominant electrostatic interactions between the negative charges of the nano-emulsion and the positive charges of chitosan or PLL. This event, as already seen, is characterized by a favourable enthalpic contribution, higher for PLL/nano-emulsion interactions. In any case, the binding is also entropically favoured, probably because of the release of ordered water by the hydration shells around the positive and negative charges in disordered bulk water as well as counterion release after

the binding process (30,31). The second binding event may involve both the backbone and the charged groups of the molecules; the resulting low values of the enthalpy reflect the balance of different endothermic and exothermic contributions. However, the binding is entropically driven also for this second event, and the conformational rearrangements of chitosan or PLL chains play a fundamental role in the overall energetic balance, together with the counterion release and the water molecules of solvation released to the bulk water. The entropic gain consequent to a polyelectrolyte deposition has already been reported in the literature (25,32,33). The two binding events are followed by a third event, which is due to an aggregation phenomenon centred at about N = 0.2 for both chitosan (Fig. 2.2C and Table 2.1) and PLL (Fig. 2.2D and Table 2.1). This third event is characterized by an endothermic enthalpy change and is attributed to a depletion flocculation, which was already described as entropically favorable but enthalpically unfavourable (34). The classic interpretation in terms of an entropydriven phenomenon is based on the Asakura−Oosawa model that describes the interaction energy on the basis of geometric analysis (35,36). The model assumes that two spherical participles are dispersed in a solution of rigid spherical polymer coils. The theory predicts that the addition of a small amount of polymer to a sterically stabilized nano-emulsion can lead to flocculation. The Gibbs energy is then calculated on the simplified approach for hard-sphere models. In particular, the increase in the entropy of the system is explained in terms of excluded volumes of hard spheres overlapping with the resulting increase in the total volume available to the polymer chains, which allows them greater translational freedom and, consequently, lowers the Gibbs energy. Overall, the thermodynamic data

show a first stronger binding event dominated by electrostatic interactions (panels C and D of Fig. 2.1) and a second weaker binding event where a number of interactions, such as hydrophobic, electrostatic, and polymer chain conformational rearrangements, compact chitosan (or PLL) coating on the nano-emulsion surface, stabilizing the secondary nano-emulsion. Finally, the depletion flocculation happens at higher polyelectrolyte concentrations (panels C and D of Fig. 2.2). ζ-Potential measurements only give a picture of the overall binding event; ITC finely distinguishes among three consecutive events.

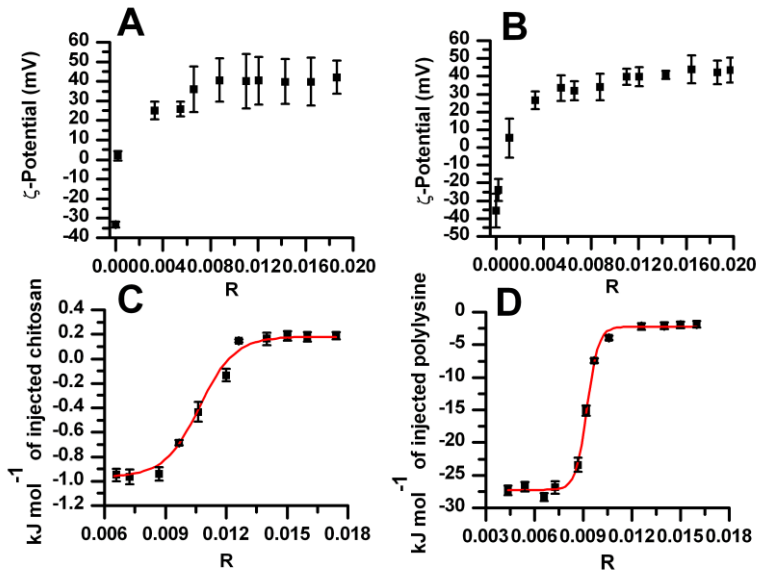

Fig 2.1 *ζ-Potential data for 1 wt % O/W NE titrated with (A) chitosan or (B) PLL at 25 °C. ITC data for the titration by single injection of (C) chitosan or (D) PLL into 1 wt % O/W NE at 25 °C. R is the ratio between the concentration of chitosan or PLL and the concentration of nano-emulsion, both expressed as weight percentage. The bars correspond to the errors. The red lines represent the best fit obtained with the independent-site model.*

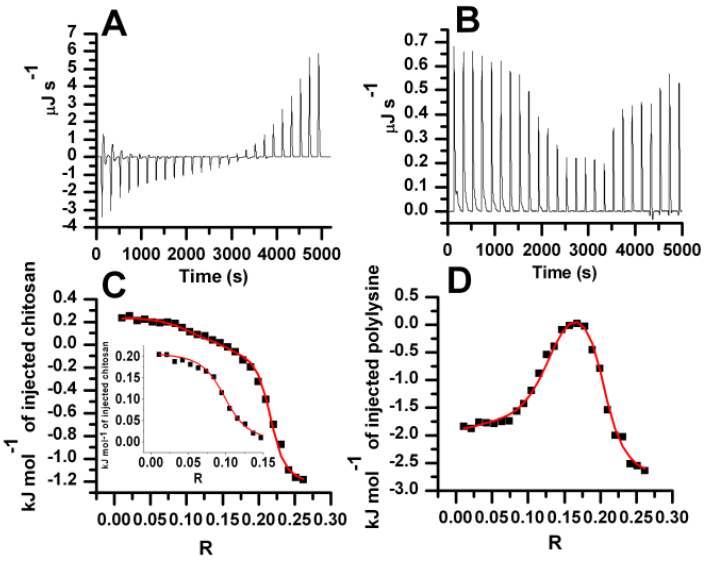

Figure 2.2 *ITC data for titration by stepwise injections of (A and C) chitosan or (B and D) PLL into 1 wt % O/W NE at 25 °C. (A and B). Heat flow and respective integrated binding heat corrected for dilution heat are plotted as a function of R. The solid curves fit according to the independent-site model. The inset in panel C represents the zoom of the first part of the curve.*

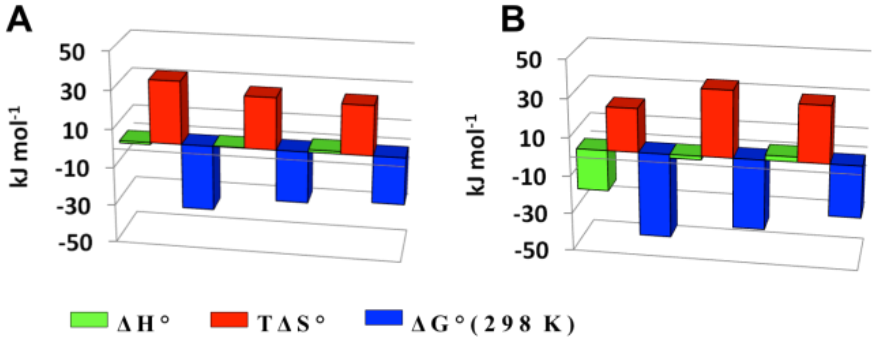

Figure 2.3 *Schematic diagram presenting the thermodynamic signature for (A) titration by single injection of chitosan and titration by stepwise injection of chitosan or (B) titration by single injection of PLL and titration by stepwise injection of PLL.*

Previous studies carried out in our laboratory showed that secondary nano-emulsions with very prolonged stability can be obtained only after reaching this second event possibly because of a more compact coverage of the emulsion (27). Therefore, an ITC study not only confirms the complete coating after the second event but also gives a deeper insight on the thermodynamics of the nanocapsule formation. The final saturation ratio is approximately the same (N = 0.1) for the two systems, but the comparison between the binding constants for the two systems highlights which couple emulsion−polyelectrolyte provides the stronger association. In the present study, PLL showed stronger association than chitosan, reflected on all of the thermodynamic parameters and, in particular, the Gibbs energy values. Such behavior could be due to steric hindrance, resulting from the relatively lower flexibility of chitosan compared to that of PLL, whose absorption is more effective on the nano-emulsion. Indeed, in a previous study, the chitosan molecules were defined "rather stiff" (37); in quantitative studies of the interaction between alginate and chitosan compared to the interaction between alginate and PLL, the faster binding of PLL was attributed to its higher flexibility (38). As a proof of the difference in the affinity between the two polymers with the nano-emulsion, some experiments were performed by varying the pH and depositing a bilayer of heparin, as shown in Fig. 2.4.

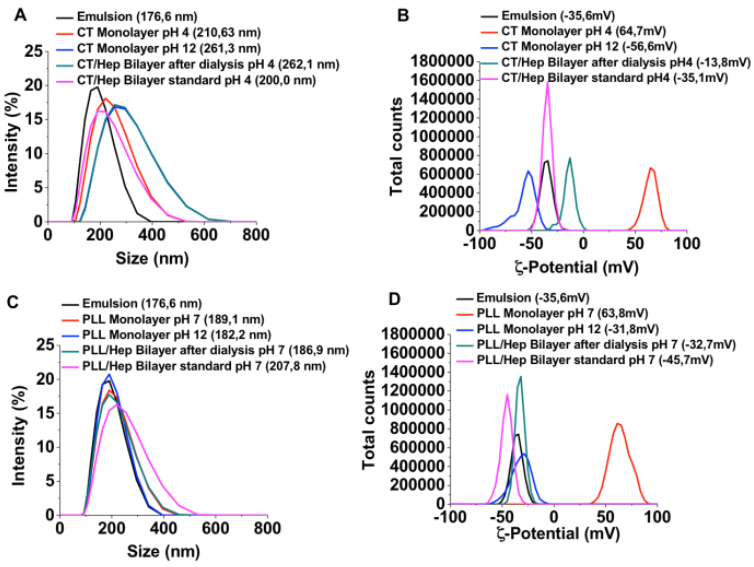

Figure 2.4 *(A and B) Size and ζ-potential data of a heparin bilayer made on a chitosan monolayer at pH 4 (standard conditions) compared to the same made at pH 12 and dialyzed until pH 4. (C and D) Size and ζ-potential data of a heparin bilayer made on a PLL monolayer at pH 7 (standard conditions) compared to the same made at pH 12 and dialyzed until pH 7.*

A layer of heparin was deposited first on a monolayer of chitosan (pH 4) and then on a monolayer of PLL (pH 7) without modifying the pH of the monolayer. In both cases, we obtained bilayer nanoparticles with good values of size, polydispersity index (PDI), and ζ-potential. In particular, the size of the bilayer was quite similar (around 200 nm), as reported in panels A and C of Fig. 2.4. The same experiments were conducted after raising the pH of the monolayers to 12. In these conditions, chitosan and PLL invert their charge. As a consequence, the chitosan monolayer shows an increase in size and PDI values, possibly because of the separation of the polymer from the nano-emulsion and/or the formation of some bridges between adjacent droplets. On the contrary, the PLL monolayer preserves good

values of size and PDI, showing no destabilization. Then, after modification of the pH of the two secondary nano-emulsions, heparin was added as a second layer; a dialysis was conducted to reach the pH at which chitosan and PLL are again positively charged (pH 4 in the case of chitosan and pH 7 in the case of PLL). The data show larger sizes and PDI and lower ζ-potential values for the heparin−chitosan bilayer (panels A and B of Fig. 2.4) than the values obtained for the heparin−PLL bilayer (panels C and D of Fig. 2.4) because of the starting destabilization of the chitosan-based secondary emulsions at pH 12. These results proved that, as also shown by ITC, PLL deposition on O/W NE is stronger than that of chitosan. It was actually so strong as to be stable against the repulsion phenomenon established between polymer and oil−lecithin at pH 12.

2.3.3. Isothermal Titration Calorimetry Analysis of PLL Interactions with Different O/W NE Percentages

PLL showed a higher affinity for the nanoemulsion than chitosan. The following step was to prepare PLL-based secondary O/W NEs at different oil concentrations. Specifically, 5 and 10 wt % were compared to the 1 wt % O/W NE to check their ability to interact with PLL. For these experiments, we started from the 20 wt % O/W NE (size, 178 nm; PDI, 0.028; and ζ potential, −47 mV). The same two sets of ITC measurements described above were performed: a single-injection experiment was made to study the first binding event (Fig. 2.5), and a typical titration experiment was

accomplished to study the second binding event and third event because of depletion flocculation (Fig. 2.6).

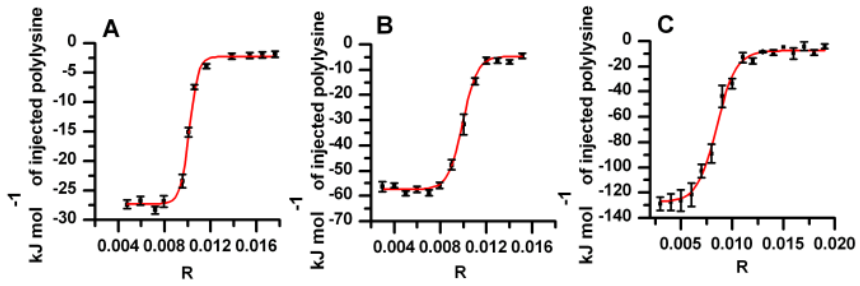

Figure 2.5 *ITC data for titration by single injection of PLL into (A) 1 wt % O/W, (B) 5 wt % o/w, and (C) 10 wt % O/W NE at 25 °C. The solid squares are the experimental data obtained by integrating the raw data and subtracting the heat of PLL dilution into the buffer. The bars correspond to the errors on the data. The red lines represent the best fit obtained with the independent-site model.*

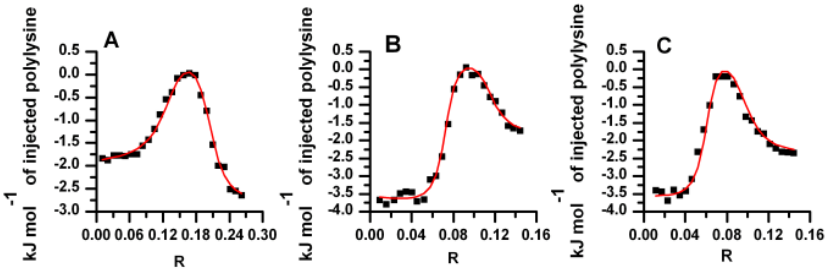

Figure 2.6 *ITC data for titration by stepwise injection of PLL into (A) 1 wt % O/W, (B) 5 wt % O/W, and (C) 10 wt % O/W NE at 25 °C. The solid squares are the experimental data obtained by integrating the raw data and subtracting the heat of PLL dilution into the buffer. The red lines represent the best fit obtained with the independent-site model.*

The thermodynamic parameters are collected in Table 2.1. Interestingly, the first event (previously referred to as predominant electrostatic interactions between PLL and the nano-emulsion) is centered at the same N value for all of the oil in water percentages, but the second and third events show decreasing N values and increasing oil in water percentage. Another interesting result is that the enthalpy of the first event becomes more favourable at increasing oil in water percentages, whereas the entropic contribution inverts its sign and becomes unfavourable. Indeed, all types of interactions are water mediated, and when the water content decreases, electrostatic interactions are favoured because the water-charged group competition is reduced. This phenomenon is enthalpically favourable. Moreover, the water content decrease in the nanoemulsion significantly varies the extension of ordered water molecules in the hydration shells of the charged groups and gives a minor contribution to the overall entropy of binding given that the charged groups are partially dehydrated prior to binding. The binding constants remain unaffected by the increase in the oil in water percentage. However, the result that appears noteworthy for practical applications is that the complete coating, referred to the second events, occurs closer and closer to the first event at increasing oil in water percentages, as shown in Table 2.1. The same happens for the third event, associated with flocculation, which also occurs closer and closer to the second event at increasing oil in water percentages (Table 2.1). These findings suggest very precisely the range of stability of a secondary nano-emulsion in relation to the final concentration of the dispersion, and at the same time, they provide the thermodynamic signature of all of the interactions.

Table 2.1 Thermodynamic parameters of the interaction between chitosan or PLL and O/W NE at 1, 5, and 10 wt %.

		N	**K_b**	**ΔH° (kJ mol^{-1})**	**TΔS° (kJ mol^{-1})**	**ΔG°(298K) (kJ mol^{-1})**
Chitosan						
1% O/W	I event	1.1± (0.1) x10^{-2}	9.2±(0.5) x10^{5}	-1.1±0.2	32.9±4.0	-34.0±3.8
	II event	9.9± (0.5) x10^{-2}	5.2± (0.2) x10^{4}	0.20±0.02	27.1±3.2	-26.9±2.4
	III event	22.0± (1.1) x10^{-2}	2.0± (0.1) x10^{4}	1.3±0.1	25.8±3.1	-24.5±2.0
Poly-L-lysine						
1% O/W	I event	1.0±(0.1) x10^{-2}	6.1± (0.5) x10^{7}	-21.5±2.0	22.9±2.8	-44.4±4.5
	II event	10.4±(0.6) x10^{-2}	2.9± (0.1) x10^{6}	-1.9±0.1	34.9±3.5	-36.8±3.0
	III event	21.0±(1.1) x10^{-2}	6.0± (0.5) x10^{4}	2.6±0.1	29.8±2.8	-27.2±2.1
5% O/W	I event	1.0± (0.1) x10^{-2}	5.2± (0.5) x10^{7}	-50.0±6.0	-6.0±0.8	-44.0±5.0
	II event	7.0±(0.4) x10^{-2}	2.8± (0.1) x10^{6}	-3.7±0.3	33.1±3.4	-36.8±2.9
	III event	11.0±(0.6) x10^{-2}	2.8± (0.1) x10^{4}	2.0±0.1	27.4±2.8	-25.4±2.0
10 % O/W	I event	0.9±(0.1) x10^{-2}	2.0± (0.2) x10^{7}	-122±10	-80.4±10.4	-41.6±4.2
	II event	6.0±(0.5) x10^{-2}	2.0± (0.1) x10^{6}	-3.5±0.3	32.5±3.4	-36.0±2.9
	III event	9.2±(0.5) x10^{-2}	3.0± (0.1) x10^{4}	2.3±0.1	27.8±2.9	-25.5±2.1

2.4. Conclusions

ITC was employed for the first time to study the optimal conditions for nano-emulsion coating. ITC measurements on the layer-by-layer interactions are rapid, accurate, and informative and constitute a substantial added value if compared to information derived from ζ-potential measurements. ITC data allowed for the acquisition of the thermodynamic signature of the investigated systems and the dissection of the Gibbs energy into entropic and enthalpic contributions. In particular, we found that the O/W NE/ polyelectrolyte structures are entropically driven. The entropic driving force may be explained as a result of several contributions: the release of ordered water from the hydration shells of the two interacting partners to the bulk water upon the direct interactions, the counterion release, the conformational rearrangements of polymeric chains, and the hydrophobic interactions. Calorimetric measurements proved that complementary and more accurate information than ζ-potential measurements can be obtained on layer-by-layer interactions between polyelectrolytes and O/W NEs; on the basis of the knowledge of the energetics of the interactions, we were able to identify the binding strength of chitosan and PLL with lecithin O/W NEs. In addition, in comparison of ITC to ζ-potential analysis, it was possible to detect two separate binding events, instead of just one saturation event. It confirms previous results regarding the dependence of secondary emulsion stability on the level of coating and allows to understand the increase of stability with the oil concentration. For the purpose of identifying the two different binding events, a combination of two sets of ITC experiments was for the first time

designed and carried out. Moreover, ITC accurately defines when flocculation starts, allowing for a fine modulation of the O/W NE percentage and the achievement of the optimal conditions for their use. Finally, the knowledge of the energetics of overall interactions may help to select the coating that guarantees the best performance in the field of drug administration.

References

(1) Lovelyn, C.; Attama, A. A. *Current state of nanoemulsions in drug delivery*. J. Biomater. Nanobiotechnol. 2011, 2, 626−639.

(2) Azeem, A.; Rizwan, M.; Ahmad, F. J.; Iqbal, Z.; Khar, R. K.; Aqil, M.; Talegaonkar, S. *Nanoemulsion components screening and selection: A technical note*. AAPS PharmSciTechnol 2009, 10, 69−76.

(3) Wei, H.; Yanan, T.; Zhiqiang, T.; Lingyun, C.; Fuqiang, H.; Wei, W. *Food protein-stabilized nanoemulsions as potential delivery systems for poorly water-soluble drugs: Preparation, in vitro characterization, and pharmacokinetics in rats*. Int. J. Nanomed. 2011, 6, 512−533.

(4) Kreilgaard, *M. Assessment of cutaneous drug delivery using microdialysis*. Adv. Drug Delivery Rev. 2002, 54, S99−S121.

(5) Shakeel, F.; Ramadan, W. *Transdermal delivery of anticancer drug caffeine from water-in-oil nanoemulsions*. Colloids Surf., B 2010, 75 (1), 356−362.

(6) Desai, A.; Vyas, T.; Amiji, M. M. *Cytotoxicity and apoptosis enhancement in brain tumor cells upon coadministration of paclitaxel and ceramide in nanoemulsion formulations*. J. Pharm. Sci. 2008, 97, 2745−2756.

(7) Tiwari, S. B.; Tan, Y. M.; Amiji, M. M. *Preparation and in vitro characterization of multifunctional nanoemulsions for simultaneous MR imaging and targeted drug delivery*. J. Biomed. Nanotechnol. 2006, 2 (3−4), 217−224.

(8) Gianella, A.; Jarzyna, P. A.; Mani, V.; Ramachandran, S.; Calcagno, C.; Tang, J.; Kann, B.; Dijk, W. J. R.; Thijssen, V. L.; Griffioen, A. W.; Storm,

G.; Fayad, Z. A.; Mulder, W. J. M. *Multifunctional nanoemulsion platform for imaging guided therapy evaluated in experimental cancer*. ACS Nano 2011, 5, 4422−4433.

(9) Jarzyna, P. A.; Skajaa, T.; Gianella, A.; Cormode, D. P.; Samber, D. D.; Dickson, S. D.; Chen, W.; Griffioen, A. W.; Fayad, Z. A.; Mulder, W. J. M. *Iron oxide core oil-in-water emulsions as a multifunctional nanoparticle platform for tumor targeting and imaging*. Biomaterials 2009, 30, 6947−6954.

(10) Yoo, H. S.; Mazda, O.; Lee, H. Y.; Kim, J. C.; Kwon, S. M.; Lee, J. E.; Kwon, I. C.; Jeong, H.; Jeong, Y. S.; Jeong, S. Y. *In vivo gene therapy of type I diabetic mellitus using a cationic emulsion containing an Epstein Barr Virus (EBV) based plasmid vector.* J. Controlled Release 2006, 112, 139−144.

(11) Brusewitz, C.; Schendler, A.; Funke, A.; Wagner, T.; Lipp, R. *Novel poloxamer-based nanoemulsions to enhance the intestinal absorption of active compounds*. Int. J. Pharm. 2007, 329 (1−2), 173− 181.

(12) McClements, D. J. Edible nanoemulsion: Fabrication, proprieties and functional performance. Soft Matter 2011, 7, 2297−2316.

(13) Patravale, V. B.; Mandawgade, S. D. *Novel cosmetic delivery systems: An application update*. Int. J. Cosmet. Sci. 2008, 30, 19−33.

(14) Sonneville-Aubrun, O.; Simonnet, J. T.; L'Alloret, F. *Nanoemulsions: A new vehicle for skincare products.* Adv. Colloid Interface Sci. 2004, 108−109, 145−149.

(15) Kabri, T. H.; Arab-Tehrany, E.; Belhaj, N.; Linder, M. *Physicochemical characterization of nano-emulsions in cosmetic matrix enriched on omega-3.* J. Nanobiotechnol. 2011, 9, 41.

(16) Eskandar, N. G.; Simovic, S.; Prestidge, C. A. *Nanoparticle coated submicron emulsions: Sustained in-vitro release and improved dermal delivery of all-trans-retinol*. Pharm. Res. 2009, 26, 1764−1775.

(17) Shah, P.; Bhalodia, D.; Shelat, P. *Nanoemulsion: A pharmaceutical review*. Syst. Rev. Pharm. 2010, 1 (1), 24−32.

(18) Rahn-Chique, K.; Puertas, A. M.; Romero-Cano, M. S.; Rojas, C.; Villalba, G. U. *Nanoemulsion stability: Experimental evaluation of the flocculation rate from turbidity measurements*. Adv. Colloid Interface Sci. 2012, 178, 1−20.

(19) Guzey, D.; McClements, D. J. *Formation, stability and properties of multilayer emulsions for application in the food industry*. Adv. Colloid Interface Sci. 2006, 128-130, 227−248.

(20) Cummaro, A.; Fotticchia, I.; Franceschin, M.; Giancola, C.; Petraccone, L. *Binding properties of human telomeric quadruplex multimers: A new route for drug design*. Biochimie 2011, 93, 1392−1400.

(21) Pagano, B.; Cosconati, S.; Gabelica, V.; Petraccone, L.; De Tito, S.; Marinelli, L.; La Pietra, V.; di Leva, F. S.; Lauri, I.; Trotta, R.; Novellino, E.; Giancola, C.; Randazzo, A. *State-of-the-art methodologies for the discovery and characterization of DNA G-quadruplex binders*. Curr. Pharm. Des. 2012, 18 (14), 1880−1899.

(22) Giancola, C.; Pagano, B. *Energetics of ligand binding to Gquadruplexes*. Top. Curr. Chem. 2013, 330, 211−242.

(23) Ravi, V.; Binz, J. M.; Rioux, R. M. *Thermodynamic profiles at the solvated inorganic−organic interface: The case of gold−thiolate monolayers*. Nano Lett. 2013, 13 (9), 4442−4448.

(24) Bouchemal, K. New challenges for pharmaceutical formulations and drug delivery systems characterization using isothermal titration calorimetry. Drug Discovery Today 2008, 13, 960−972.

(25) Thongngam, M.; McClements, D. J. *Characterization of interactions between chitosan and an anionic surfactant*. J. Agric. Food Chem. 2004, 52 (4), 987−991.

(26) Mertins, O.; Dimova, R. *Binding of chitosan to phospholipid vesicles studied with isothermal titration calorimetry*. Langmuir 2011, 27 (9), 5506−5515.

(27) Vecchione, R.; Ciotola, U.; Sagliano, A.; Bianchini, P.; Diaspro, A.; Netti, P. A. *Tunable stability of monodisperse secondary O/W nano-emulsions.* Nanoscale 2014, 6 (15), 9300−9307.

(28) Preetz, C.; Rübe, A.; Reiche, I.; Hause, G.; Mäder, K. *Preparation and characterization of biocompatible oil-loaded polyelectrolyte nanocapsules.* Nanomedicine 2008, 4, 106−114.

(29) Szczepanowicz, K.; Dronka Góra, D.; Para, G.; Warszyński, P. *Encapsulation of liquid cores by layer-by-layer adsorption of polyelectrolytes*. J. Microencapsulation 2010, 27 (3), 198−204.

(30) Ben-Amotz, D.; Underwood, R. *Unravelling water's entropic mysteries: A unified view of nonpolar, polar, and ionic hydration*. Acc. Chem. Res. 2008, 41 (8), 957−967.

(31) Wong, G. C.; Pollack, L. *Electrostatics of strongly charged biological polymers: Ion-mediated interactions and self-organization in nucleic acids and proteins.* Annu. Rev. Phys. Chem. 2010, 61, 171−189.

(32) von Klitzing, R. *Internal structure of polyelectrolyte multilayer assemblies*. Phys. Chem. Chem. Phys. 2006, 8 (43), 5012−5033.

(33) Dubas, S. T.; Schlenoff, J. B. *Factors controlling the growth of polyelectrolyte multilayers.* Macromolecules 1999, 32 (24), 8153−8160.

(34) Chanamai, R.; McClements, D. J. *Isothermal titration calorimetry measurement of enthalpy changes in monodisperse oilin- water emulsions undergoing depletion flocculation.* Colloids Surf., A 2001, 181 (1−3), 261−269.

(35) Asakura, S.; Oosawa, F. *On interaction between two bodies immersed in a solution of macromolecules*. J. Chem. Phys. 1954, 22, 1255.

(36) Asakura, S.; Oosawa, F. *Interaction between particles suspended in solutions of macromolecules*. J. Polym. Sci., Part A: Polym. Chem. 1958, 33 (126), 183−192.

(37) Kubota, N.; Shimoda, K. *Macromolecular complexes of chitosan. In Polysaccharides: Structural Diversity and Functional Versatility*, 2nd ed.; Dumitriu, S., Ed.; CRC Press: Boca Raton, FL, 2004; Chapter 29, pp 679−706.

(38) Gåserød, O.; Smidsrød, O.; Skjåk-Braek, G. *Microcapsules ofalginate-chitosan A quantitative study of the interaction between alginate and chitosan.* Biomaterials 1998, 19 (20), 1815−1825.

CHAPTER 3 Synthesis and Characterization of Bioactive Conjugated O/W Secondary Nanoemulsions for Drug Delivery

3.1. Introduction

The vascular endothelium lines the inner surface of blood vessels. It is the first interface between circulating blood and surrounding extravascular tissues (1). Vascular endothelium not only regulates blood delivery and perfusion but also provides a semipermeable barrier that controls blood–tissue exchange of fluids, nutrients, and metabolic wastes (2). Unfortunately, this fundamental organ can be affected by different types of dysfunction which can occur during different inflammation states or tumors. Vasculitis provides an example of vascular endothelium inflammatory disease (3). The exact cause of vasculitis is not fully understood. Some types are related to a person's genetic makeup. Others result from the immune system attacking blood vessel cells by mistake. The pathology causes changes in the walls of blood vessels, including thickening, weakening, narrowing and scarring. These changes restrict blood flow, resulting in organ and tissue damage (Fig. 3.1). Depending on the type of blood vessel that is affected (small, medium, or big sized vessel) different types of vasculitis have been identified (5,6). Drugs used to treat vasculitis include corticosteroids to control inflammation (prednisone or methylprednisolone) and immune-suppressants that decrease the function of immune system cells causing the inflammation (azathioprine, methotrexate

and cyclophosphamide) (7). Another example of vascular endothelium dysfunction is represented by angiogenesis which is the growth of new vessels from pre-existing vasculature that supply oxygen and nutrients to proliferating tumor cells (8). In normal physiological circumstances, angiogenesis is well controlled by pro- and anti-angiogenic factors. Though, in cancer, this balance is disturbed because tyrosine kinases, that are pro-angiogenic factors are over-expressed. In the past two decades, inhibitors of angiogenic tyrosine kinases receptors have been developed as a systemic treatment strategy for cancer (9,10).

In this work, we synthetized and characterized a biodegradable O/W SNE decorated with PEG chains and the peptide gH-(625-644) able to accumulate in the endothelium barrier and sustainably release its lipophilic cargo making possible therapy of the endothelium layer or drug release from the layer to the tissue. The incorporation of lipophilic drugs in O/W NEs is a smart way to overcome the solubility problems. A great deal of research is ongoing on this field especially because many of the newly discovered drugs have a low solubility in water (11). Nanoemulsions present high solubilization capacity of hydrophobic drugs, ease of production, long-term stability, ability to reduce the toxicity of cytotoxic drugs, and ability to protect drugs from hydrolysis and enzymatic degradation under physiological conditions which make them promising drug delivery systems (12). A number of drug-containing nanoemulsion formulations have been already introduced in the pharmaceutical market and several others are under preclinical and clinical stage of development (13). Anyway, it is known that cationic surface charges on nanoparticles, support better the transfer through negatively charged bio-membranes (14). For this reason we

prepared an O/W SNE through the deposition of a positively charged polyelectrolyte, poly-L-lysine, where electrostatic forces facilitate layer build-up. This strategy appears also as the main way to improve nanoemulsion stability (15). On the other hand phagocytosis by the mononuclear phagocyte system (MPS) is unfortunately higher for positively charged particles. To inhibit the clearance of positively charged nanoparticles, we decorated them with poly(ethylene glycol) (PEG) chains. PEG is a coiled polymer of repeating ethylene ether units with dynamic conformation (16). The movement of PEG chains conjugated on nanoparticles reduces MPS uptake and association with non-targeted serum and tissue proteins. Due to this attribute, PEGylated nanoparticles generally have an increased circulation time in blood stream and accumulate in the liver a half to a third of the amount of non-PEGylated nanoparticles (17). Further in order to enhance the nanocapsules entrance in endothelium barrier, we functionalized them with the peptide gH-(625-644) which is able to merge the cellular membranes. It was diffusely demonstrated that the peptide gH-(625-644), previously identified as a membrane-perturbing domain in glycoprotein H (gH) of herpes simplex virus 1, is able to traverse the membrane bilayer (18). gH-(625-644) once bound to membranes tends to adopt a stable-helical conformation characterized by a strong amphipathic propensity since one side is constituted by aromatic and hydrophobic residues, whereas the other side is formed by hydrophilic or small residues. This characteristic enables the peptide to associate and fuse with the membrane (19). In vitro studies on a model of endothelial barrier showed that conjugation of gH625 to the surface of polystyrene nanoparticles enhances their transport across the endothelial cells (20).

In this work, we synthetized and characterized step by step PEGylated nanocapsules (NCs) decorated with the gH-(625-644) peptide which allows them to escape the endocytic pattern. We also demonstrated that differently from studies done on rigid nanoparticles a consistent amount of NCs accumulates in the endothelium vessel with consequent possibility to release its cargo over the time and treat the endothelial barrier dysfunction attacking from the inside of the cells.

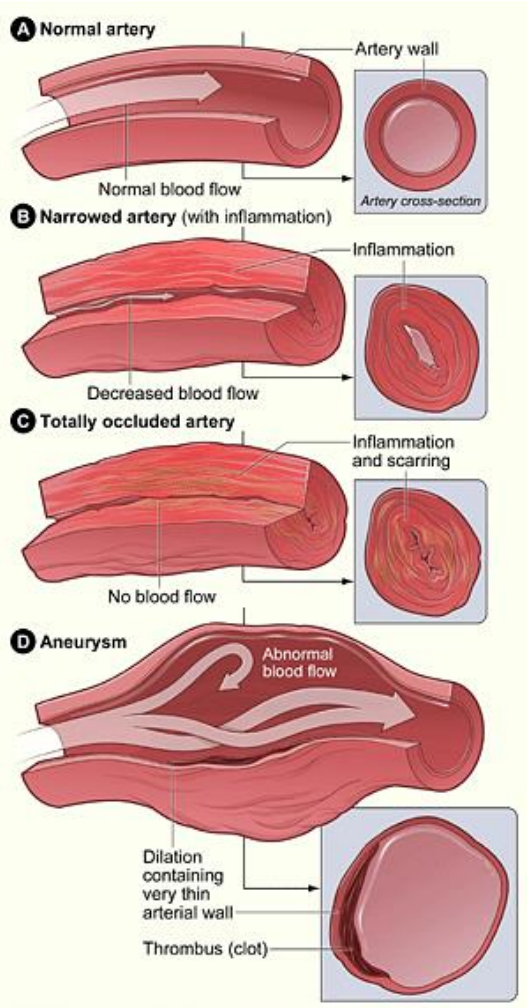

Figure 3.1 *shows a normal artery with normal blood flow. The inset image shows a cross-section of the normal artery. Figure B shows an inflamed, narrowed artery with decreased blood flow. The inset image shows a cross-section of the inflamed artery. Figure C shows an inflamed, blocked (occluded) artery and scarring on the artery wall. The inset image shows a cross-section of the blocked artery. Figure D shows an artery with an aneurysm. The inset image shows a cross-section of the artery with an aneurysm (4).*

3.2. Materials and Methods

3.2.1. Polylysine Functionalization with Biotin

Biotin (0,224 mmol) was solubilized in 25 ml N,N-dimethilformamide (DMF). PLL (0,0448 mmol), N-(3-dimethylaminopropyl)-N′-ethylcarbodiimide (EDC) (0,224 mmol) end N-hydroxysuccinimide (NHS) (0,112 mmol) were added to 5 ml of carbonate buffer. The two solutions were mixed and the reaction was carried on for 6 h adding other EDC (0,224 mmol) after the first hour. The product was lyophilized, solubilized in water, centrifuged and then dialyzed. All the reagents and solvents were purchased from Sigma Aldrich. Nuclear Magnetic Resonance (NMR) spectra were recorded using an Agilent 600 MHz (14 T) spectrometer equipped with a DD2 console and a One NMR HX probe. PLL and PLL-biotin samples (1 mg) were dissolved in 600 µl of 90/10 H2O/D2O solution. 1H 1D spectra were recorded at 300 K using 1024 scans to obtain a good signal-to-noise ratio. Water signal was reduced using a PRESAT pulse sequence. Spectra were transformed and analysed using VNMRJ4 software. Chemical shift scale was referenced to the solvent residual peak signal.

3.2.2. Peptide Synthesis and PEGylation

gH625 peptide was synthesized in a modified version, with a spacer of three glycine residues from the C-terminal amino acid, a cystein residue, and with a β-alanine at the N-terminal. Briefly, synthesis was performed on a fully automated multichannel peptide synthesizer Biotage Syro Wave. It was

assembled on a rink-amide resin (0.71 mmol/g; Sigma Aldrich) using fluorenylmethyloxycarbonyl (Fmoc) solid-phase peptide synthesis. Activation of Fmoc-protected amino acids was achieved using 2-(1H-benzotriazole-1-yl)-1,1,3,3-tetramethyluroniumhexafluorophosphate: hydroxybenzotriazole: N,N-diisopropylethylamine (HBTU:HOBt:DIEA) (1:1:2). Fmoc deprotection was carried out using 20% piperidine in DMF. All couplings were performed for 15 min and deprotections for 10 min. The entire synthesis was conducted under microwave (Mw) treatment. The following protecting groups were used: Trt (Asn), tBu (Ser, Thr, Tyr), Boc (Trp), Mmt (Cys). The N-terminal was then conjugated to fluorescein isothiocyanate (1:3) using DIEA (1:6). The 4-methoxytrityl protector group (Mmt) was removed selectively from the lateral chain of the cystein residue using trifluoroacetic acid/triisopropyl-silane/dichloromethane (TFA/TIS/DCM) (1:2:97). The –SH free group was conjugated to the malemide group of biot-PEG2000-Mal (NanoCS) (1:2) under Mw for 4h at 50°C in N,N-diisopropylethylamine/dimethylformamide (DIEA/DMF) (pH 8-9), 0,1 mM tris-(2-carboxyethyl)-phosphine hydrochloride (TCEP). PEGylated peptide was removed from the resin, by treatment with a TFA/TIS/H2O (90:5:5, v/v/v) mixture for 90 min at room temperature, then precipitated in cold diethyl ether, dissolved in a water/acetonitrile (1:1, v/v) mixture, and lyophilized. Products were purified by reversed-phase high performance liquid chromatography (RP-HPLC) using a Waters 2535 Quaternary Gradient Module, equipped with a 2489 UV/Visible detector and with an X-Bridge BEH300 preparative 10× 100 mm C8, 5μm column and applying a linear gradient of 0.1% TFA in acetonitrile (CH3CN)/ 0.1% TFA in water from 30% to 95% over 30 min at flow rate of 5 ml/min. The

negative control sequence was synthetized, PEGylated and purified in the same way. PEGylated peptide purity and identity were confirmed by LC-MS (Agilent 6530 Accurate-Mass Q-TOF LC/MS spectrometer). Zorbax RRHD Eclipse Plus C18 2.1 x 50 mm, 1.8 µm columns were used for these analyses.

Reagents for peptide synthesis (Fmoc-protected amino acids, resins, activation, and deprotection reagents) were from Iris Biotech GMBH. Solvents for peptide synthesis and HPLC analyses were from Sigma Aldrich; reversed phase columns for peptide analysis were supplied from Waters. Circular dichroism (CD) spectra curves were recorded on a Jasco-1500 circular dichroism spectrophotometer in a 0.2 cm path length cuvette and the wavelength was varied from 190 to 260 nm. A time constant of 4 s, a 2 nm bandwidth, and a scan rate of 20 nm/min were used to acquire the data. The spectra were signal-averaged over at least three scans and baseline corrected by subtracting a water spectrum.

3.2.3 NCs Preparation

First, a 20 wt % oil in water pre-emulsion (130-140 nm, ∼−30 mV, pH 4.3) was prepared by dissolving the surfactant (egg lecithin) in the oil phase (soybean) and adding all to the aqueous phase. The pre-emulsion was then homogenized by a high-pressure homogenizer (110P series microfluidizer)

to obtain the final nano-emulsion (1). PLL-biotin solution was prepared by dissolving 10 mg in 1 ml Milli-Q water. The first positively charged layer of PLL-biotin was obtained by adding in one shot the polymer solution to the emulsion solution under vigorous stirring (1500 rpm) and then homogenized for 100 steps at a pressure of 700 bar by a high-pressure homogenizer (110P series microfluidizer). The secondary nanoemulsion solution was 0,0125 wt% of PLL-biotin and 1 wt% of oil. The streptavidin (Sigma Aldrich) solution was prepared by dissolving 1 mg in 1 ml of Milli-Q water (166 µM). The streptavidin solution was added to the O/W (0,5 wt%) PLL-biotin (0,00625 wt%) SNE under sonication at a final concentration 1,45 µM. In the same way the compound FITC-gH625-PEG-biotin was added under sonication to the PLL-biotin-streptavidin secondary nanoemulsion at a ratio 1:1 between FITC-gH625-PEG-biotin and the streptavidin. The NCs were characterized at each step of preparation measuring size and ζ-potential by dynamic light scattering (Malvern Zetasizer). Before each experiment, 50 µl aliquots were withdrawn from each sample and diluted 1:40 (v/v) with Milli-Q water. The diluted samples were poured into disposable cells, and the size and ζ-potential was determined at least 3 times for each sample at 25 °C. In particular, the particle size distribution was measured by DLS (λ= 632.8 nm) using a detecting angle of 173°.

The final nanoparticles were also characterized by confocal microscopy. A treatment of the WillCo dish was performed with a solution of poly-L-lysine (4-15 kDa): the solution 1mg/mL of poly-L-lysine was deposited for 10 min on the WillCo dish and then washed two times with Milli-Q water. The sample of NCs was diluted up to an oil concentration of 0.001 wt % using Milli-Q water and leaved in the dish for 30 min, then one part and half of

the diluted sample was substituted with a solution of 1,4-diazobiciclo-(2.2.2)-benzeneoctane 5 wt % (in water). Confocal microscopy was performed by a confocal and multiphoton micro-scope system (Leica TCS SP5 MP, (Wetzlar). The lambda of the argon ion laser was set at 488 nm. Fluorescence emission was revealed by band pass 500–530. 1,4-diazobiciclo-(2.2.2)-benzeneoctane and WillCo dishes were respectively from Sigma Aldrich and WillCo Wells B.V.

3.2.4 Isothermal Titration Calorimetry Analysis

Isothermal titration calorimetry (ITC) experiments were performed using a Nano ITC Low Volume from TA Instruments (USA) with a cell volume of 170 μl. Titration experiments were carried out at 25 °C. 25 injections of 2 μl each of streptavidin solution (10,41 μM) were added to the PLL-biot NCs solution (0,00625% PLL-biot) every 200 s at a continuous stirring rate of 200 rpm. Measurements were carried out to calculate the heat of dilution for streptavidin solution. Control experiments were performed between the streptavidin solution (10,41uM) and the PLL NCs solution (0,00625% PLL). The binding constant (K_b), enthalpy change ($\Delta_b H°$), and stoichiometry of the interaction process were obtained by fitting the binding isotherm to the equivalent and independent binding sites model, by using the NanoAnalyze software, version 2.4.1 (TA Instruments). The remaining

thermodynamic parameters of the interaction were calculated using the relationships:

$\Delta_b G° = -RT\ln K_b$

$\Delta_b G° = \Delta_b H° - T\Delta_b S°$

3.2.5 Permeability Experiments

Cells were seeded at a density of 9×10^4 cells/cm^2 on transwell permeable inserts (6.5 mm in diameter, 3 μm pores size; Corning Incorporated, Corning, NY). Transendothelial electrical resistance (TEER) was measured by using Millicell1-ERS voltohmmeter (Millipore, Billerica, MA) to assess the growth of cells on inserts. Permeability experiments were performed on the monolayer 7 days after cell seeding, allowing sufficient time for the cells to develop the junctions between cells. On the day of experiment, transwell insert filter was washed with PBS, and then the media of the donor chamber was filled with 150 μl cell culture medium without phenol red and containing 4.3×10^8 NPs/ml while the acceptor chamber was filled with 400 μl cell culture medium without phenol red. The samples of 400 μl were drawn every 30 min for 240 min from the acceptor chamber and were then replaced with the same amount of fresh medium. The fluorescence tracer concentration in the samples was determined by a spectrofluorometer

(Victor, Wallac, PerkinElmer), and the excitation and emission wavelengths were set respectively to 488 nm and 530 nm. The cell nuclei were stained with 4′,6-diamidine-2′-phenylindole dihydrochloride (DAPI). Fluorescence analyses were performed by a confocal and multiphoton micro-scope system (Leica TCS SP5 MP). Images were acquired with a resolution of 1024 × 1024 pixels by an oil-immersion 63× objective.

3.3. Results and Discussion

Oil in water primary and secondary poly-L-lysine nanoemulsions were previously reported and well characterized (21,22). In the latter case, it was utilized PLL modified with biotin (PLL-biotin), followed by the linker protein, streptavidin, and biotin end-functionalized PEGylated peptide (biotin-PEG-gH625-FITC). In Fig 3.2 it is shown a schematic illustration of the decorated NCs assembly. The first PLL-biotin layer is able to gain cellular entry of NCs indeed the mechanism of uptake for positively charged nanoparticles is energy driven due to the interaction with charged heparin sulfate on the cell surface that plays an important role for nanoparticles invagination (14). The streptavidin bridges PLL-biotin and biotin-PEG-gH625 via streptavidin-biotin affinity interaction. Further, PEG has the role to enable the NCs to avoid clearance by mononuclear phagocytic system. It allows NCs to stay in the blood for extended period (23). Lastly, the

terminal peptide gH625 is able to traverse the membrane bilayer and transport the NCs into the cytoplasm and across the endothelium barriers.

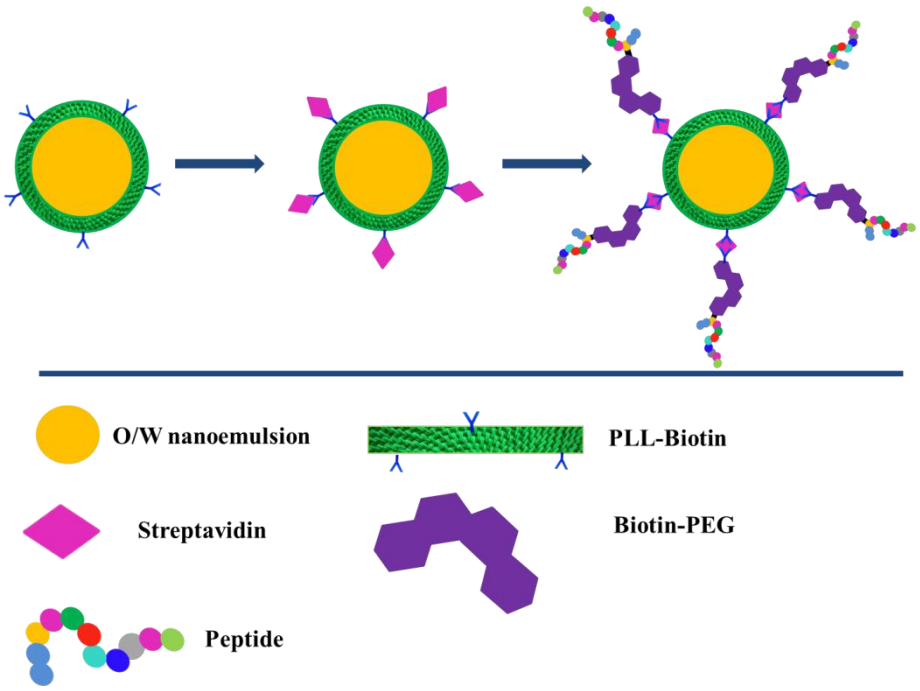

Figure 3.2 *Schematic representation of PEG-gH625 decorated NCs formulation.*

As previously mentioned, the PLL was functionalized with biotin (Fig. 3.3) in order to create biotinylated NCs. The functionalization was detected by nuclear magnetic resonance (NMR). The peak at 3.0 ppm was assigned to the epsilon protons of free Lys (as confirmed by spectrum of PLL shown in Fig. 3.4 B) whereas peak at 2.9 ppm was assigned to the epsilon protons of Lys bound to biotin. The integration of those two peaks gives the percentage

of biotin bound to PLL in the PLL-biotin sample showing a yield of functionalization of 5%. This degree of polymer functionalization resulted a good compromise between the reduction of the polymer solubility induced by the biotin conjugation and the amount of new sites able to link PEG-peptide necessary to improve cellular uptake. Further, PEG is able to explicate its anti-opsonic properties only if its density on nanoparticles surface is relatively low to allow the single chains to move freely.

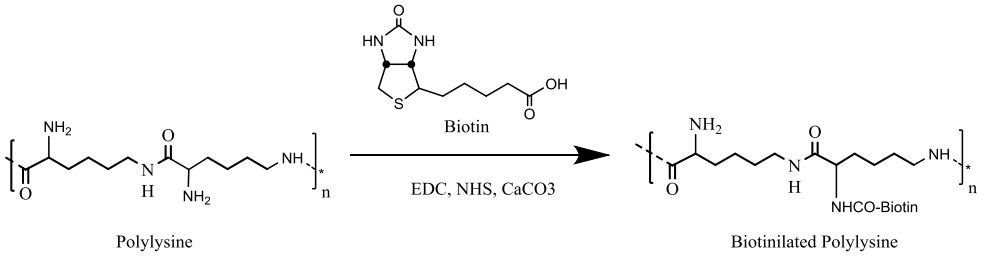

Figure 3.3 *Scheme of poly-L-lysine functionalization with biotin.*

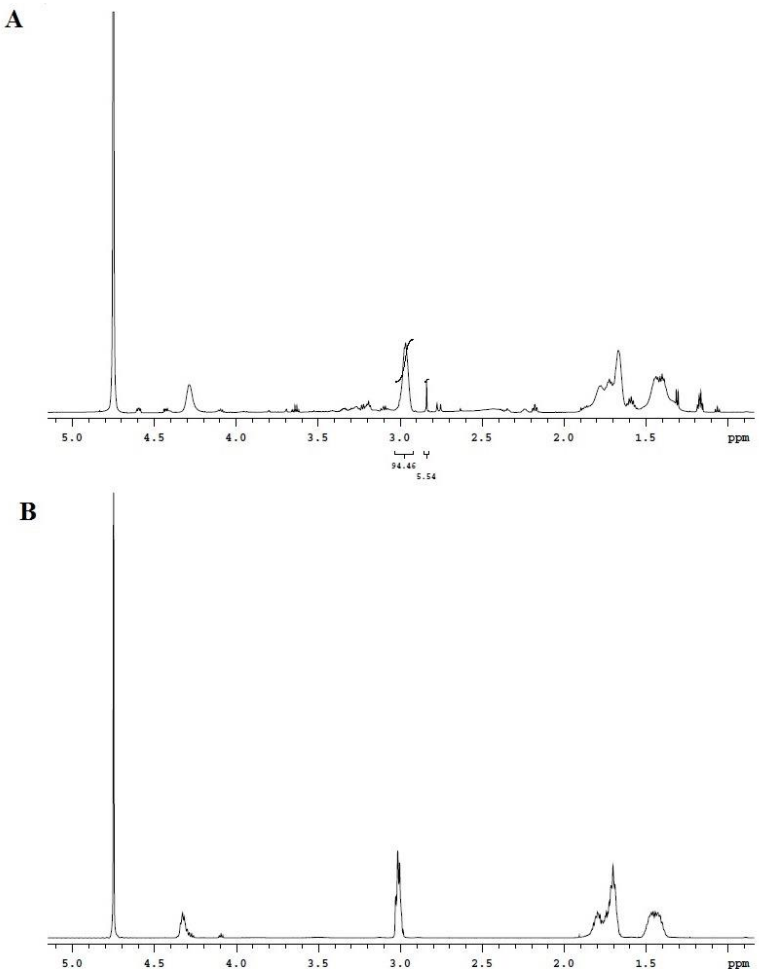

Figure 3.4 *1H1D NMR spectra of PLL-biotin (A) and PLL (B) in 90/10 H2O/D2O.*

The O/W (1 wt%) PLL-biotin (0,0125 wt%) SNE was prepared and characterized by dynamic light scattering analysis which showed good results of size, polydispersity index and ζ-potential. The results demonstrated an increment of size from the primary nanoemulsion (137,3 nm) to the PLL-biotin secondary nanoemulsion (154,3 nm) (Fig 3.5A).

Further, an inversion of nanoparticles charge was shown. Indeed, the ζ-potential results negative in the primary nanoemulsion due to the presence of charged carboxylic acid groups along the lecithin chain (used as surfactant) and becomes positive in the secondary nanoemulsion due to the coating of the positively charged polymer (poly-L-lysine) (Fig. 3.5B).

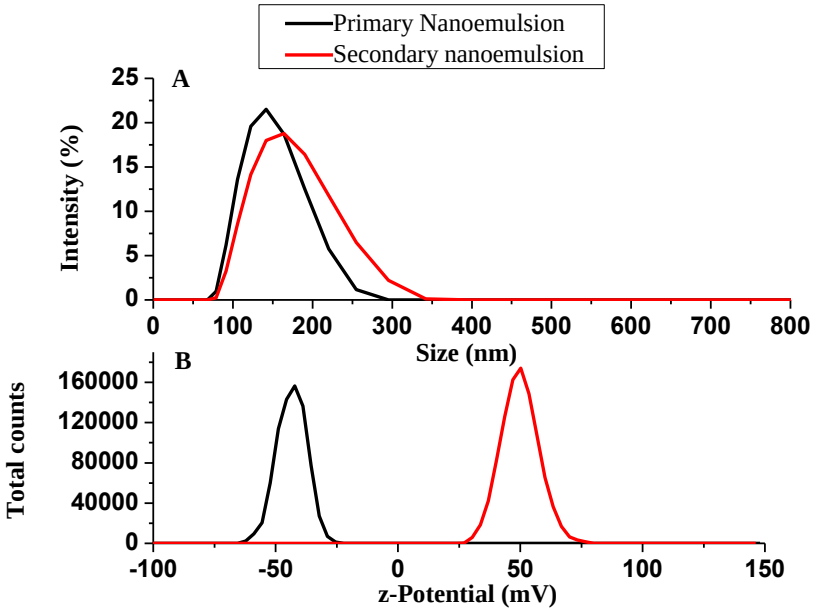

Figure 3.5 *Size data of O/W primary nanoemulsion compared with O/W (1 wt%) PLL-biotin (0,0125 wt%) secondary nanoemulsion (A). ζ-Potential data of primary nanoemulsion compared with O/W (1 wt%) PLL-biotin (0,0125 wt%) secondary nanoemulsion (B).*

Overall, DLS periodicals measurements showed that the PLL-biotin secondary nanoemulsion maintains its hydrodynamic diameter until about 49 days, thus demonstrating its good stability (Fig. 3.6).

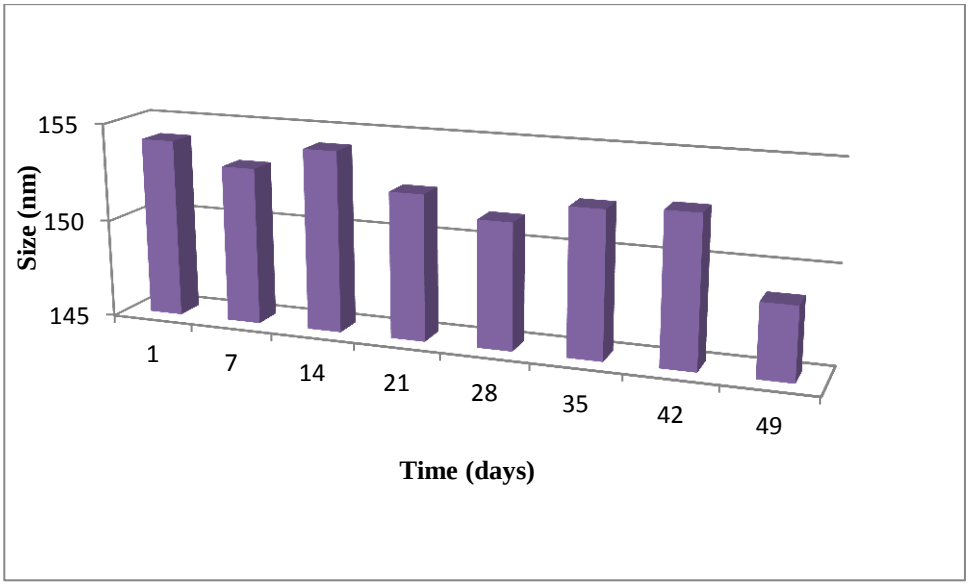

Figure 3.6 *Dimensional behaviour over time for O/W (1 wt%) PLL-biotin (0,0125 wt%) secondary nanoemulsion measured by DLS analysis.*

In order to establish the precise amount of streptavidin able to saturate all the biotin groups exposed on the surface of NCs, isothermal titration calorimetry experiments were carried out. The methodology is based on the measurement of the heat absorbed or released following titration by injecting a solution of one of the interacting molecules (the ligand) into a cell containing a solution of the other molecule (a macromolecule). In this case an O/W (0,5 wt%) PLL-biotin (0,00625 wt%) SNE was titrated with a solution of streptavidin (10,41 μM) (Fig. 3.7A). The ITC binding curve obtained from the integration of the heat data has a sigmoidal behaviour and was fitted with an independent and equivalent-sites model, the best-fit parameters are reported in Table 3.1. As shown in Table 3.1, the affinity between PLL-biotin NCs and streptavidin is very high, K_d (K_d=1⁄K_b) values

are in the order of nM. The thermodynamic signature, traced by the thermodynamic parameters collected in Table 3.1 and depicted in Fig. 3.7B, clearly shows that the interaction is exothermic and enthalpically driven. The process is enthalpically driven counterbalanced by an unfavourable entropic contribution to Gibbs energy. The favourable enthalpy is ascribable to the formation of new interactions between biotin and streptavidin upon binding. The unfavourable entropy contribution upon binding, suggests that the unfavourable conformational rearrangements due to the loss of conformational degrees of freedom for both the interacting molecules, emerge predominant. To confirm that the obtained binding curve is only due to the interaction between the biotin and the streptavidin, the same experiment without biotin was carried out. In particular O/W (0,5 wt%) PLL (0,00625 wt%) SNE was titrated with a solution of streptavidin (10,41 µM). Raw data (Fig. 3.7C) showed only small peaks of dilution demonstrating no interaction between the streptavidin and O/W PLL SNE.

Table 3.1 Thermodynamic parameters of the interaction between streptavidin and O/W (0,5 wt%) PLL-biotin (0,00625 wt%) SNE at 25 °C.

molar enthalpy, **$\Delta H°$ (kJ mol^{-1})**	entropic contribution, **$T\Delta S°$ (kJ mol^{-1})**	Gibbs energy, **$\Delta G°$(25 °C) (kJ mol^{-1})**	binding constant, **Kb (M^{-1})**
-510,1	-463,24	-46,86	$1,6*10^{8}$

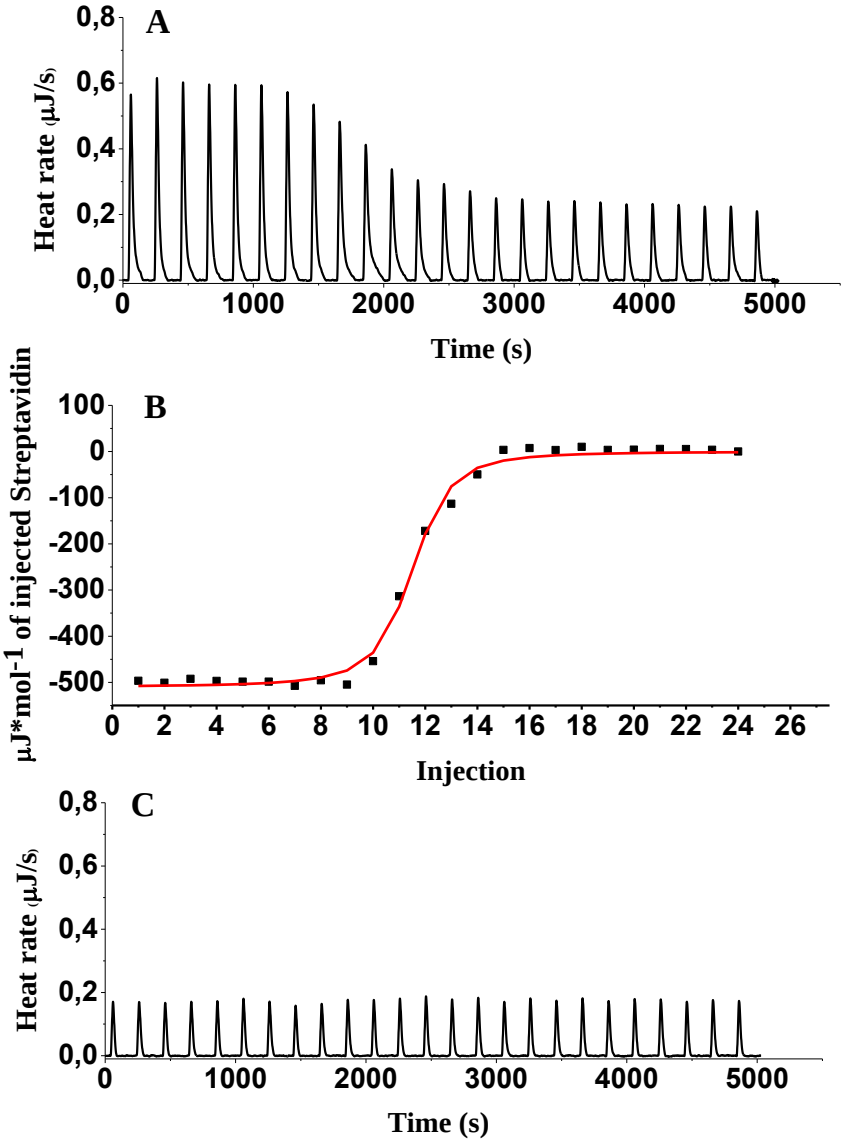

Figure 3.7 *ITC data for titration by stepwise injections of streptavidin into 0,5 wt% O/W PLL-biotin SNE at 25 °C (A). Normalized heat of interaction between PLL-biotin SNE and streptavidin. The solid circles are the experimental data obtained by integrating the raw data and subtracting the heat of ligand dilution into the buffer. The lines represent the best fit obtained with the independent-sites model (B). ITC data for titration by stepwise injections of streptavidin into 0,5 wt% O/W PLL SNE at 25 °C (C).*

According to the NMR data the solution of O/W (0,5 wt%) PLL-biotin (0,00625 wt%) SNE is 14,5 µM concentrated in biotin (5% biotin on the total amount of PLL monomers used for the NCs formulation). Whereas ITC data show that the same NCs solution saturated by means of streptavidin is 1,45 µM concentrated in streptavidin. This means that 10% of biotins are exposed on the NCs surface and able to bind the streptavidin added to the solution. ITC experiments allowed to determine the exact amount of biotin exposed on the NCs surface with respect to the total quantity. These data were of fundamental importance to continue the decorated NCs assembly and avoid nonspecific interactions due to the addition of a larger amount of the biomolecules than the available sites.

Regarding the peptide synthesis three glycines and a cysteine were added to the C-terminal (gH625-GGGC). The three glycines had a role of spacer in order to make the peptide free to acquire its conformation when conjugated. Whereas at the N-terminal a fluoresceine 5(6)-isothiocyanate (FITC) residue was added in order to dye the compound and detect its conjugation on the NCs (FITC-gH625-GGGC). The protector group was selectively removed from the thiol group of the last cysteine residue, still linked to the resin, then was conjugated to the maleimide group of a bifunctionalized polyethylenglycol (Mal-PEG-biotin, 2000 Da) obtaining the PEGylated peptide (FITC-gH625-PEG-biotin) (Fig. 3.8). PEG 2000 was chosen for its known capability to extend the circulation time and decrease accumulation in liver of nanoemulsion better than smaller or longer PEG (24). In literature it is reported that PEG2000-nanoemulsion has a 7-fold increased half-time after injection in rats (25).

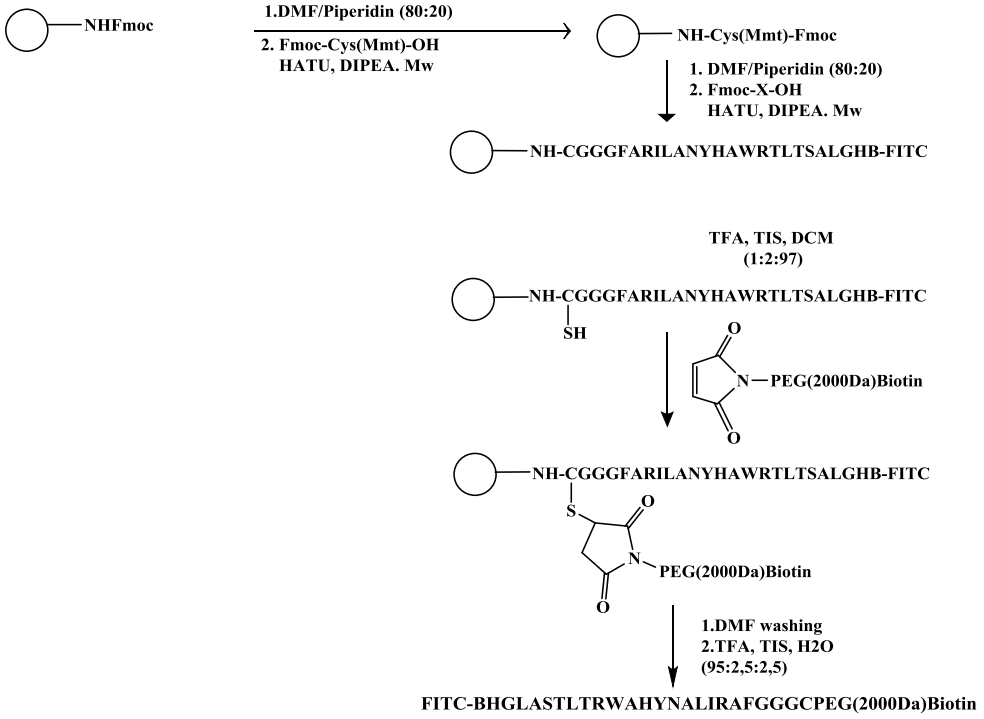

Figure 3.8 *Scheme of peptide synthesis on solid phase, PEGylation and washing.*

Analytical high pressure liquid chromatography and mass spectroscopy showed both the presence of the unreacted peptide and the PEGylated peptide with a yield of 37% (Fig. 3.9). The first main peak was associated to the peptide, the second to the PEGylated peptide. The two compounds were separated by RP-HPLC (reverse phase-high performance liquid chromatography).

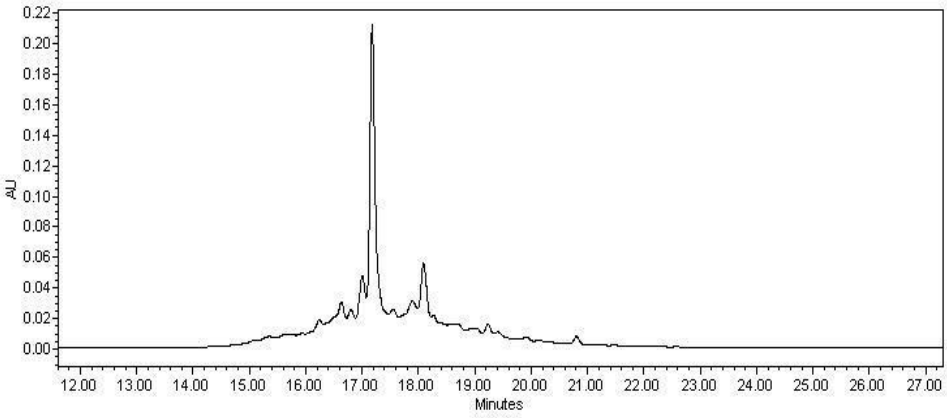

Figure 3.9 *RP-HPLC spectra at 220 nm of the reaction products.*

The secondary structures of gH625-GGGC and gH625-GGGC-PEG were determined in water by CD spectroscopy in the far-UV spectral region (195–260 nm). CD spectra performed on gH625-GGGC revealed spectra with minima at ∼200–205 nm, indicating the presence of a random coil conformation. This spectral characteristic is consistent with the CD spectra of gH625 reported in literature (26) demonstrating that the insertion of amino acids at the C-terminal does not disturb the peptide conformation. Further, the CD spectra performed on gH625-GGGC-PEG showed the same trend proving that the long PEG chain does not interfere with the peptide secondary structures (Fig. 3.10).

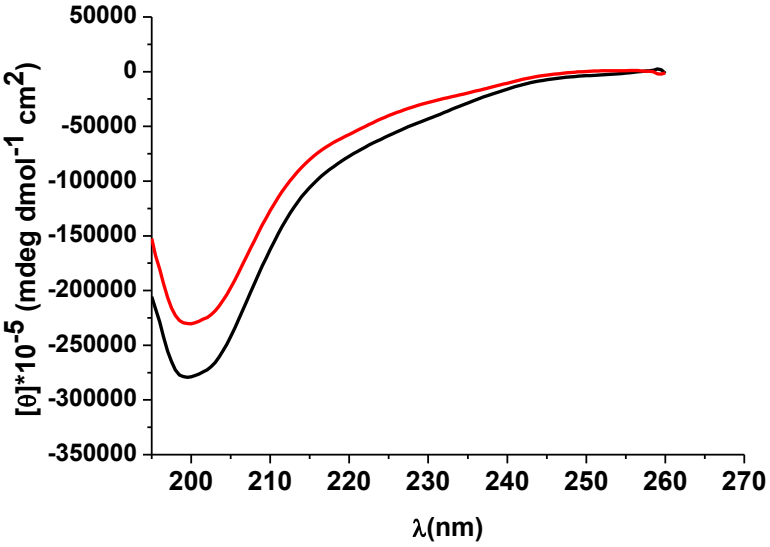

Figure 3.10 *CD spectra of gH625-GGGC (black) and gH625-GGGC-PEG (red) in water. The spectra were recorded using 0.2 cm path length cells.*

The FITC-gH625-PEG-biotin was then added to the O/W PLL-biotin-streptavidin SNE under sonication at a ratio 1:1 with the streptavidin. The completed functionalized NCs were characterized by DLS. The hydrodynamic diameter of these fluorescent nanoparticles was ~156 nm, as illustrated by the typical light scattering measurement shown in Fig. 3.11A. Such systems were also evaluated by fluorescence confocal microscopy and, in order to improve NCs imaging resolution, stimulated emission depletion microscopy (STED) was also performed. Confocal imagine (Fig. 3.11 B) shows the good monodispersity of the colloidal system and absence of aggregates in accordance with DLS data.

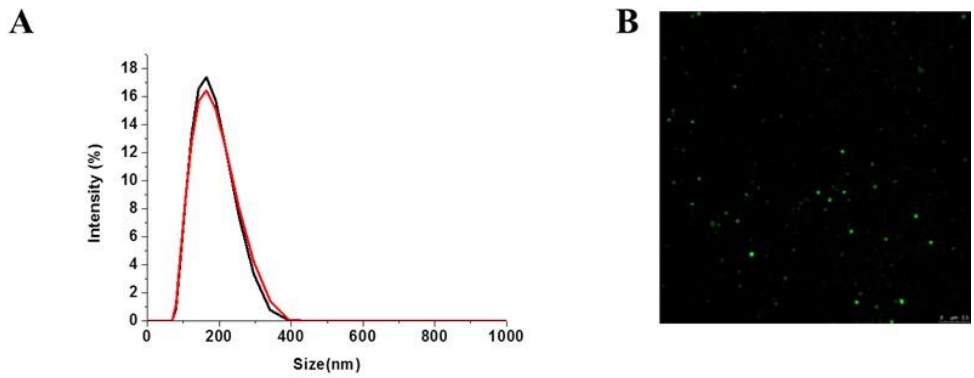

Figure 3.11 *Size data of PLL-biotin-streptavidin secondary nanoemulsion (black) and PLL-biotin-streptavidin-PEG-gH625 secondary nanoemulsion (red)(A). Confocal imagine of PLL-biotin-streptavidin-PEG-gH625 secondary nanoemulsion. The scale bars is 2,5µm (B).*

In Table 3.2 size and ζ-potential measurements of NCs during each step of preparation are shown. As illustrated, an increment of size (from 137±0,56 to 153,5±0,88) and a ζ-potential inversion (from -43,3±1,90 to 45,9±0,91) occurred in the passage from O/W NE to O/W SNE since the polymer forms a positively charged layer around the negatively charged oil droplets increasing their overall size. The next steps of conjugation did not change significantly the nanoparticle size in agreement with the fact that the functionalization degree is low and the conjugated compound is small with respect to the NC, in fact as reported in literature streptavidin hydrodynamic diameter is 7 nm (27).

Table 3.2 Size and ζ-potential measurements of NCs during the four steps of assembly.

	Size	**PDI**	**ζ-potential**
1.Primary nanoemulsion	137,3±0,56	0,041±0,003	-43,3±1,90
2.Secondary PLL-biotin nanoemulsion	153,5±0,88	0,054±0,013	45,9±0,91
3.Secondary PLL-biotin-streptavidin nanoemulsion	153,8±0,56	0,075±0,0063	42,9±0,83
4.Secondary PLL-biotin-streptavidin-PEG-gH nanoemulsion	155,9±2,00	0,099±0,01	47,5±0,60
4.Secondary PLL-biotin-streptavidin-PEG- negative control peptide nanoemulsion	154,8±2,90	0,068±0,02	48,6±3,39

To study the effect of the functionalization of gH625-PEG on O/W SNE (gH-NCs), transcytosis experiments were performed. In particular, to confirm the peptide capability to enhance NCs crossing of a confluent monolayer of endothelial cells, gH-NCs were compared with NCs functionalized with a peptide that acts as negative control , whose sequence

was opportunely modified, through the substitution of amino acids considered fundamental for the interaction (named negative control peptide-NCs). The negative control sequence (FITC-BDGGAAAGAEEADAGAGGEAWGGGC) was synthetized on solid phase, PEGylated and conjugated on the nanocapsule surface in the same way practiced for gH625 peptide. bEnd3 cells are usually used as a BBB model system due to their rapid growth end capability to form a confluent monolayer that mimics the endothelium permeability (28-29). As shown in Fig. 3.12, after 60 minutes of incubation, both gH-NCs and negative control peptide-NCs crossed bEnd3 cells in the same amount. In both cases the number of internalized nanocapsules increases as a function of incubation time. However, the amount of crossing gH-NCs is higher than negative control peptide-NCs and this effect is more evident at longer incubation time. After 4 hours the bEnd confluent monolayer was washed and treated with a paraformaldehyde solution. Cells nuclei were DAPI stained and confocal microscope analyses were performed to confirm gH-NCs enhanced uptake (Fig. 3.13). Very interestingly, this analysis showed that despite the slight difference in terms of crossing gH-NCs accumulate much more than negative control peptide-NCs.

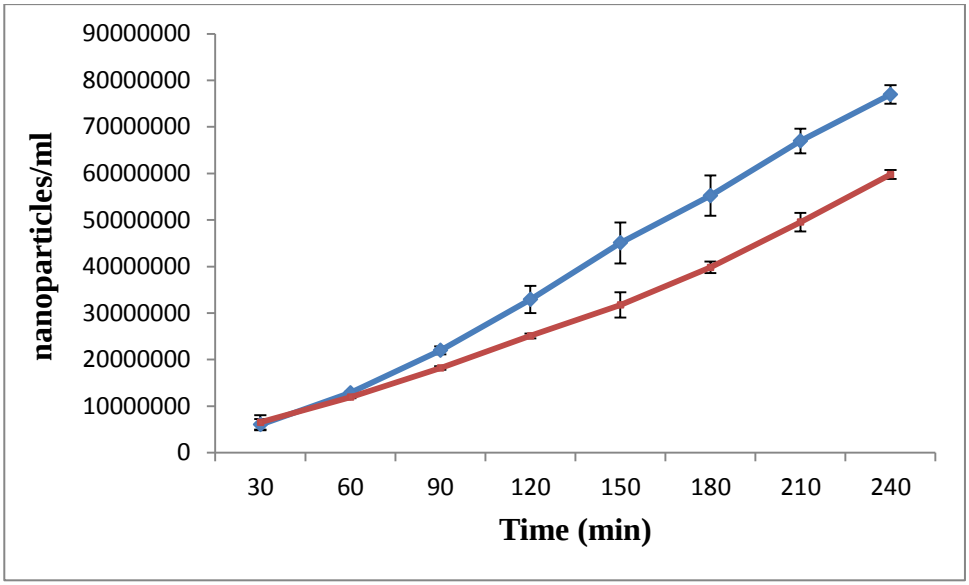

Figure 3.12 *Transcytosis of gH-PEG-NCs (blue) and negative control peptide –PEG-NCs (red) in bEnd3 cells over 4hour.*

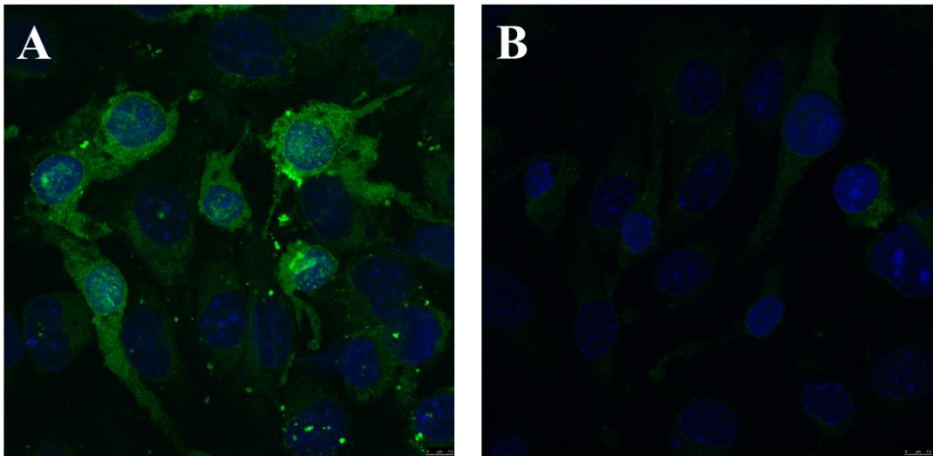

Figure 3.13 *Confocal imagines for bEnd3 confluent monolayer after four hours in contact with gH-PEG-NCs (A) and negative control peptide PEG-NCs (B) .The scale bars is 2,5µm.*

A possible explanation is that the peptide induces much higher internalization.

Very interestingly, due to the soft nature of the secondary nanoemulsions once internalized they tend to destabilize and remain in the cellular layer. This can be of particular importance when the release has to be localized in the layer of cells.

Conversely, to enhance transcytosis properties of the above described nanocarrier one way, under investigation, is to reinforce NE system by thickening the shell through the layer by layer of further polymers.

3.4 Conclusions

In this work we synthetized and characterized O/W PEGylated SNEs decorated with gH-(625-644), a peptide that merges with biological membranes. The strong affinity interaction streptavidin-biotin was used for the PEGylation and the peptide conjugation. In vitro studies showed that gH625-644 enables the O/W NE both to cross and accumulate in the endothelial barriers. This propriety permits the NCs to be used in a double path. One as pharmaceutical form that accumulates in the vessel endothelium barrier, and in a sustained way releases its lipophilic cargo in the layer of cells making possible therapy of the endothelium layer or drug release from the layer to the tissue. The other as drug delivery system able to cross endothelium barriers; in this case we want to enhance the

transcytosis by reinforcing the shell through the layer by layer of further polymers.

References

1) Folkman, J.; D' Amore, P. A. *Blood Vessel Formation: What Is Its Molecular Basis?* Cells. 1996, 87, 1153–1155.
2) Yuan, S. Y.; Rigor, R. R. *Regulation of Endothelial Barrier Function*. University of California Davis. 2010.
3) Gary S. Hoffman, G, S.; Calabrese, L. H. *Vasculitis: determinants of disease patterns.* Nature Reviews Rheumatology. 2014, 10,454–462.
4) Diseases and Conditions Vasculitis. Mayo Clinic
5) J. C. Jennette, R. J. Falk, P. A. Bacon, N. Basu, M. C. Cid, F. Ferrario, L. F. Flores-Suarez, W. L. Gross,L. Guillevin, E. C. Hagen, G. S. Hoffman, D. R. Jayne, C. G. M. Kallenberg, P. Lamprecht,C. A. Langford, R. A. Luqmani, A. D. Mahr, E. L.*2012 Revised International Chapel Hill Consensus Conference Nomenclature of Vasculitides.* Arthritis & Rheumatism. 2013. 65, 1–11.
6) Watts, R. A.; Lane, S.; Bentham, G.; Scott, D. G. *Epidemiology of Systemic Vasculitis*. Arthritis & Rheumatism. 2000, 43, 414–419.
7) Miller, A.; Chan, M.; Wiik, A.; Misbah, S. A.; Liqmani, R. A. *An approach to the diagnosis and management of systemic vasculitis.* Clinical & Experimental Immunology. 2010, 160, 143–160.
8) Papetti, M.; Herman, I.M. *Mechanisms of normal and tumor-derived angiogenesis.* American Journal of Physiology. 2002. 282, 947-C970.
9) Gotink, K. J.;Verheul, H. M.W.*Anti-angiogenic tyrosine kinase inhibitors: what is their mechanism of action?* 2010, 13, 1-14.
10) Folkman, J. *Tumor angiogenesis: therapeutic implications*. 1971 The New England Journal of Medicine 1971; 285:1182-1186.

11) Hörmann, K.; Zimmer, A.*Drug delivery and drug targeting with parenteral lipid nanoemulsions: A review*. Journal of Controlled Release. 2016, 223:85-98.

12) Ganta, S.; Paxton, J. W.; Baguleyc, B. C.; Garga, S. *Pharmacokinetics and pharmacodynamics of chlorambucil delivered in parenteral emulsion*. International Journal of Pharmaceutics. 2008,360, 115–121.

13) Ganta, S.; Talekar, M.; Singh, A.; Coleman, T. P.; Mansoor, M.*Nanoemulsions in Translational Research—Opportunities and Challenges in Targeted Cancer Therapy*. AAPS PharmSciTech. 2014, 15, 694-708.

14) .Poon, Z.; Chang, D.; Zhao, X.; Hammond, P. T. *Layer-by-Layer Nanoparticles with a pH Sheddable Layer for In Vivo Targeting of Tumor Hypoxia.* ACS Nano. 2011, 5 (6), 284–4292.

15) McClements, D. J. *Edible nanoemulsion: Fabrication, proprieties and functional performance*. Soft Matter 2011, 7, 2297−2316.

16) Moril, A.; Klibanov, A. L.; Torchilin, V. P.; Huangl; L. *Influence of the steric barrier activity of amphipathic poly(ethyleneglycol) and ganglioside GM, on the circulation time of liposomes and on the target binding of immunoliposomes in vivo*. FEBBS letters. 1991, 284, 263-266.

17) Jokerst, J. V.; Lobovkina, T.; Zare, R. N.; Gambhir, S. S. *Nanoparticle PEGylation for imaging and therapy*. Nanomedicine. 2011, 6(4): 715–728.

18) Galdiero, S.; Falanga, A.; Morelli, G.; Galdiero, M. *gH625: a milestone in understanding the many roles of membranotropic*

peptides.. Biochimica et Biophysica Acta (BBA) - Biomembranes. 2015, 1848, 16–25.

19) Galdiero, S.; Falanga, A.; Vitiello, M.; Raiola, L.; Fattorusso, R.; Browne, H.; Pedone, C.; Isernia, C.; Galdiero, M. *Analysis of a Membrane Interacting Region of Herpes Simplex Virus Type 1 Glycoprotein H*. Biochimica et Biophysica Acta (BBA) - Biomembranes. 2008, 283(44): 29993–30009.

20) . Guarnieri, D.; Falanga, A.; Muscetti, O.; Tarallo, R.; Fusco, S.; Galdiero, M.; Galdiero, S.; Netti, P.A.*Shuttle-mediated nanoparticle delivery to the blood–brain barrier* Small. 2013,9(6):853–862.

21) Vecchione, R.; Ciotola, U.; Sagliano, A.; Bianchini, P.; Diasproc, A.; Netti, P.A. *Tunable stability of monodisperse secondary O/W nano-emulsions.* Nanoscale. 2014, 6, 9300.

22) Fotticchia, I.; Fotticchia, T.; Mattia, C. A.; Antonio Netti, P. A.; Vecchione, R.; Giancola, C.*Thermodynamic Signature of Secondary Nano-emulsion Formation by Isothermal Titration Calorimetry*. Langmuir. 2014, 30 (48), 14427–14433.

23) Torchilin, V. *Tumor delivery of macromolecular drugs based on the EPR effect*. Advanced Drug Delivery Reviews. 2011, 63, 131–135.

24) Owens, D. E.; Peppas,. N. A. *Opsonization, biodistribution, and pharmacokinetics of polymeric nanoparticles*. International Journal of Pharmaceutics. 2006, 307, 93–102.

25) Alayoubi, A.; Alqahtani, S.; Kaddoumi, A.; Nazzal, S. *Effect of PEG Surface Conformation on Anticancer Activity and Blood Circulation of Nanoemulsions Loaded with Tocotrienol-Rich Fraction of Palm Oil*. AAPS J. 2013, 15(4): 1168–1179.

26) Smaldone, G.; Falanga, A.; Capasso, D.; Guarnieri, D.; Correale, S.; Galdiero, M.; Netti, P. A.; Zollo, M.; Galdiero, S.; Di Gaetano, S.; Pedone, E. *gH625 is a viral derived peptide for effective delivery of intrinsically disordered proteins*. Int J Nanomedicine. 2013. 8:2555-65.

27) Perrault, S. D.; Chan, W. C. W. *In vivo assembly of nanoparticle components to improve targeted cancer imaging*. Proc Natl Acad Sci U S A. 2010, 22;107(25):11194-9.

28) Brown, R. C.; Morris, A. P.; O'Neil, R. G. *Tight junction protein expression and barrier properties of immortalized mouse brain microvessel endothelial cells*. Brain Res. 2007, 1130,17.

29) Omidi, Y.;Campbell, L.; Barar, J.; Connell, D.; Akhtar, S. *Evaluation of the immortalised mouse brain capillary endothelial cell line, b.End3, as an in vitro blood-brain barrier model for drug uptake and transport studies.* Brain Res. 2003;990(1-2):95-112.

CHAPTER 4 Energetics of Ligand-Receptor Binding Affinity on Endothelial Cells: an In Vitro Model

4.1. Introduction

Biological signaling plays a key role in cellular uptake of molecules by receptor mediated transport (RMT) (1). This mechanism is still not well understood, but binding of a specific ligand to its corresponding receptor is believed to induce an endocytic event that triggers the formation of endocytic vesicles (2). This mechanism is widely used to promote drug passage through cells or a layer of cells such as the blood brain barrier (BBB), which is a specialized vasculature and it is considered as the main barrier in preventing molecules from reaching the brain parenchyma (3-5). In the latter case the strategy consists in conjugating the drug or the system of the drug carrier with a molecule that recognize the overexpressed receptor on the BBB (6-9). As a consequence of the binding of the specific ligand to its corresponding receptor, endocytosis takes place via membrane invagination and the formation of an intracellular vesicle, which contains receptor-ligand complexes, occurs. Then, the vesicle is shuttled to the basolateral membrane (brain-side) releasing the vesicle content into the brain parenchyma (10). Thus, a detailed characterization of the cell membranes is of fundamental importance in order to identify the overexpressed receptors in each district and design the drug targeting to the

desired site. In particular, many studies show that, in the BBB, receptors of folate (11), insulin (12), low-density lipoprotein (LDL) (13), lactoferrin (14), and transferrin (Tf) (15) are overexpressed (16). Up to now, several studies, based on the conventional analytical methods mainly involving the fluorescence (i.e. immunofluorescence microscopy, flow cytometry and immunohistochemistry), aimed to the receptor quantification (17). Nevertheless, it is widely known that fluorescence spectroscopy is a non-quantitative technique, strongly influenced by the surrounding environment. Thus, most of the developed assays provide only a relative assessment of protein level, rather than absolute quantification. In addition, imaging differences in receptor expression are often not very accurate because background fluorescence reduces precision of fluorescence intensity measurements (18). Recently, a quantification method for the determination of receptors levels, based on liquid chromatography–tandem mass spectrometry (LC–MS/MS), had been developed. This method requires a long and elaborate process (19), in particular, it requires membrane protein extraction, protein triptic digestion, choice of a stable isotope-labeled peptide as internal standard and finally a mass spectroscopy quantification that needs a highly selective detector.

Herein, we propose for the first time a rapid, simple and quantitative methodology based on Isothermal Titration Calorimetry (ITC) coupled with confluent cell layers cultured around biocompatible templating microparticles to evaluate the number of transferrin receptors (TfRs) onto the cell membrane and study the energetics of their interaction with the transferrin. Thus far, ITC has been specially used to study interactions between molecules of biological interest (i.e. proteins-proteins, nucleic

acids-proteins, small molecules-nucleic acids) and in the last years it has been successfully applied to nanosystems (20-23).

4.2. Materials and Methods

4.2.1 Cell Culture

Immortalized mouse cerebral endothelial cells, (bEnd3; American Type Culture Collection, Manassas, VA) were maintained in Dulbecco′s Modified Eagle′s Medium (DMEM) with 4.5 g/l w/o phenol red (Gibco-Thermo Fisher Scientific), supplemented with 10 % fetal bovine serum (FBS), 3.7 g/l sodium bicarbonate and 4 mM glutamine, 100U/ml penicillin and 0.1 mg/mL streptomycin, 1% non-essential aminoacids. bEnd3 cells used in all experiments from passage 21 to 30. Primary human umbilical vein endothelial cells (HUVECs; Lonza), used from passage 3 to 8, were cultured in Medium-200 (Cascade Biologics) supplemented with low serum growth supplement kit (LSGS kit) both purchased from Life Technologies of Thermo Fisher Scientific. Cells were grown at 37 °C and 5 % CO2.

4.2.2 Immunofluorescence Analysis

Transferrin receptor (TfR) expression on cell membrane was evaluated by indirect immunofluorescence. Briefly, cells seeded on 12 mm diameter glass coverslips were fixed with 4 % paraformaldehyde at room temperature (RT) and incubated overnight at 4 °C with anti-transferrin receptor polyclonal primary antibodies (Invitrogen) diluted 1:1000 in blocking buffer (0.5 % bovine serum albumin (BSA) in PBS). Then, cells were incubated 1 h, at RT with anti-rabbit secondary antibodies Alexa-488 (Invitrogen) diluted 1:1000 in the blocking buffer. Cell nuclei were stained with 4',6-diamidino-2-phenylindole blue nuclear dye (DAPI) purchased from Sigma. Samples were mounted on a glass slide and observed by confocal microscope (MP Leica TCS SP5) equipped with a 63 × oil immersion objective.

4.2.3 Cell Seeding on Cytodex Microspheres

Pyrex glass vial was coated with Sigmacote (Sigma) for 5 min before use to prevent cell adhesion on the walls. Dextran microcarrier beads (Cytodex® 3 purchesed from Sigma) were weighed in the vial and swelled with PBS for 3 h, at RT under gentle stirring. Afterwards the vial was autoclaved to prevent contamination. After sterilization, Cytodex suspension was decanted and PBS was removed to resuspend the beads at a concentration of 5 mg/ml in

cell culture medium. 2 ml of Cytodex suspension were transferred into each well of a low attachment 6-well plate (Corning). 8 × 105 cells in 100 µl of cell culture medium were added to the Cytodex in the well. In order to allow cell adhesion to the surface of the microspheres, the 6-well plate was kept under stirring at 80 rpm overnight in incubator at 37 °C and 5 % CO2. Stirring was stopped for 1 min every 15 min for the first 3 h from the seeding. After overnight incubation, 7 ml of Cytodex with adhered cells were collected and cells were fixed with 4 % paraformaldehyde for 10 min before ITC analysis. Cell adhesion on Cytodex was monitored by phase contrast microscopy. After cell seeding procedure, cell suspension was analyzed by Neubauer chamber to verify that all the seeded cells were adhered to the microspheres. Moreover, in order to further verify cell adhesion on the Cytodex microspheres, after fixation, cells were stained with Phalloidin–Tetramethylrhodamine B isothiocyanate (Phalloidin-TRITC) by Invitrogen to detect actin filaments and with DAPI to detect nuclei. Samples were observed by confocal microscope with a 10 × objective.

4.2.4 Sample Preparation

Holo-Transferrin was purchased from Sigma Aldrich, the solution was prepared by dissolving the lyophilized compound in a fresh PBS buffer

solution pH = 7.4 every time before each ITC measurement. The concentration of Tf solution was determined by UV adsorption measurements at 295 K using sequence based molar extinction coefficient values (280nm) of 85240 $M^{-1}cm^{-1}$. bEnd3 or HUVEC cells cultured on Cytodex microbeads solutions were suspended in PBS buffer solution pH = 7.4, as these systems tend to settle as sediment after few minutes, all the solutions were maintained under soft stirring conditions until the loading in the ITC cell in order to ensure homogeneity of the samples.

4.2.5 Isothermal Titration Calorimetry

ITC experiments were performed using a Nano ITC Low Volume from TA Instruments (Lindon, UT, USA) with a cell volume of 170 µl. All solutions were accurately degassed before the ITC experiments to avoid the formation of air bubbles in the calorimeter cell. The sample cell was loaded with bEnd3 or HUVEC cells cultured on Cytodex microbeads in PBS buffer solution, Tf instead was loaded into the computer-controlled microsyringe in the same buffer conditions. Injections were started after baseline stability had been achieved. Titration experiments were carried out at 298 K, 10 injections of 5 µl of Tf 1- 0.1 µM were added to the bEnd3 or HUVEC cells cultured on Cytodex microbeads (1800000 - 5600000 cells/mL) every 250 s. Control experiments were carried out to calculate the heat of dilution for Tf

in PBS solution. All the measurements were conducted at a continuous stirring rate of 250 rpm.

Raw data were obtained as a plot of heat released against time and featured as a series of peaks for each injection. The calorimetric enthalpy for each injection was calculated after correction for the heat of Tf dilution, the area under raw data peaks was integrated by the analysis software of the instrument (NanoAnalyze software, version 2.4.1 (TA Instruments)) to obtain a plot of enthalpy change per mole of injectant (Tf) against the number of TfRs per cell. From the number of cells/ml was calculated the number of cells for each experiment. The number of TfRs was calculated taking into account the moles of added Tf, until the saturation occurs, this value correspond to half of the TfRs present in the sample cell. Holo - transferrin was previously shown to bind to the receptor with a stoichiometry of one Tf molecule per TfR monomer (stoichiometry Tf-TfR 2:1) (24). Each experiment was repeated up to three-five times in order to ensure reproducibility. Integrated heat data obtained for the titrations were fitted using a nonlinear least-squares minimization algorithm to a theoretical titration curve, using NanoAnalyze software, version 2.4.1 (TA Instruments). $\Delta_b H°$ (reaction enthalpy change in kJ mol^{-1}), K_b (binding constant in M^{-1}), and n (number of binding sites) were the fitting parameters obtained by the equivalent and independent binding sites model.

The remaining thermodynamic parameters of the interaction were calculated using the following equations:

$\Delta_b G° = -RT \ln K_b$, ($R = 8.314$ J mol^{-1} K^{-1}, and $T = 298$ K)

$T\Delta_b S° = \Delta_b H° - \Delta_b G°$

The values in the Table 4.1 show the determination of average and average deviation of ITC measurements.

4.3. Results and Discussion

4.3.1 Choice of Cells and Microparticles

In this study, we use mouse brain endothelial cells (bEnd3) and primary human umbilical vein cells (HUVEC) cultured on dextran microbeads with size ranging from 67 µm to 80 µm (Cytodex) (25). The bEnd3 cells are usually used as a BBB model system due to their numerous advantages: rapid growth, formation of functional barriers, amenability to numerous molecular interventions and preservation of blood–brain barrier properties over repeated experiments (26-30).

We chose to compare bEnd3 cell line and HUVEC cells because they have different expression levels of TfR. We firstly evaluated TfR expression levels on bEnd3 and HUVEC by indirect immunofluorescence microscopy. As reported in Fig. 4.1A, bEnd3 cells showed a brighter fluorescent signal than that of HUVECs (Fig. 4.1B). These observations indicate that the TfR expression level on the membrane surface of bEnd3 is higher than that of HUVEC cells.

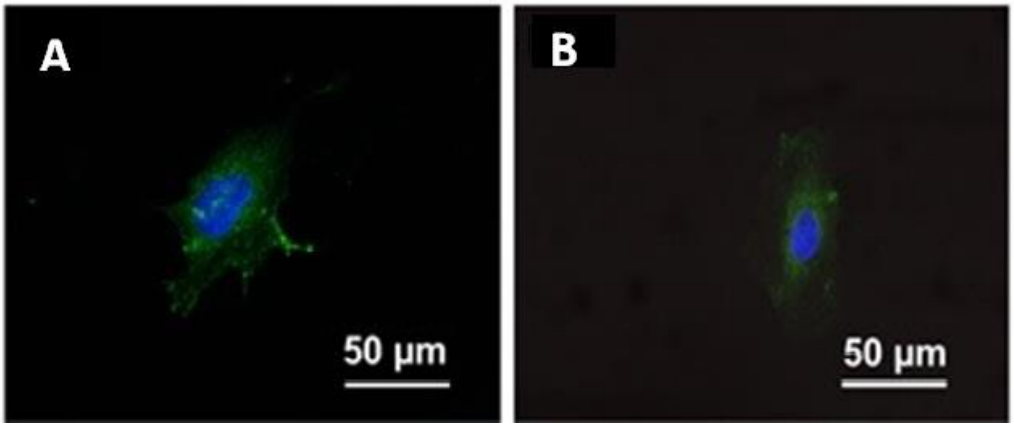

Figure 4.1 *TfR expression in bEnd3 (A) and HUVECs (B) evaluated by indirect immunofluorescence without cell permeabilization. Images were acquired by confocal miscroscope with 63 × oil immersion objective. Green fluorescence represents TfR proteins, blue fluorescence indicates cell nuclei stained with DAPI.*

4.3.2 Optimization of Cell Seeding on Cytodex Microspheres

Starting from these preliminary results, we optimized the procedure of cell seeding on Cytodex microspheres. Cytodex system allows having a higher number of cells in a small volume maintaining the correct morphology of adherent cells compared to cell suspensions obtained upon trypsin treatment. In the latter case, in fact, cells become round in shape thus losing their canonical phenotype of adherent cells. Transmitted light microscope images show Cytodex beads with a smooth surface (Fig. 4.2A). After cell seeding, the surface of Cytodex beads appears rough compared to original beads indicating the presence of the cells on it (Fig. 4.2B).

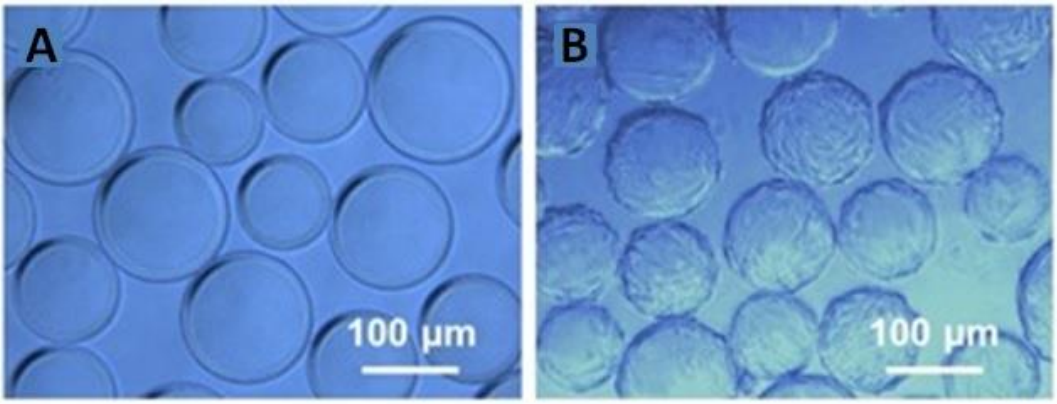

Figure 4.2 *Phase contrast microscopy micrographs of Cytodex microsphere suspension before (A) and after (B) cell seeding.*

Moreover, confocal microscopy images further confirm the presence of a confluent layer of cells on the Cytodex surface (Fig. 4.3). In particular, phalloidin staining of the actin cytoskeleton demonstrates the correct spreading of the cells (Fig. 4.3).

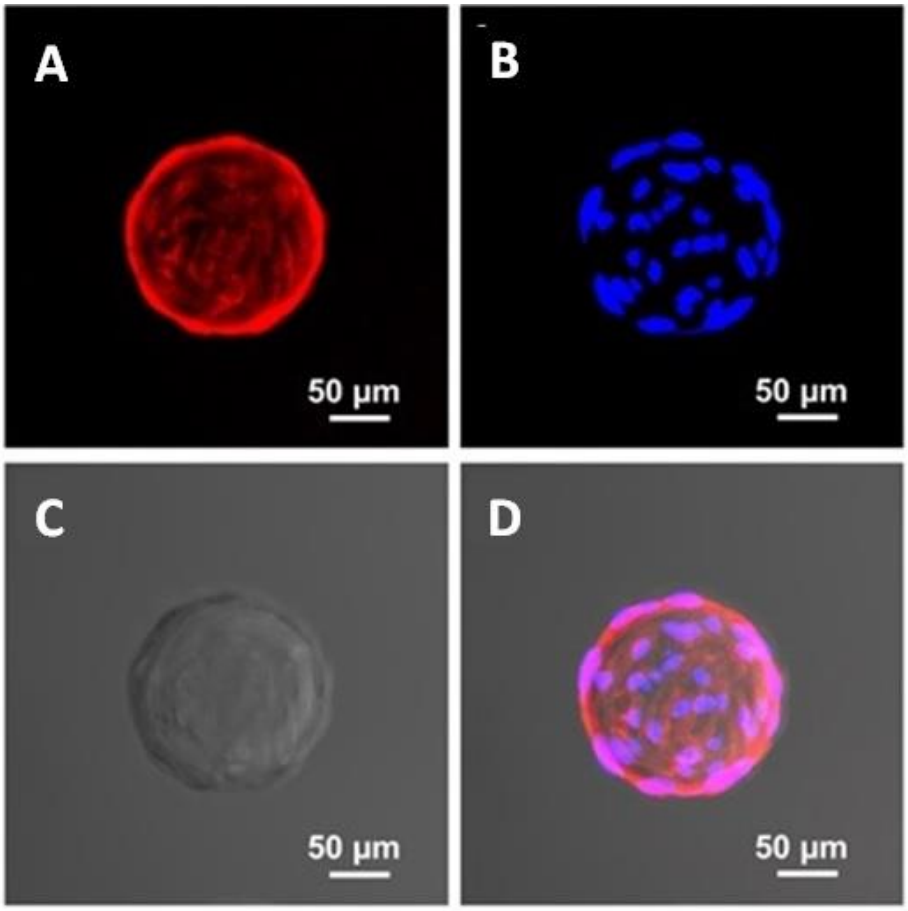

Figure 4.3 *Maximum projection of z-sectioning images obtained by confocal microscopy with 10 × objective of a Cytodex microsphere after bEnd3 cell seeding (A-D). Actin microfilaments are stained in red by Phalloidin-TRITC (A), cell nuclei are represented in blue by DAPI (B) and the Cytodex is acquired in transmitted light (B). Merge of the three channels is reported in D.*

4.3.3 Isothermal Titration Calorimetry Experiments

ITC experiments allowed us to monitor the binding between Tf and TfRs present on the cell membrane simply measuring the heat released upon molecular interactions (31). The binding curve provided the complete thermodynamic profile (i.e., binding constant (K_b), enthalpy change ($\Delta H°$), entropy change ($\Delta S°$), Gibbs energy change ($\Delta G°$)) of the interaction. Taking into account that two molecules of Tf bind to one molecule of TfR (32), the number of TfRs/cell was calculated considering the Tf moles necessary to saturate all the TfRs present in the sample and dividing for the number of loaded cells. The assessment of TfR number on cells by ITC, obtained from the specific interaction between Tf and TfR, is very important to overcome the problem of nonspecific interactions that could occur at higher Tf concentration. Indeed, most of conventional analytical methods are conducted adding an excess of Tf to the cell culture and then removing the unbinding molecules by washing (33, 34). This could provide an overestimation of receptor numbers, due to the nonspecific interactions, that is detrimental for an effective targeting action. The ITC experiments, performed by using bEnd3 and HUVEC cells cultured on Cytodex microbeads are shown in Fig. 4.4 and Fig. 4.5.

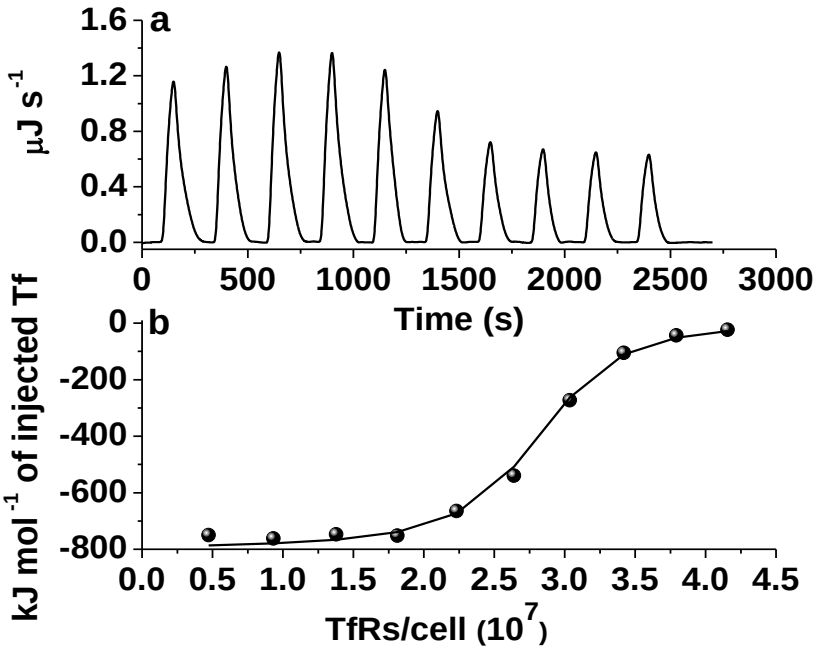

Figure 4.4 *ITC raw data for titration of Tf solution (1µM) into the solution of bEnd3 cells (1800000 cells/mL) cultured on Cytodex microbeads (a). The solid circles are the experimental data obtained by integrating the raw data and subtracting the heat of Tf dilution into the buffer. The solid line represents the best fit obtained with the independent-binding site model (b).*

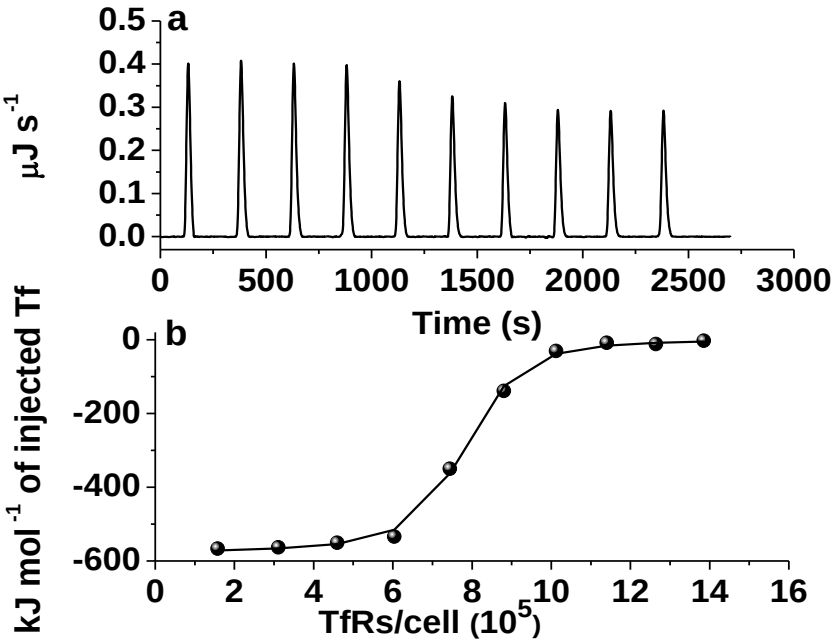

Figure 4.5 *ITC raw data for titration of Tf solution (0.1μM) into the solution of HUVEC cells (5600000 cells/mL) cultured on Cytodex microbeads (A). The solid circles are the experimental data obtained by integrating the raw data and subtracting the heat of Tf dilution into the buffer. The solid line represents the best fit obtained with the independent binding site model (B).*

ITC results showed that the binding reaction between Tf and TfRs on bEnd3 and HUVEC cells was exothermic and accomplished by an unfavorable entropy, indicating that the interaction is enthalpically driven (Table 4.1).

Table 4.1. Thermodynamic parameters of the interaction between Tf protein and TfR on bEnd3 and HUVEC cells cultured on Cytodex microbeads.

	n [a]	K_d [nM] [b]	ΔH° [kJ mol^{-1}] [c]	TΔS° [kJ mol^{-1}] [c]	ΔG°(298 K) [kJ mol^{-1}] [b]
bEnd3	$2.7\ 10^7$	3.7	-794	-746	-48
HUVEC	$4.5\ 10^5$	4.4	-575	-528	-47

a) n refers to the number of TfRs per cell; b) The experimental error for K_d and Gibbs energy is <20%; c) The experimental error for enthalpy and entropy change is < 25%.

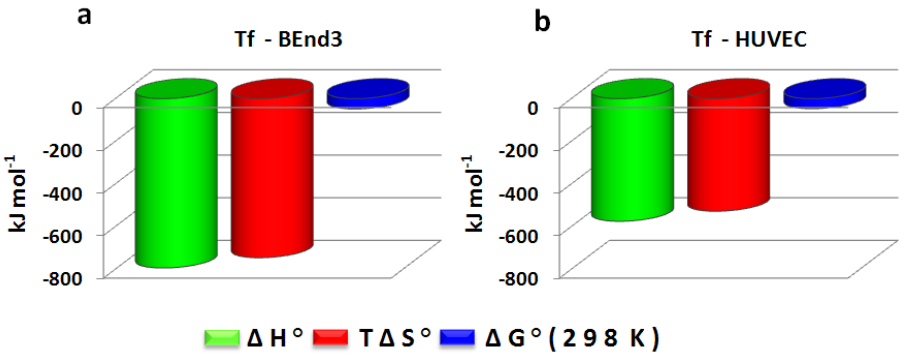

Figure 4.6 *Schematic diagram presenting the thermodynamic signature for the Tf- TfR binding on bEnd3 cells cultured on Cytodex microbeads (A) and Tf- TfR binding on HUVEC cells cultured on Cytodex microbeads (B).*

ITC experiments were also performed titrating the Tf solution into the solution of Cytodex microbeads without cells. With each injection of ligand, constant heat release was observed due only to Tf dilution, proving that it is no longer able to interact with microbeads without cell. An example of the raw ITC data is shown in Fig. 4.7.

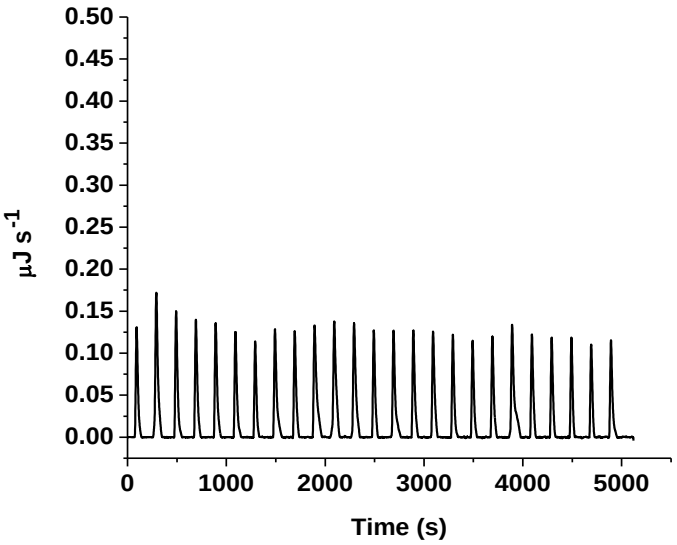

Figure 4.7 *ITC raw data for the titration of Tf solution (1µM) into the solution of Cytodex microbeads (35 mg in 1.5 mL) into PBS buffer solution.*

ITC experiments of Tf injected into free bEnd3 cells in solution without Cytodex microbeads showed irresolvable binding isotherm, with scattered points, which do not allow to evaluate the thermodynamic parameters (Fig. 4.8). These findings confirm the validity of the experiments conducted using bEnd3 and HUVEC cells cultured on Cytodex microbeads.

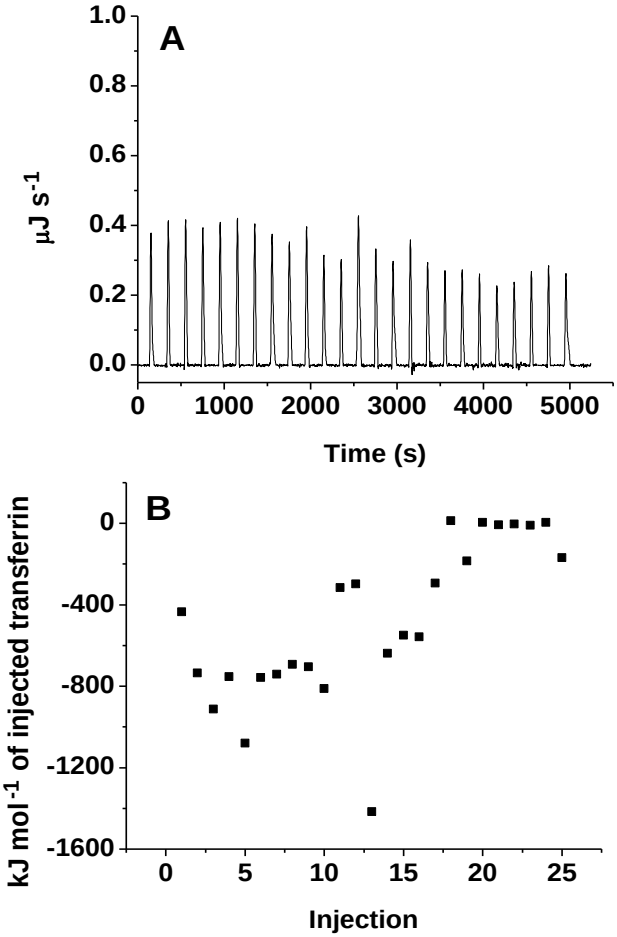

Figure 4.8 *ITC raw data for the titration of Tf solution (1µM) into the solution of 1800000 cells/ml bEnd3 cells without Cytodex microbeads (A). The solid squares are the experimental data obtained by integrating the raw data and subtracting the heat of Tf dilution into the PBS buffer solution (B).*

4.3.4 Energetics of Tf-TfRs Binding on Cells

The energetics of interactions is context-dependent, for this reason thanks to the use of Cytodex, we studied the binding in near-physiological conditions, where the TfRs are in their natural location, which is the membrane of cells residing in a continuous and confluent layer.

As shown in Table 4.1, the affinity between Tf and TfRs in both systems is very high, K_d (K_d=1⁄K_b) values are in the order of nM. Conversely, the value of TfRs/cell reveals a 100-fold increase in the number of TfRs per bEnd3 cells compared to HUVEC cells. The values in Table 4.1 show the number of receptors/cell that, divided by the Avogadro number, gives 45 attomol/cells and 0.74 attomol/cells for bEnd3 and HUVEC cells, respectively. These values are comparable with those recently obtained for TfRs on other kinds of cells, assessing the validity of our method which conversely is much more simple than the proposed quantification method based on LC-MS/MS (19). In addition, the number of receptors has never been calculated for a continuous layer of cells such as a BBB mimicking model system. Analogously, due to the lack of a realistic model, previous ITC studies even showing similar affinity (K_d~ 1nM) for the Tf-TfR interaction with just the proteins in solution provided both enthalpically and entropically driven binding, in contradiction with our findings (24). Indeed, the thermodynamic signature of the binding, i.e. the proportion by which the enthalpy and entropy contribute to the Gibbs energy, illustrated in Fig. 4.6, clearly shows that the binding is enthalpically driven for our systems. The measured enthalpy changes are the result of the formation and breakage of many interactions: protein–water and ligand-water hydrogen bonds, van der

Waals interactions, water network reorganisation near the protein surface, direct ligand-protein bonds, such as salt bridges, hydrogen bonds and van der Waals contacts, and many others. Each of these sub-contributions is attributable to non-covalent interaction contribute to measured enthalpy change, but it is not possible quantify each of them. Nevertheless, we can assume that the establishment of new interactions between interacting proteins and water network reinforcement near complex surface (favorable enthalpy) overcome the breaking of many other interactions, among these the loss of water molecules from a binding pocket (unfavorable enthalpy). However, for both the systems, the favorable enthalpic contribution is partially counterbalanced by the unfavorable entropic contribution to Gibbs energy. Consequently, the Gibbs energy is around values of a few tens of $kJmol^{-1}$. The cause lies in the thermodynamic behaviour, known as enthalpy-entropy compensation, and it is common to many receptor–ligand complexes, whose ITC thermodynamic data have been collected by Li et al. (35). Actually, the observed enthalpy-entropy compensation lies in the different structural properties of water molecules surrounding the interacting partners (36). The water contribution, indeed, is important as well as the direct interactions between the receptor and the ligand in shaping the thermodynamic signature of molecular interactions. Particularly, for binding entropy, it is known that two main contrasting terms are important, the favorable release of water due to the desolvation of the interacting groups of the proteins and unfavorable conformational rearrangements due to the loss of conformational degrees of freedom for both the interacting proteins upon binding. As our findings, show an unfavorable entropy contribution upon binding, they suggest that the latter contribution described emerges

predominant when TfRs are on the cells in contrast to a favorable entropic contribution for free proteins in solution mainly ascribable to the release of water. Finally, our thermodynamic data that relate to a more realistic model represents a suitable tool for drug design, suggesting to move toward an improvement of the conformational freedom of a potential drug upon binding, for example introducing proper structural modifications to partially overcome the penalty in entropy (37).

4.4. Conclusions

In conclusion, our methodology provides a significant advance in the cell membrane receptor quantification. To the best of our knowledge, there has been no previous study on the energetics of interaction between a receptor on the cell membrane and its ligand. In this study, a simple assay based on Isothermal Titration Calorimetry coupled with cell layers cultured around biocompatible templating microparticles has been developed to determine TfR expression in two different kind of endothelial cells. Adhesion of cells on dextran microbeads allow them to adopt their canonical phenotype of adherent cells. The new methodology gives a more accurate quantification of proteins than the conventional analytical methods and possesses several advantages. It does not utilize complex and expensive detection systems. It does not require specific labeling of the target protein with specific

fluorophores, as for immunofluorescence microscopy, flow cytometry and immunohistochemistry. In addition, the fluorescent probes often possess limited photostability and scarce emission intensity (38). Even if photostable dyes have been recently utilized (39), they are very expensive. It does not require protein extraction, digestion and isotope-labeled peptide internal standard as for other methodologies like LC-MS/MS-based targeted proteomics assay (19).

The methodology here proposed is based instead on a direct measurement of the number of receptors on the cells together with a detailed analysis of the energetics of interaction, providing complete information on receptor overexpression in a near-physiological conditions. These findings pave the way for an optimal design of new active drugs targeting towards specific tissues and shed new insights into the emerging field of nanotechnology.

Refereces

1) Parrish, K.E.; Sarkaria, J.N.; Elmquist, W.F. *Improving Drug Delivery to Primary and Metastatic Brain Tumors: Strategies to Overcome the Blood-Brain Barrier*. Clin Pharmacol Ther. 2015, 97, 336-346.

2) Khawli, L.A.; Prabhu, S. *Drug Delivery across the Blood-Brain Barrier*. Mol Pharmaceut. 2013, 10, 1471-1472.

3) Turowski, P.; Kenny, B.A. *The blood-brain barrier and methamphetamine: open sesame?* Front Neurosci-Switz. 2015, 9.

4) Cecchelli, R.; Berezowski, V.; Lundquist, S.; Culot, M.; Renftel, M.; Dehouck, M.P.; Fenart, L. *Modelling of the blood-brain barrier in drug discovery and development*. Nat Rev Drug Discov. 2007, 6, 650-661.

5) Chen, Y.; Liu, L.H. *Modern methods for delivery of drugs across the blood-brain barrier*. Adv Drug Deliver Rev. 2012, 64 640-665.

6) Staquicini, F.I.; Ozawa, M.G.; Moya, C.A.; Driessen, W.H.P.; Barbu, E.M.; Nishimori, H.; Soghomonyan, S.; Flores, L.G.; Liang, X.W.; Paolillo, V.; Alauddin, M.M.; Basilion, J.P.; Furnari, F.B.; Bogler, O.; Lang, F.F.; Aldape, K.D.; Fuller, G.N.; Hook, M.; Gelovani, J.G.; Sidman, R.L.; Cavenee, W.K.; Pasqualini, R.; Arap, W. *Systemic combinatorial peptide selection yields a non-canonical iron-mimicry mechanism for targeting tumors in a mouse model of human glioblastoma*. J Clin Invest. 2011, 121,161-173.

7) van Rooy, Mastrobattista, E.; Storm, G.; Hennink, W.E.; Schiffelers, R.M. *Comparison of five different targeting ligands to enhance accumulation of liposomes into the brain*. J Control Release. 2011, 150 30-36.

8) Mu, C.F.; Dave, N.; Hu, J.; Desai, P.; Pauletti, G.; Bai, S.H.; Hao, J.K. *Solubilization of flurbiprofen into aptamer-modified PEG-PLA micelles for targeted delivery to brain-derived endothelial cells in vitro*. J Microencapsul. 2013, 30, 701-708.

9) Zhang, P.C.; Hu, L.J.; Yin, Q.; Zhang, Z.W.; Feng, L.Y.; Li, Y.P. *Transferrin-conjugated polyphosphoester hybrid micelle loading paclitaxel for brain-targeting delivery: Synthesis, preparation and in vivo evaluation.* J Control Release. 2012, 159, 429-434.

10) Lajoie, J.M.; Shusta, E.V. *Targeting receptor-mediated transport for delivery of biologics across the blood-brain barrier*. Annu Rev Pharmacol. 2015, 55, 613-631.

11) Wu, D.F.; Pardridge, W.M. *Blood-brain barrier transport of reduced folic acid.* Pharm Res-Dordr. 199, 16, 415-419.

12) Frank, H.J.; Pardridge, W.M.; Jankovic-Vokes, T.; Vinters, H.V.; Morris, W.L. *Insulin binding to the blood-brain barrier in the streptozotocin diabetic rat*. J Neurochem. 1986, 47 405-411.

13) Dehouck, B.; Fenart, L.; Dehouck, M.P.; Pierce, A.; Torpier, G.; Cecchelli, R. *A new function for the LDL receptor: Transcytosis of LDL across the blood-brain barrier*. J Cell Biol. 1977, 138, 877-889.

14) Fillebeen, C.; Descamps, L.; Dehouck, M.P.; Fenart, L.; Benaissa, M.; Spik, G.; Cecchelli, R.; Pierce, A. *Receptor-mediated transcytosis of lactoferrin through the blood-brain barrier*. J Biol Chem. 1999, 274, 7011-7017.

15) Descamps, L.; Dehouck, M.P.; Torpier, G.; Cecchelli, R. *Receptor-mediated transcytosis of transferrin through blood-brain barrier endothelial cells*. Am J Physiol. 1996, 270,1149-1158.

16) Chang, J.; Jallouli, Y.; Kroubi, M.; Yuan, X.B.; Feng, W.; Kang, C.S.; Pu, P.Y.; Betbeder, D. *Characterization of endocytosis of transferrin-coated PLGA nanoparticles by the blood-brain barrier.* Int J Pharmaceut. 2009, 379, 285-292.

17) Brockhoff, G.; Hofstaedter, F.; Knuechel, R. *Flow cytometric detection and quantitation of the epidermal growth factor receptor in comparison to Scatchard analysis in human bladder carcinoma cell lines*. Cytometry. 1994, 17, 75-83.

18) Waters, J.C. *Accuracy and precision in quantitative fluorescence microscopy.* J Cell Biol. 2009, 185, 1135-1148.

19) Yang, T.; Xu, F.; Zhao, Y.; Wang, S.; Yang, M.; Chen, Y. *A liquid chromatography-tandem mass spectrometry-based targeted proteomics approach for the assessment of transferrin receptor levels in breast cancer*. Proteomics Clin Appl. 2014, 8 (2014) 773-782.

20) Fotticchia, I.; Fotticchia, T.; Mattia, C.A.; Netti, P.A.; Vecchione, R.; Giancola, C. *Thermodynamic signature of secondary nano-emulsion*

formation by isothermal titration calorimetry. Langmuir. 2014, 30, 14427-14433.

21) Mertins, O.; Dimova, R. *Binding of chitosan to phospholipid vesicles studied with isothermal titration calorimetry*. Langmuir. 2011, 27, 5506-5515.

22) Petraccone, L.; Fotticchia, I.; Cummaro, A.; Pagano, B.; Ginnari-Satriani, L.; Haider, S.; Randazzo, A.; Novellino, E.; Neidle, S.; Giancola, C. *The triazatruxene derivative azatrux binds to the parallel form of the human telomeric G-quadruplex under molecular crowding conditions: biophysical and molecular modeling studies*. Biochimie. 2011, 93, 1318-1327.

23) Di Maro, S.; Zizza, P.; Salvati, E.; De Luca, V.; Capasso, C.; Fotticchia, I.; Pagano, B.; Marinelli, L.; Gilson, E.; Novellino, E.; Cosconati, S.; Biroccio, A. *Shading the TRF2 recruiting function: a new horizon in drug development*. J Am Chem Soc. 2014, 136, 16708-16711.

24) Bou-Abdallah, F.; Terpstra, T.R. *The thermodynamic and binding properties of the transferrins as studied by isothermal titration calorimetry*. Biochim Biophys Acta. 2012, 1820, 318-325.

25) AD Cell culture Cytodex 1, Cytodex 3, GE Healthcare, 18,60.

26) Guarnieri, D.; Torino, E.; Vecchione, R.; Netti, P.A. Conference on Colloidal Nanoparticles for Biomedical Applications X, in: W.J. Parak, M. Osinski, X.J. Liang (Eds.) Proceedings of SPIE, SPIE-International Society for Optical Engineering, San Francisco, CA, USA, 2015, pp. 2-10

27) Guarnieri, D.; Muscetti, O.; Netti, P.A. *A method for evaluating nanoparticle transport through the blood-brain barrier in vitro*. Methods Mol Biol. 2014, 1141, 185-199.

28) Guarnieri, D.; Falanga, A.; Muscetti, O.; Tarallo, R.; Fusco, S.; Galdiero, M.; Galdiero, S.; Netti, P.A. *Shuttle-mediated nanoparticle delivery to the blood-brain barrier.* Small. 2013, 9 853-862.

29) Brown, R.C.; Morris, A.P.; O'Neil, R.G. *Tight junction protein expression and barrier properties of immortalized mouse brain microvessel endothelial cells*. Brain Res. 2007, 1130, 17-30.

30) Montesano, R.; Pepper, M.S.; Mohle-Steinlein, U.; Risau, W.; Wagner, E.F.; Orci, L. *Increased proteolytic activity is responsible for the aberrant morphogenetic behavior of endothelial cells expressing the middle T oncogene.* Cell. 1990, 62, 435-445.

31) O'Brien, R.; Haq, I. Applications of Biocalorimetry: *Binding, stability and enzyme kinetics*. Ladbury, J.E.; Doyle M.L. Biocalorimetry 2: Applications of Calorimetry in the Biological Sciences, John Wiley & Sons, Chichester, West Sussex, England, 2004, pp. 3-31.

32) Lawrence, C.M.; Ray, S.; Babyonyshev, M.; Galluser, R.; Borhani, D.W.; Harrison, S.C. *Crystal structure of the ectodomain of human transferrin receptor*. Science. 1999, 286 779-782.

33) Ciechanover, A.; Schwartz, A.L.; Lodish, H.F. *The asialoglycoprotein receptor internalizes and recycles independently of the transferrin and insulin receptors.* Cell. 1983, 32, 267-275.

34) Nuciforo, P.; Radosevic-Robin, N.; Ng, T.; Scaltriti, M. *Quantification of HER family receptors in breast cancer*. Breast Cancer Res. 2015, 17, 53.

35) Li, L.; Dantzer, J.J.; Nowacki, J.; O'Callaghan, B.J.; Meroueh, S.O. PDBcal: a comprehensive dataset for receptor-ligand interactions with three-dimensional structures and binding thermodynamics from isothermal titration calorimetry. Chem Biol Drug Des. 2008, 71, 529-532.

36) Breiten, B.; Lockett, M.R.; Sherman, W.; Fujita, S.; Al-Sayah, M.; Lange, H.; Bowers, C.M.; Heroux, A.; Krilov, G.; Whitesides, G.M. *Water networks contribute to enthalpy/entropy compensation in protein-ligand binding*. J Am Chem Soc. 2013, 135, 15579-15584.

37) Garbett, N.C.; Chaires, J.B.*Thermodynamic studies for drug design and screening*. Expert Opin Drug Discov. 2012. 7, 299-314.

38) Shaner, N.C.; Lin, M.Z.; McKeown, M.R.; Steinbach, P.A.; Hazelwood, K.L.; Davidson, M.W.; Tsien, R.Y. *Improving the photostability of bright monomeric orange and red fluorescent proteins*. Nat Methods. 2008, 5, 545-551.

39) Sakamoto, S.; Kawabata, H.; Masuda, T.; Uchiyama, T.; Mizumoto, C.; Ohmori, K.; Koeffler, H.P.; Kadowaki, N.; Takaori-Kondo, A. *H-Ferritin is preferentially incorporated by human erythroid cells through transferrin receptor 1 in a threshold-dependent manner*. Plos One. 2015, 10, 0139915.

CHAPTER 5 Preliminary Characterization of O/W Nanoemulsions Electrostatically Bioconjugated

5.1 Introduction

Nowadays, cancer is one of the leading causes of death, in particular American Cancer Society estimates that one in 4 deaths in the United States is due to cancer (1). As already said, nanocarriers (NCs) for the delivery of drugs are attracting increasing research interest due to their capability to carry a wide range of compounds and to release them in the ill cells/organs (2-5). We extensively discussed about the fact that accumulation of NCs in the ill tissue is due to a spontaneous phenomenon called passive targeting or "Enhanced Permeability and Retention" (EPR) coming from a damaging of the vessel walls surrounding an inflamed or tumor region (6-9). However, in the case of blood brain vessels they tend to keep their impermeable feature even in the presence of a tumor (10). Recently great attention has been forwarded to the nineteen residues peptide gH625, a membrane-perturbing domain in the glycoprotein gH of Herpes simplex virus type I (11-15). In particular, it was verified that gH625 conjugation enhances nanoparticles transport across the BBB, thereby enhancing the central nervous system (CNS) bioavailability of a possible drug (16).

Nowadays the scientific community is making great efforts to improve cancer management trying to simplify as much as possible the preparation

procedure of the nanocarriers. To this aim, since in vitro studies conducted on gH625 decorated O/W NCs showed good results (chapter 3), herein an easy electrostatic strategy has been proposed to bind gH625 on the external surface of polymeric nanocapsules prepared via layer by layer using an O/W nanoemulsion as template (17).

The peptide was synthetized in a novel way with a tail of six charged amino acids which confers the peptide electrostatic proprieties and so the possibility to be bound using the layer by layer's main principle. Peptide deposition was followed by analyzing surface charge through ζ-potential measurements in combination with ITC analysis as a fine method which also provides thermodynamic information on the peptide coating.

5.2 Materials and Methods

5.2.1 Nanocapsules Preparation

First, a 20 wt % oil in water pre-emulsion (130-140 nm, ∼−30 mV, pH 4.3) was prepared by dissolving the surfactant (egg lecithin) in the oil phase (soybean) and adding all to the aqueous phase. The pre-emulsion was then homogenized by a high-pressure homogenizer (110P series microfluidizer) to obtain the final nano-emulsion (18). The first positively charged layer of poly-L-lysine-FITC (PLL-FITC) was obtained by adding in one shot the polymer solution to the emulsion solution under vigorous stirring (1500 rpm). The SNE was 0,0125 wt% of PLL and 1 wt% of oil. The right amount of polymer coating was previously discussed (19). The second negatively charged layer (heparin) was obtained in the same way by adding the

negatively charged polymer, heparin, to the positively charged SNE; final heparin concentration was 0,009375 wt%. At the same way the PLL-FITC third layer was obtained by adding the polymer solution into the bilayer nanocapsules solution, it was 0,02812% of PLL-FITC. Whereas the bilayer constituted by hyaluronic acid (HA) on PLL was obtained by adding a solution of HA to the PLL SNE under stirring; in the final preparation HA was 0,0156 wt%. Poly-L-lysine (PLL, 4−19 kDa) and heparin sodium salt from porcine intestinal mucosa (Hep, 18000 kDa) were purchased from Sigma-Aldrich.

The polymeric nanocapsules were characterized measuring size and ζ-potential by dynamic light scattering (Malvern Zetasizer). In the ζ-potential measurement a voltage gradient is applied across a pair of electrodes of the cell containing the particle dispersion. Charged particles are attracted to the oppositely charged electrode, and their velocity can be measured and expressed in unit field strength as an electrophoretic mobility. ζ-potential measures were conducted in the same way described in chapter 3. The diluted samples were poured into disposable cells, and the ζ-potential was determined at least 3 times for each sample at 25 °C. Size measurements were also performed by a Malvern Zetasizer. In particular, the particle size distribution was measured by laser DLS (λ= 632.8 nm). This technique correlates the fluctuations of scattered light intensity I(t) during time with the Brownian motion of colloidal particles associated with the diffusion coefficient D, which is related to the hydrodynamic radius Rh of the particles. A detecting angle of 173° was used. All samples were diluted up to a droplet concentration of approximately 0.025 wt % using Milli-Q water.

5.2.2 Peptide Synthesis

gH625 peptide was synthesized in a modified version, with a spacer of three glycines and a tail of six lysines at the C-terminal (gH625(6K)) in the first case. In the second case it was added a tail of six glutamic acids (gH625(6E)). It was employed the solid-phase method and standard Fmoc strategies. Rink-amide resin (substitution 0.48 mmol/g) was used as solid support. Activation of amino acids was achieved using 2-(1H-Benzotriazole-1-yl)-1,1,3,3-tetramethyluroniumhexafluorophosphate: hydroxybenzotriazole: N,N-diisopropylethylamine (HBTU/HOBt/DIEA) (1 : 1 : 2). All couplings were performed for 15 min and deprotections for 10 min. All the synthesis were conducted under Mw treatment. Peptides were removed from the resin, after acetylation step, by treatment with a TFA/TIS/H2O (90 : 5 : 5, v/v/v) mixture for 90 min at room temperature, then, crude peptide was precipitated in cold ether, dissolved in a water/acetonitrile (1:1, v/v) mixture, and lyophilized. Products were purified by RP-HPLC applying a linear gradient of 0.1% TFA in CH3CN/ 0.1% TFA in water from 15% to 75% over 25 min using a semipreparative 10 x 100 mm C18 column at flow rate of 5 mL/min. Peptides purity and identity were confirmed by LC-MS (Agilent 6530 Accurate-Mass Q-TOF LC/MS spectrometer). Purified peptide was lyophilized and stored at 4 °C until use. Reagents for peptide synthesis (Fmoc-protected amino acids, resins, activation, and deprotection reagents) were from Iris Biotech GMBH. Solvents for peptide synthesis and HPLC analyses were from Sigma Aldrich; reversed phase columns for peptide analysis were supplied from Waters. Solid phase peptide synthesis was performed on a fully automated

multichannel peptide synthesizer Biotage. Preparative RP-HPLC was carried out on a Waters 600 Controlled, equipped with a Waters 2489 UV/Visible detector and with a Waters C18 column (10 x 100 mm, 5 µm).

5.2.3 Isothermal Titration Calorimetry Analysis

Isothermal titration calorimetry (ITC) experiments were performed using a Nano ITC Low Volume from TA Instruments (Lindon, UT, USA) with a cell volume of 170 µl. Titration experiments were carried out at 25 °C. Two set of experiments were performed: in the first experiment 10 injections of 5 µl each of gH625(6K) solution (145,7 µM) were added to the nanocapsules solution (5,2 µM of heparin, 0,5% oil) every 250 s at a continuous stirring rate of 250 rpm, in the second experiment 10 injections of 5 µl each of gH625(6K) solution (3084 µM) were added to the nanocapsules solution (5,2 µM of Heparin, 0,5% oil) in order to test higher ratios .Control experiments were carried out to calculate the heat of dilution for gH625(6K). The binding constant (K_b), enthalpy change ($\Delta_b H°$), and stoichiometry of the interaction process were obtained by fitting the binding isotherm to the equivalent and independent binding sites model, by using the NanoAnalyze software, version 2.4.1 (TA Instruments). The remaining thermodynamic parameters of the interaction were calculated using the relationships:

$\Delta_b G° = -RT\ln K_b$

$\Delta_b G° = \Delta_b H° - T\Delta_b S°$

where $\Delta_b G°$ is the binding free-energy change, $\Delta_b H°$ is the binding enthalpy change, $\Delta bS°$ is the binding entropy change, R is the gas constant (R = 8.314 J mol^{-1} K^{-1}), and T is the temperature in Kelvin (T = 298 K).

5.2.4 Circular Dicroism Analysis

Circular dichroism (CD) spectra were recorded on a Jasco 1500 circular dichroism spectrophotometer (Easton, US) in a 0,2 cm path length cuvette and the wavelength was varied from 260 to 190 nm. The spectra were recorded with a response of 4 s at 2.0 nm bandwidth and normalized by subtraction of the background scan with buffer for peptide in solution spectra and with nanocapsules solution for peptide on nanocapsules spectra. The oligonucleotide concentration was 9,8 μM.

5.2.5 Confocal Microscopy

For the confocal microscopy a treatment of the willCo dish was performed with a solution of Poly-L-lysine (4-15 kDa) 1mg/ml for ten minutes and then washed two times with Milli-Q water. The sample was diluted up to an oil concentration of 0.001 wt % using Milli-Q water and leaved in the dish for 30 minutes, then one part and half of the diluted sample was substituted with a solution of 1,4-diazobiciclo-(2.2.2)-benzeneoctane 5 wt % (in water). Confocal microscopy was performed with a confocal laser-scanner microscope SP5 Leica. The lambda of the argon ion laser was set at 488 nm. Fluorescence emission was revealed by band pass 500–530. 1,4-diazobiciclo-(2.2.2)-benzeneoctane and WillCo dishes were respectively from Sigma Aldrich and WillCo Wells B.V.

5.3 Results and Discussion

The polymeric bilayer nanocapsules (Hep/PLL) on oil core were prepared at the saturation polymer concentration for each layer and characterized by confocal microscopy (Fig. 5.1) and DLS (Fig. 5.2). Confocal imagine showed a good monodispersity of the colloidal system and absence of aggregate in accordance with DLS data which showed an hydrodynamic diameter of 144,3 nm, a polydispersity index of 0,071, and a ζ –potential of

-44,4 mV for the bilayer (Hep/PLL) NCs. In particular, in Fig. 5.2 they are shown hydrodynamic diameter and ζ-potential data of the nanocapsules during the three steps of preparation: O/W NE, poly-L-lysine-FITC monolayer, Hep/PLL bilayer. An increase of almost 10 nm in the size was observed coating the O/W NE with the first layer of polymer (poly-L-lysine), whereas no increase in the diameter was observed coating with the second layer of polymer (heparin), probably due to a better compaction of the polymeric chains on the oil droplets.

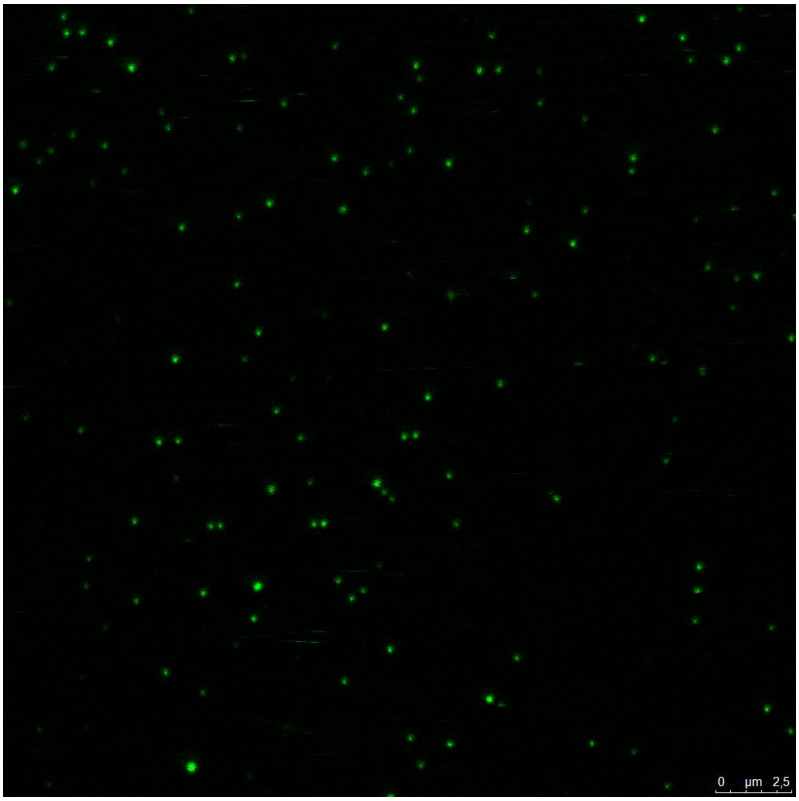

Figure 5.1 *Confocal microscope images of nanocapsules with a double layer of polymer (heparine on poly-L-lysine) on oil core. Scale bar is 2,5 µm.*

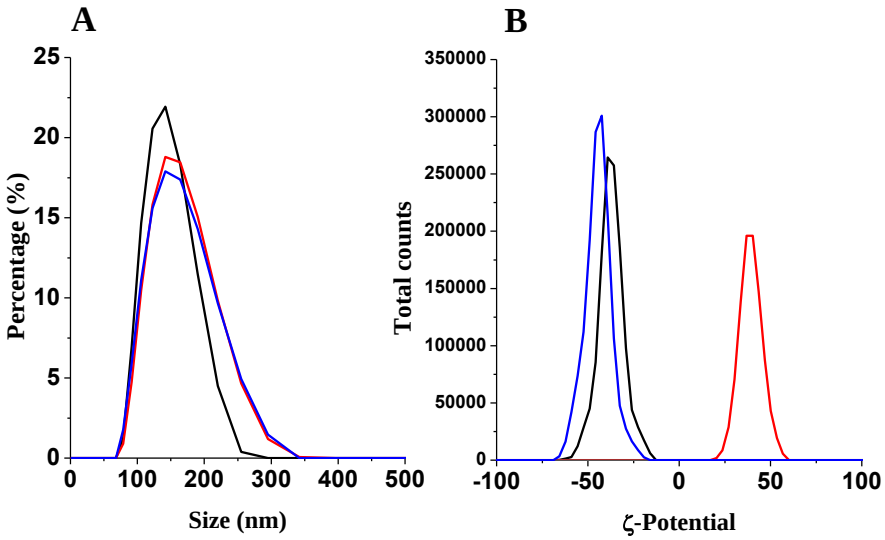

Figure 5.2 *Size (A) and ζ –potential (B) data of O/W NE in black (Size:134 nm, PDI:0,034, ζ –potential: -37,3 mV) monolayer of PLL in red (Size: 146,7 nm, PDI: 0,063, ζ –potential:38,8 mV) and the bilayer of heparin in blue (Size:144,3, PDI: 0,071, ζ –potential -44,4mV).*

The peptide gH625 was synthetized in a modified version with six residues of lysines at the C-terminal (gH625(6K)) which are positively charged at the pH of the polymeric bilayer nanocapsules solution (pH=7) and able to bind the negatively charged surface of heparin through electrostatic interaction exploiting the main principle of layer by layer methodology (Fig. 5.3). Further, a spacer of three glycines was added between the tail and the peptide in order to confer the peptide the possibility to acquire its conformation. In Fig. 5.4 is shown the UV spectrum followed at 220 nm of the Analytical RP-HPLC of the purified peptide.

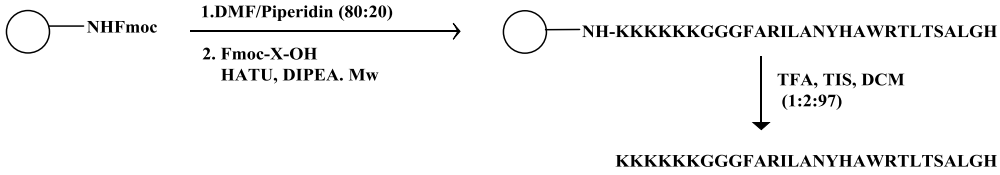

Figure 5.3 *Strategy of synthesis of gH625(6K) on solid phase.*

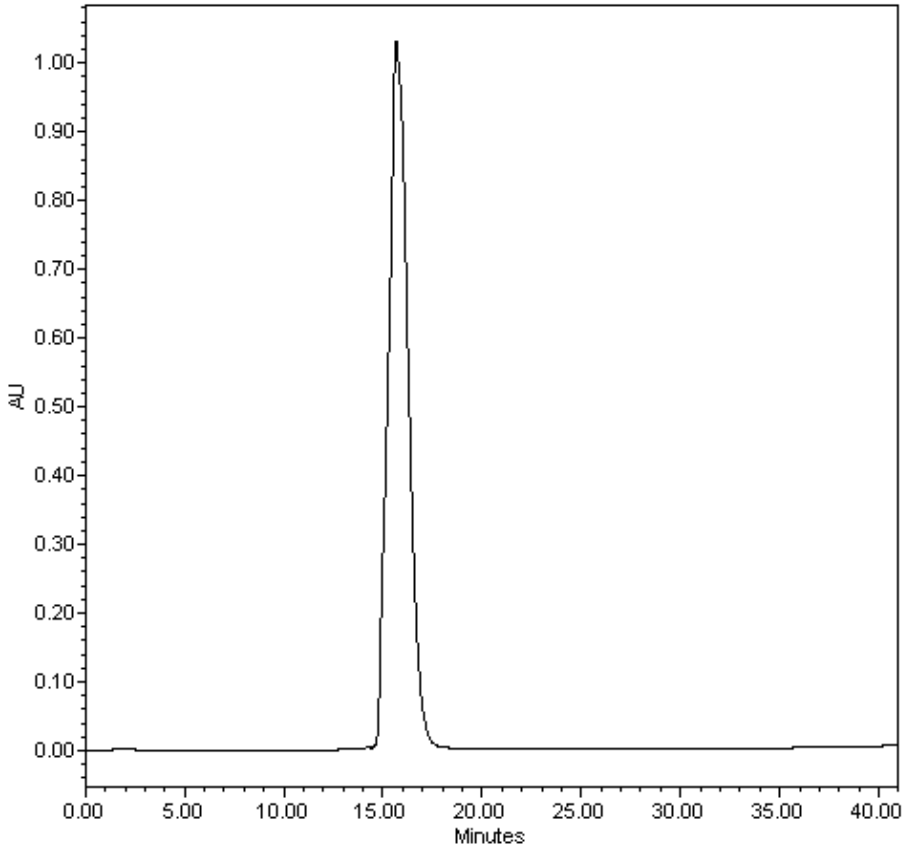

Figure 5.4 *UV profile (220 nm) of the RP-HPLC of the pure peptide gH625(6K).*

In the described conditions only the lysine's tail of the peptide is fixed on the nanocapsules, whereas the functional part is free to assume its conformation and explicate its action when in contact with cell membrane's phospholipids. CD spectra showed an unchanged conformation of the peptide when on the nanoparticles (Fig. 5.5), proving that only the peptide's electrostatic tail interacts with the nanoparticles, the rest of the peptide remains in solution free to assume its conformation.

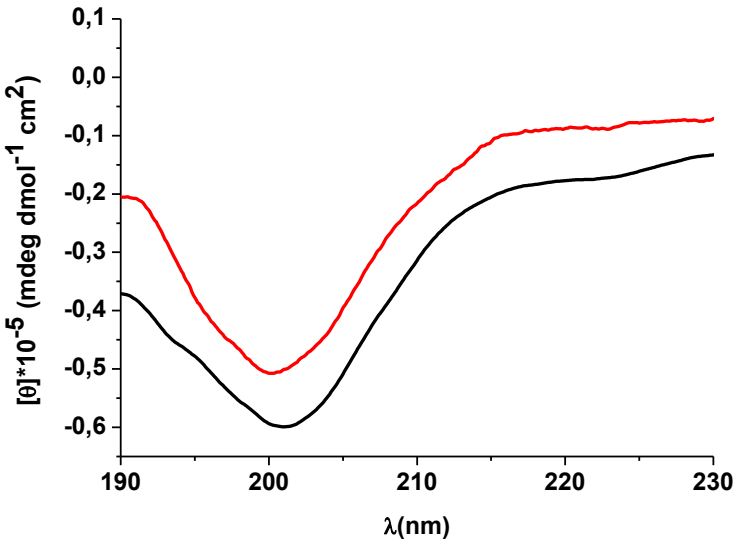

Figure 5.5 *CD spectra of the peptide in solution (red) and the peptide attached to the nanocapsules (black).*

To better explore the peptide deposition at different concentrations, it was performed a ζ-potential curve in relation to the ratio (w/w) between the

peptide and the outermost polymer layer. The ζ-potential of the bilayer nanocapsules was negative in absence of peptide which is due to the presence of carboxylic acid groups on the chains of the outermost layer of heparin. When the peptide concentration was increased, the ζ-potential initially became increasingly less negative, with a point of zero charge at around R=1,34, and reached a plateau for higher concentrations at R=16 (Fig. 5.7A). The functionalized nanocapsules resulted to have good values of size and PDI at the concentrations of peptide that gave the nanoparticles a charge minor of -6 (R<0,9) and major of +6 (R>2). Isothermal titration calorimetry analysis allowed to monitor the interaction between the negatively charged nanoparticles and the peptide's positively charged tail from a thermodynamic point of view. In order to test a wide range of concentrations of the peptide interacting with the nanoparticles two experiments were designed. In the first experiment ratios (peptide/heparin % w/w) from 0,149 to 1,49 were tested (Fig. 5.6) whereas, in the second experiment ratios were from 3 to 30 (Fig. 5.7B). In both cases low raw heat rate (μJ/sec) were registered at each injection proving that nonspecific electrostatic interactions are occurring. In the first experiment they were observed a nonspecific interaction between the peptide and the nanocapsules from ratio 0,14 to 0,74 and anomalous peaks without a significant trend from ratio 0,89, showing a destabilization of the nanocapsules due to a charge too near to zero, as already seen from DLS (Fig. 5.7A). From the second experiment it was possible to observe the right R at which the nanoparticles are saturated by means of the peptide, these data were fitted by an "independent site model" (Fig. 5.7B).

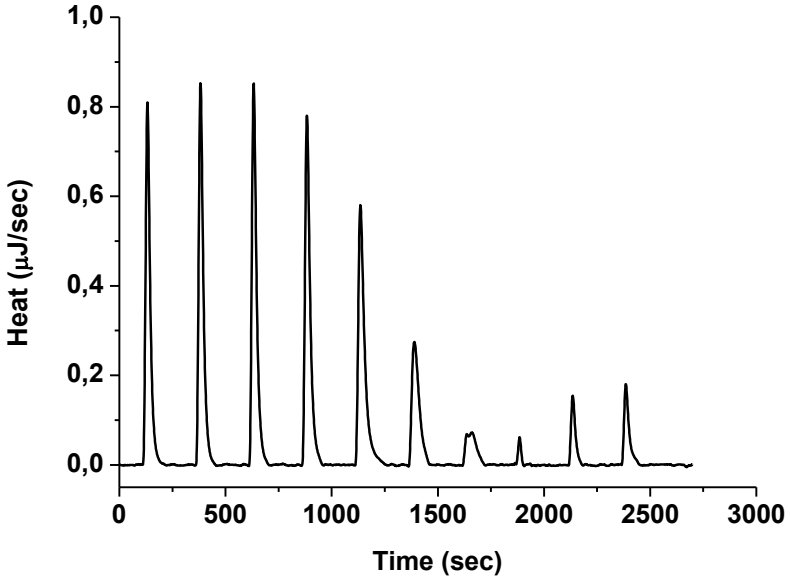

Figure 5.6 *ITC raw data for the titration of gH625 solution (145,7 μM) into the solution of Hep/PLL bilayer nanocapsules 0,5% oil.*

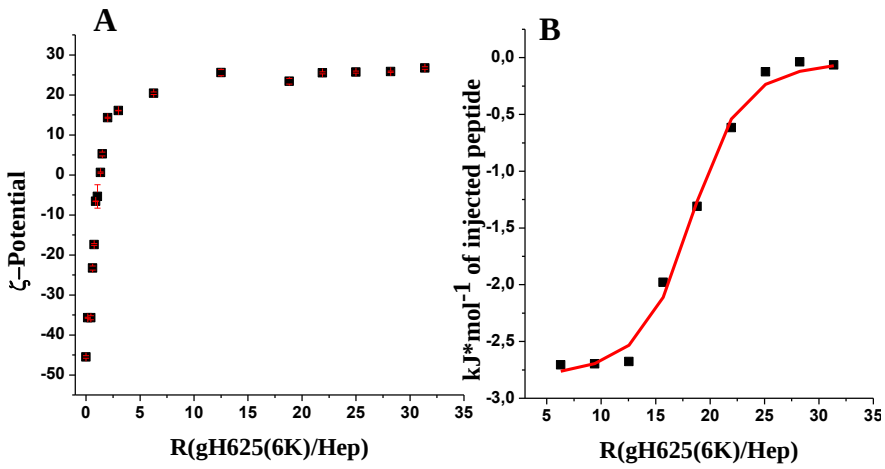

Figure 5.7 *ζ –potential curve of the functionalized nanoparticles in relation to the ratio between the peptide and the heparin (w/w)(A.) ITC data for titration by stepwise injection of gH625(6K) into nanocapsules solution 0,009375% heparin and 0,5% oil at 25 °C. The solid squares are the experimental data obtained by integrating the raw data and subtracting the heat of gH625(6K) dilution into the buffer. The red lines represent the best fit obtained with the independent-site model (B).*

From the data of the second ITC experiment emerged that the binding event is exothermic ($\Delta H° = -2,85$ kJ*mol^{-1}) and is accomplished by a favorable entropy ($T\Delta S° = 25,75$ kJ*mol^{-1}), indicating that it is entropically driven, probably because of the release of ordered water by the hydration shells around the positive and negative charges in disordered bulk water (20,21). In the complex the binding event between the peptide and the outermost polymer is a spontaneous phenomenon ($\Delta G° = -28,60$ kJ*mol-1). The low

binding constant (K_b=1,04*10^5) is a demonstration that non-specific interactions like electrostatic are occurring.

It appeared clearly that from $R_{pep/Hep}$ 0,14 to 0,89 the peptide interacts with the nanocapsules without altering their stability. Conversely, from ratio 0,89 the amount of attached peptide was such to reduce the negative charge of the nanocapsules and cause destabilization. This destabilization stopped at ratio 2 where the nanocapsules charge became enough positive to confer them the right stability.

In a first instance we conducted in vitro studies on the NCs of Hep/PLL (R=1,5), pep/Hep (R=0,4). Anyway, these studies did not show a difference of cellular uptake from functionalized and no-functionalized nanoparticles probably due to the low degree of conjugation. Then, we increased the amount of peptide testing NCs of Hep/PLL (R=1,5), pep/Hep (R=1,2). In this case to avoid the NCs destabilization (ζ –potential near to zero) it was necessary to complete the NCs saturation with PLL, adding the amount of polymer able to switch the charge to positive (~30) ($R_{PLL/Hep}$=2,2, $R_{pep/Hep}$=1,2).

In other words, we prepared positively charged nanocapsules whose saturation of the last positively charged layer of poly-L-lysine was completed with gH625(6K). In particular the heparin bilayer nanocapsules were covered by a layer of poly-L-lysine at a concentration ($R_{PLL/Hep}$=2,2) that doesn't completely cover the last layer of heparin; then the saturation was completed by gH625(6K) ($R_{pep/Hep}$ =1,2). As control saturated trilayer nanocapsules (PLL/Hep/PLL) were realized (Fig. 5.8). In Fig. 5.9 a

schematic representation of the preparation of the just mentioned nanocapsules is shown.

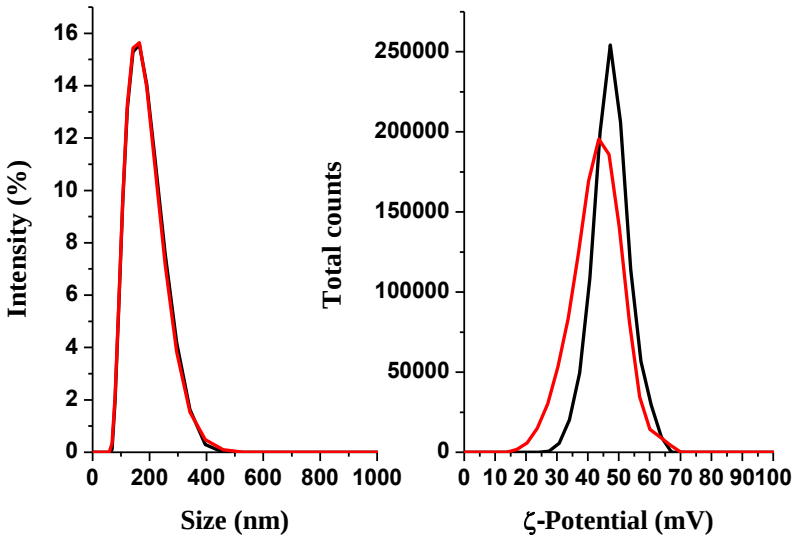

Figure 5.8 *Size (A) and ζ –potential (B) data of the trilayer PLL/Hep/PLL (Size:152,0 nm, PDI:0,091, ζ –potential: -48,2 mV) (black)and the trilayer with gH625(6K)(Size: 150,2 nm, PDI: 0,109, ζ –potential:43,2 mV) (red).*

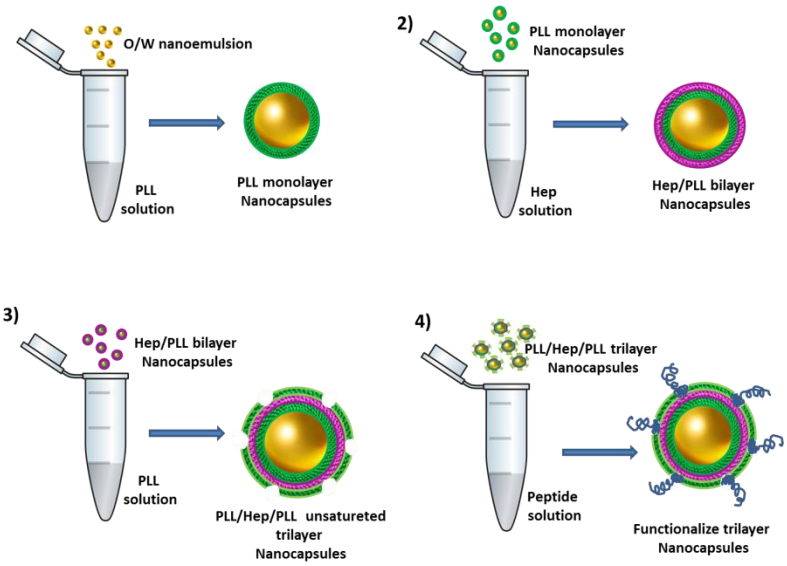

Figure 5.9 *Schematic representation of preparation of the functionalized trilayer nanocapsules. 1) The O/W nanoemulsion solution was added one shot to a solution of poly-L-lysine under stirring obtaining poly-L-lysine monolayer nanocapsules. 2) The poly-L-lysine monolayer nanocapsules solution was added one shot to a solution of heparine under stirring obtaining heparin/poly-L-lysine bilayer nanocapsules. 3) The heparin/poly-L-lysine bilayer nanocapsules solution was added one shot to a solution of poly-L-lysine (at a lower concentration of saturation) under stirring obtaining unsaturated poly-L-lysine/heparin/poly-L-lysine nanocapsules. 4) The poly-L-lysine/heparin/poly-L-lysine bilayer nanocapsules solution was added to a solution of the peptide obtaining functionalized nanoparticles.*

Also in this case in vitro studies did not show difference between NCs with and without the peptide. Probably the high interaction of PLL with cells membrane did not allow to appreciate the difference of uptake, further it was not possible to test NCs with a higher degree of functionalization due to a destabilization in the culture medium.

Therefore, we moved to the same peptide with a negatively charged tail of six residues of glutamic acid (gH625(6E)). In Fig. 5.10 is shown the UV spectrum followed at 220 nm of the Analytical RP-HPLC of the purified peptide.

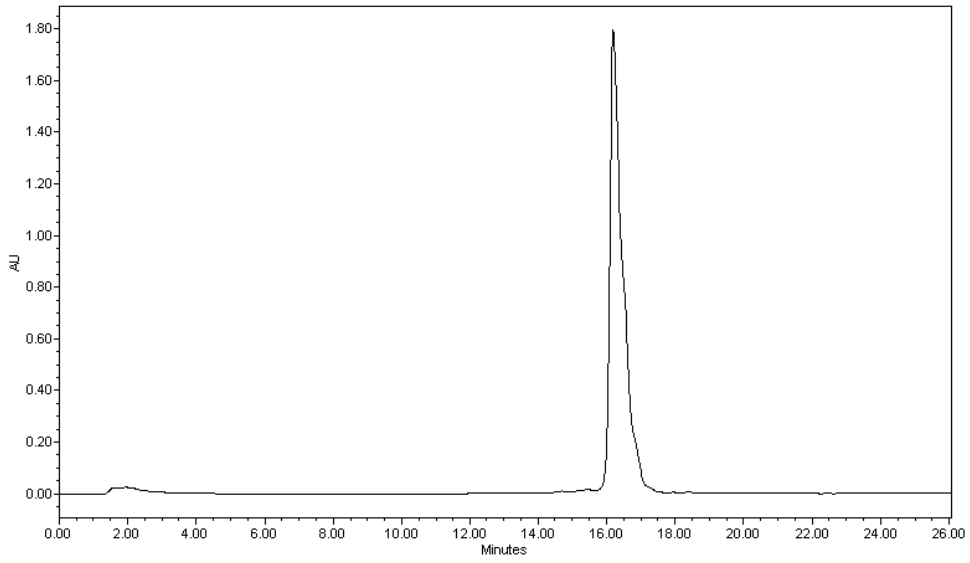

Figure 5.10 *UV profile (220 nm) of the RP-HPLC of the pure peptide gH625(6E).*

In this case the peptide was bound to PLL NCs (Pep/PLL=0,85) and the saturation was completed with HA (HA/PLL=2,5). In Fig. 5.11 data of size and ζ -potential of the just mentioned nanoparticles are represented. Experiments of uptake will be carried out to assess a difference in uptake between control and HA/PLL NCs bound to gH625 peptide by the proposed electrostatic strategy.

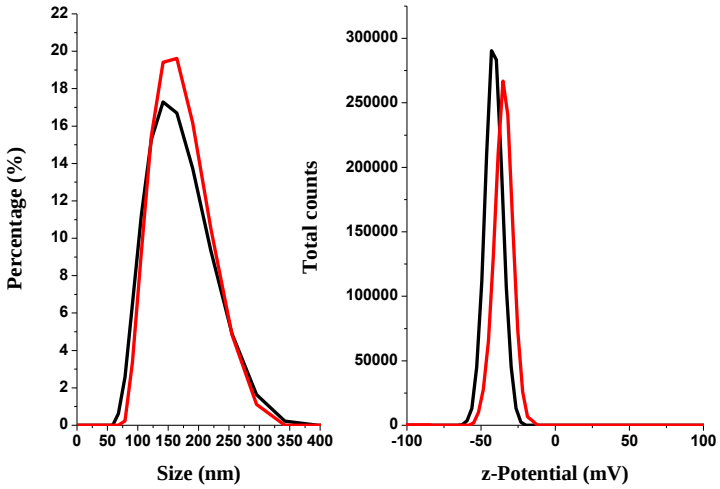

Figure 5.11 *Size (A) and ζ –potential (B) data of the bilayer HA/PLL (Size:149,2 nm, PDI:0,076, ζ –potential: -41,4 mV)(black) and the bilayer saturated with gH625(6E)(Size: 150,4 nm, PDI: 0,060, ζ –potential:-34,9 mV)(red).*

5.3 Conclusions

An easy strategy of attachment, based on electrostatic interaction, was developed in order to decorate with gH625 O/W NEs coated with a polymeric multilayer. The peptide was synthetized in a novel way with a tail of six charged amino acids in order to give it the capability to attach charged nanocapsules only by the tail and exploit the principle of deposition based on the layer by layer methodology. In this way it was possible to carry out

an easy and fast strategy of bio-conjugation of charged polymeric nanocapsules by means of a peptide projected with electrostatic properties. We first started with a positively charged peptide however final positive charged nanocapsules did not show a significant difference in uptake as compared with the control system whereas, low concentrations of peptides to keep a final negative charge was too low for a consistent and functional decoration. We have therefore moved to negative peptides with the aim to work with a final negatively charged nanocapsules and new experiments are under investigation.

References

1. Siegel, R.; Ma, J.; Zou, Z.; Jemal, A. *Cancer Statistics*. 2014. Ca Cancer J Clin. 2014,64:9–29.

2. Malakoutikhah, M.; Teixid, M.; Giralt, E. *Shuttle-Mediated Drug Delivery to the Brain*. Angew. Chem. Int. 2011, 50, 7998 – 8014.

3. Martine, J.; Brown, B.; Quattrocchi, N. Evangelopolos, M.; Ferrari, M.; Tasciotti, E. *Multifunctional to multistage delivery systems: The evolution of nanoparticles for biomedical applications.* Chinese Science Bullettin. 2012, 57, 31: 3961-3971.

4. Safari, J.; Zarnegar, Z. *Advanced drug delivery systems: Nanotechnology of health design: A review*. Journal of Saudi Chemical Society. 2014. 18, 85–99.

5. Kumar, A.; Chen, F.; Mozhi, A.; Zhang, X.; Zhao, Y.; Xue, X.; Hao, Y.; Zhang, X.; Wang, P. C.; Liang, X. J. *Innovative pharmaceutical development based on unique properties of nanoscale delivery formulation*. Nanoscale. 2013, 5(18):8307–8325.

6. Gerlowski, L. E.; Jain, R. K. *Microvascular permeability of normal and neoplastic tissues.* Microvasc Res. 1986, 31(3):288-305.

7. Rakesh, K. J. *Delivery of Molecular Medicine to Solid Tumors.* Science. 1996, 271, 1079-1080.

8. Jain, R. *Transport of molecules across tumor vasculature.* Cancer Metastasis Rev. 1987, 6, 559–593.

9. Hobbs, S. K.; Monsky, W.; Yuan, L. F.; Gregory Roberts, W.; Griffith, L.; Torchilin, V. P.; Jain. R. K. *Regulation of transport pathways in tumor vessels: role of tumor type and microenvironment*. Proc. Natl. Acad. Sci. U.S.A. 1998. 95, 4607–4612.

10. Neuwelt, E.; Abbott, N. J.; Abrey, L.; Banks, W. A.; Blakley, B.; Davis, T.; Engelhardt, B.; Grammas, P.; Nedergaard, M.; Nutt, J.; Pardridge, W.; Gary A. Rosenberg, G. A.; Smith, Q.; Drewes, L. R. *Strategies to advance translational research into brain barriers.* Lancet Neurol. 2008, 7: 84–96.

11. Jafari, S.; Maleki Dizaj, S.; Adibkia, K. *Cell-penetrating peptides and their analogues as novel nanocarriers for drug delivery*. BioImpacts, 2015, 5(2), 103-111.

12. Matjaz,ˇ Z.; Langel, U. *Cell-penetrating peptides: mechanism and kinetics of cargo delivery*. Advanced Drug Delivery Reviews. 2005, 57 529–545.

13. Translocation of Human Calcitonin in Respiratory Nasal Epithelium Is Associated with Self-Assembly in Lipid Membrane. Maria Christiane Schmidt, M.; Rothen-Rutishauser, B.; Rist, B.; Beck-Sickinger, A.; Wunderli-Allenspach, H.; Rubas, W.; Sade´e, W.; and Merkle, H. P. *Translocation of human calcitonin in respiratory nasal epithelium is associated with self-assembly in lipid membrane*. Biochemistry. 1998, 37, 16582– 16590.

14. Carberry, T. P.; Tarallo, R.; Falanga, A.; Finamore, E.; Galdiero, M.; Weck, M.; Galdiero, S. *Dendrimer Functionalization with a Membrane-*

Interacting Domain of Herpes Simplex Virus Type 1: Towards Intracellular Delivery. Chem. Eur. J. 2012, 18, 13678 – 13685.

15. Stefania Galdiero, Annarita Falanga, Mariateresa Vitiello, Luca Raiola, Roberto Fattorusso, Helena Browne, Carlo Pedone, Carla Isernia, and Massimiliano Galdiero. Analysis of a Membrane Interacting Region Simplex Virus Type 1 Glycoprotein H. Journal of Biological Chemistry. 2008. 283:29993-30009.

16. Guarnieri, D.; Falanga, A.; Muscetti, O.; Tarallo, R.; Fusco, S.; Galdiero, M.; Galdiero, S.; Netti, P. A, *Shuttle-Mediated Nanoparticle Delivery to the Blood–Brain Barrier.* Small. 2013, 9, 6, 853–862

17. Kim, J. S.; Rieter, W. J.; Taylor, K. M. L.; An, H.; Lin, Lin, W. *Self-Assembled Hybrid Nanoparticles for Cancer-Specific Multimodal Imaging.* J Am Chem Soc. 2007, 129(29): 8962–8963.

18. Vecchione, R.; Ciotola, U.; Sagliano, A.; Bianchini, P.; Diasproc, A.; Netti. P. A. *Tunable stability of monodisperse secondary O/W nano-emulsions*. Nanoscale. 2014, 6, 9300.

19. Fotticchia, I.; Fotticchia, T.; Mattia, C. A.; Netti, P. A.; Vecchione, R.; Giancola, C. *Thermodynamic Signature of Secondary Nano-emulsion Formation by Isothermal Titration Calorimetry*. Langmuir. 2014, 9, 30(48):14427-33.

20. Ben-Amotz, D.; Underwood, R. *Unravelling water's entropic mysteries: A unified view of nonpolar, polar, and ionic hydration.* Acc.Chem. Res. 2008, 41,8, 957−967.

21. Wong, G. C.; Pollack, L. *Electrostatics of strongly charged biological polymers: Ion-mediated interactions and self-organization in nucleic acids and proteins*. Annu. Rev. Phys. Chem. 2010, 61, 171−189.

Concluding Remarks and Applications

Nanocapsules are colloidal drug carrier systems composed of an oily or an aqueous core surrounded by a thin polymer membrane. In particular biodegradable, oil core nanocapsules represent a suitable platform for entrapment and delivery of lipophilic drugs to treat various diseases (including cancer and infections). Herein, we designed injectable PEGylated oil core nanocapsules with a size below 200 nm, which can reach the area with the increased vascular permeability, and release there the active drug since they are completely composed of biodegradable materials (fatty acids and biodegradable polymers). This type of nanoparticles could represent a versatile platform for the treatment of different types of solid tumors. Anyway, in the case of brain tumors the blood brain vessels tend to keep their impermeable feature. For this reason, we decorated the injectable PEGylated oil core nanocapsules with a cell penetrating peptide (gH625) which, due to its amphipathic character, is able to perturb temporarily phospholipidic membrane organization and cross the blood brain barrier (BBB) carrying its cargo with it. This type of nanocapsules can also have a second functionality. They can accumulate in the endothelium vessels where could have the possibility to release their cargo over the time and treat an endothelial barrier dysfunction attacking inside the cell.

In the synthesis of oil core nanocapsules ITC was employed for the first time to study the optimal conditions for nano-emulsion coating. As result a new method, based on the knowledge of the energetics of overall

interactions, was developed to select the polymer coating that guarantees the best performance in the field of drug administration.

ITC allowed also to develop a new methodology for the measurement of the number of receptors on the cells. This methodology, based on the analysis of the energetics of interaction with a ligand, provided complete information on receptor overexpression in a near-physiological conditions. These findings could give fundamental information for an optimal design of new active drugs targeting towards specific tissues and shed new insights into the emerging field of nanotechnology.

In this regards future in vitro experiments could be conducted to confirm the good effects that the accumulation in the endothelium vessels of biodegradable oil core NCs, loaded with a drug, could provide on an endothelial barrier dysfunction. Moreover, studies could be designed to identify the optimal NCs rigidity to improve their crossing through the endothelial barrier like the blood brain barrier in order to optimize the drug delivery formulation for a CNS disease. The NCs rigidity could be increased switching from a monolayer to a multilayer polymeric coating or a solid shell of silica. Finally, in view of decorating the oil core polymeric NCs with a targeting molecule, the ITC methodology, already developed to study the receptor overexpression on cells, could be used to study the energetics of interaction directly between NCs and cells with the aim to optimize the formulation itself on the basis of the results.